THESIS

EFFECT OF ANNEALING UNDER AMBIENT AND HIGH-HUMIDITY CONDITIONS ON THE STRUCTURAL AND OPTICAL PROPERTIES OF A-GEO2 AND 44% A-TI:GEO2 THIN-FILM COATINGS

Submitted by

Tatiana Savicheva

Department of Electrical and Computer Engineering

In partial fulfillment of the requirements

For the Degree of Master of Science

Colorado State University

Fort Collins, Colorado

Summer 2026

Master's Committee:

Advisor: Carmen Menoni

Jorge Rocca
Jesse Wilson
Justin Sambur

ABSTRACT

EFFECT OF ANNEALING UNDER AMBIENT AND HIGH-HUMIDITY CONDITIONS ON THE STRUCTURAL AND OPTICAL PROPERTIES OF A-GEO2 AND 44% A-TI:GEO2 THIN-FILM COATINGS

Amorphous GeO_2 and *a*-44%Ti-doped GeO_2 thin films are promising high-index materials for low-loss optical coatings in gravitational wave detectors and high-power lasers, but their annealing response due to uncontrolled atmospheric conditions remains not fully understood. The goal of this thesis is to investigate how humidity during annealing affects the thin film materials structural stability, chemical bonding, and surface morphology, addressing a critical gap in amorphous oxide thin film processing.

Ion-beam sputtered amorphous (*a-)* GeO_2, *a*-44%Ti-doped GeO_2, SiO_2, Al_2O_3 and multilayer stacks formed by combining these materials were synthesized and were annealed at 600°C for 10 hours in controlled ambient air and high-humidity annealing environments. Transformations were characterized using powder X-ray diffraction (PXRD), Fourier-transform infrared spectroscopy (FTIR), and Nomarski optical microscopy.

Key findings reveal humidity as a dominant factor controlling the modifications in the structural properties of *a*-GeO_2. PXRD showed pure *a*-GeO_2 films crystallized under high humidity, exhibiting a peak at $2\theta \approx 26.5°$ after 600°C for 10h annealing while remaining amorphous when annealed in ambient air conditions. FT-IR confirmed water incorporation through enhanced O-H stretching (3000-3700 cm^{-1}) and H-O-H bending ($\sim$1630 cm^{-1}) bands as well as Ge-O network reorganization. Nomarski microscopy revealed stress-induced micro-cracking and bubbling in high

humidity annealed *a*-GeO_2. In contrast *a*-44%Ti-doped GeO_2 films remained amorphous at 600°C even under high humidity annealing, demonstrating the Ti's network-stabilizing effect. *a*-SiO_2 and *a*-Al_2O_3 exhibited superior moisture resistance. Multilayer coating stacks showed behavior dependent on their materials: structures containing *a*-GeO_2 layers showed sensitivity to humid annealing, while stacks incorporating TiO_2 demonstrated improved stability.

These results demonstrate that water vapor is a critical variable lowering *a*-GeO_2 crystallization temperature while Ti doping enhances amorphous stability. Humidity-driven effects previously overlooked in "ambient air" annealing studies explain the lack of exact irreproducibility in *a*-GeO_2-based oxide processing and necessitate controlled atmospheres for reproducible low-loss coatings. Future work includes high-resolution PXRD, ellipsometry, X-Ray Photoelectron Spectroscopy and multilayer stability tests to optimize processing protocols.

ACKNOWLEDGEMENTS

I would like to acknowledge my advisor, Carmen Menoni, for her guidance, support and funding throughout my graduate studies. I would like to thank Aaron Davenport and Ramon Rodriguez for their valuable advice, as well as their coatings development for this work and fabrication of the coatings. I am also grateful to Ela Jankowska for her guidance and constant positivity. I would like to acknowledge Vladimir Savichev and Tarkan Takil for their support and for answering my questions related to laser topics. I also thank Ethan Crace and Rebecca Miller for teaching me how to use PXRD and FT-IR, and for their assistance when issues with these facilities arose.

I acknowledge the Analytical Resource Core at Colorado State University for their support in learning X-ray techniques (Research Resource ID: SCR_021758), as well as the Department of Chemistry at CSU.

AI-based tool (Perplexity) was used to assist with language refinement and organization of Chapters 1 and 2. All technical content, analysis, and conclusions were developed and verified by me.

TABLE OF CONTENTS

CHAPTER 1 INTRODUCTION

1.1 Oxide thin films in modern technologies

Oxide thin films occupy a central position in modern materials science and engineering due to their wide range of physical and chemical properties and their importance in numerous technological applications. They are extensively used in optics, microelectronics, photonics, and sensor technologies. In optical systems, amorphous (*a*-) oxide films such as SiO_2, TiO_2, Ta_2O_5, HfO_2, and their mixtures are key components of high-reflective mirrors, antireflection coatings, and interference filters, where precise control of refractive index, absorption, and thickness is required. In microelectronics, amorphous oxide films serve as gate dielectrics, insulating layers, and diffusion barriers, where electrical stability and interface quality are of critical importance.

The functional performance of an oxide thin film is not determined solely by its nominal chemical composition. Instead, it depends on a complex interplay between composition, microstructure, density, defect population, and interface quality with the substrate. Parameters such as porosity, internal stress, and the presence of point defects or impurities can strongly influence refractive index, electrical conductivity, leakage current, and long-term stability. As a result, two films with identical stoichiometry but prepared or processed under different conditions can exhibit significantly different properties [1,2].

Thin film deposition techniques such as ion beam sputtering and electron-beam evaporation typically produce films that are far from thermodynamic equilibrium. As-deposited oxide films are often amorphous or nanocrystalline, may contain a high density of defects, and can exhibit voids, residual stress, or non-ideal stoichiometry. For this reason, post-deposition processing is commonly required to stabilize and optimize film properties [3].

Among post-deposition treatments, thermal annealing plays a particularly important role. Annealing is widely used to relax internal stresses, densify the film, reduce defect concentrations, promote structural ordering, and, in many cases, induce crystallization. [4,5] The impact of annealing on oxide thin films has been demonstrated in numerous material systems. For example, tantalum pentoxide (Ta_2O_5) films deposited by electron beam evaporation were shown to undergo structural changes and phase transitions upon annealing, accompanied by measurable modifications of optical and electrochemical properties [5]. Such results illustrate that annealing is not just a secondary processing step, but often a decisive factor that determines the final functional performance of oxide thin films. For example, Figure 1.1.1. shows cross sectional SEM images of Ta_2O_5 thin films annealed at different temperatures. Here particle size of Ta_2O_5 films decreases greatly with increasing of the annealing temperatures (from 300 to 700°C) but significant changes occurred at 900°C, where the film surface morphology becomes texturized.

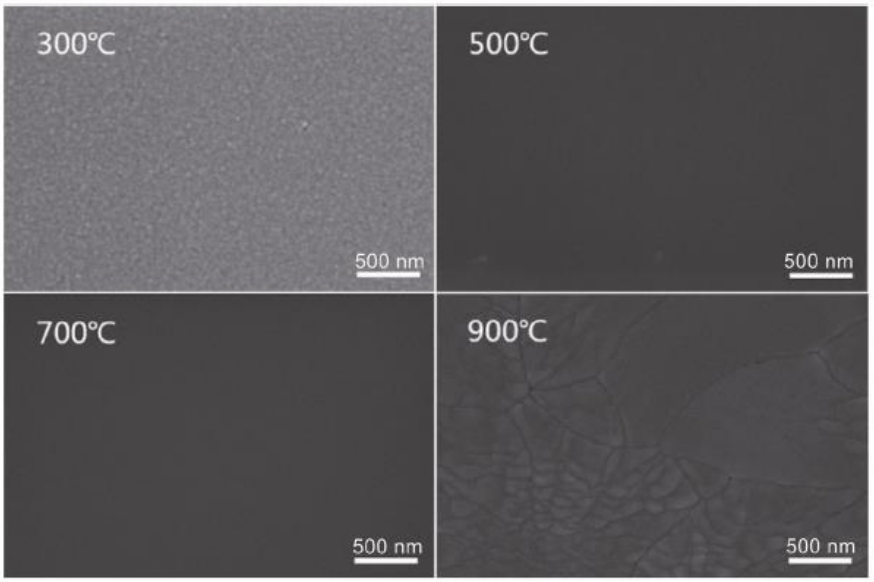

Figure 1.1.1. - Scanning Electron Microscopy images of Ta_2O_5 thin films annealed at different temperatures. The samples presented were annealed for 2 hours at each given temperature [5].

1.2 Physical mechanisms present when annealing amorphous oxide thin films

The effects of annealing on oxide thin films arise from a combination of thermally activated physical and chemical processes. At elevated temperatures, atomic mobility within the film increases, enabling structural relaxation and reorganization of the atomic network [4]. In amorphous oxides, this often leads to densification, reduction of excess free volume, and a decrease in the concentration of weakly bonded or highly strained structural units [4]. Figure 1.2.1. shows the microstrain and the d-spacing (distance between crystal lattice planes) evolution with annealing in polycrystalline Al:ZnO films under different temperatures [6].

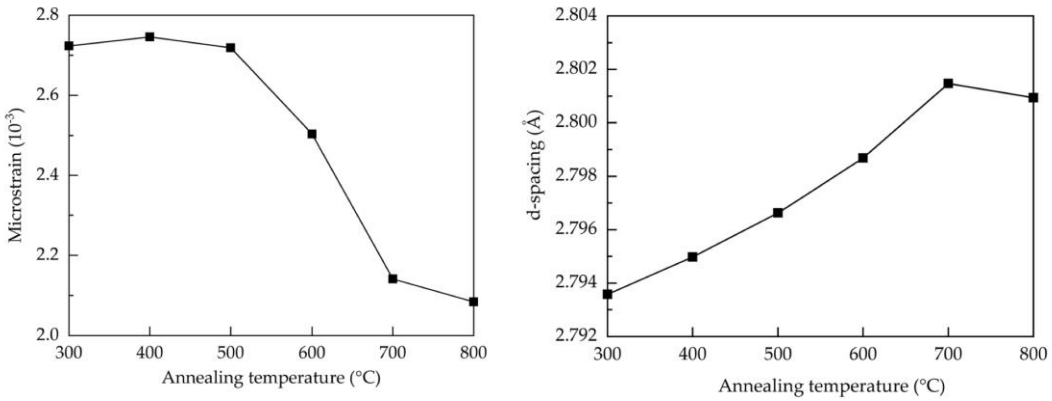

Figure 1.2.1. - Microstrain and d-spacing evolution with annealing in polycrystalline Al:ZnO films under different temperatures [6].

Micro-strain reduces and the increase in the d-spacing is interpreted as a repair of the crystalline structures [6]. These changes are accompanied by an increase in refractive index, which is consistent with a higher density alloy.

Figure 1.2.1. from the Al:ZnO study illustrates polycrystalline behavior, but parallel annealing effects occur in amorphous high-index oxides like Sc_2O_3. In Erik Krous's thesis, XRD analysis of e-beam evaporated scandia films showed that post-deposition annealing from 100–400°C progressively reduced microstrain while slightly shifting d-spacing, reflecting densification and structural relaxation without crystallization [6].

Another important consequence of annealing is the modification in the shallow defect population. As-deposited oxide films can contain a variety of point defects, such as oxygen vacancies, interstitials, or undercoordinated atoms, depending on the deposition technique and conditions [7]. Annealing leads to reduction or redistribution of these defects, either through diffusion-driven recombination processes or through reactions with the surrounding annealing atmosphere, like O_2 filling vacancies, or inert gases like Ar/N_2 limiting oxidation [24,25]. Since many optical and electrical properties of oxides are strongly defect-sensitive, such changes can have a pronounced impact on film performance [7].

At sufficiently high temperatures, annealing can also induce phase transformations. Amorphous films may crystallize, and new alloys may form. This was observed in the crystallization of 25%TiO_2:Ta_2O_5 [11]. In some material systems, such as Ta_2O_5, the transition from amorphous to polycrystalline phases upon annealing is accompanied by changes in optical band gap and functional stability [5]. Similar amorphous-to-crystalline transformations have been observed in many other oxide systems, including GeO_2-based films [9].

The temperature at which amorphous oxide crystallize can be altered when synthesizing mixture alloys. It has been shown that adding other cations, i.e. Hf, Ti, Si, and others with approximately 20% content to Ta_2O_5 increases the crystallization temperature [10]. In Ti:doped Ta_2O_5 annealing to 650°C revealed the presence of a new stable phase [11].

In addition to purely structural effects, annealing can drive chemical changes within the film. These may include oxidation or reduction reactions, changes in stoichiometry, diffusion of elements toward or away from the surface, and reactions at the film to substrate interface [12]. The extent and nature of these chemical processes depend not only on temperature and time, but also on the chemical environment during annealing [7]. As a result, annealing must be regarded as a coupled thermo-chemical treatment rather than a purely thermal one.

Annealing plays a critical role in reducing optical absorption in amorphous oxide thin films. During deposition, films often contain structural defects such as oxygen vacancies and impurities including molecular water and hydroxyl groups. Thermal annealing can promote structural relaxation, densification, and defect reduction.

However, annealing also can induce the structural changing of the amorphous network. At sufficiently high temperatures, this may lead to crystallization. Crystallization is generally unacceptable for optical coatings, as it introduces refractive index change that increases optical scattering, as well as morphological defects and stress.

1.3 *a*-GeO_2 as a functional oxide material

a-GeO_2 is an oxide material of considerable interest for applications in microelectronics and optics. In comparison to the technologically dominant silicon dioxide (SiO_2), *a*-GeO_2 is also a glass former that however exhibits a number of distinctive features that make it both attractive and challenging as a thin film material.

One of the key differences between *a*-GeO_2 and *a*-SiO_2 lies in their chemical behavior and oxidation chemistry [13]. While silicon forms a single Ge stable oxidation state (Si^{4+}) in *a*-SiO_2, Ge can exist in multiple oxidation states, most notably Ge^{2+} and Ge^{4+}. Surface science studies using high-resolution photoelectron spectroscopy have demonstrated that Ge surfaces exposed to oxygen can exhibit several distinct oxidation states, and that annealing can drive redistribution among these states, favoring specific bonding configurations depending on thermal history [14]. This multi-valent nature of *a*-GeO_x implies a more complex chemical landscape than in the case of *a*-SiO_2 and suggests a higher sensitivity of *a*-GeO_2 to thermal and chemical processing conditions [15].

In thin film form, *a*-GeO_2 has been investigated using a variety of deposition techniques. Hsu et al. studied *a*-GeO_2 thin films prepared by a sol-gel method and demonstrated that annealing

in air between 500 °C and 700 °C leads to significant microstructural and morphological changes, including grain growth, reduction of surface roughness, and improvements in electrical leakage behavior. Figure 3 from Hsu et. al [16] shows atomic force microscope (AFM) images of *a*-GeO_2 film surfaces annealed at 500°C for 2 hours, shown on the left part of the figure. This sample has the roughest surface. Annealing at 600°C for 2 hours (central picture) provides smoother surface with larger grains than the sample annealed at 700°C for 2 hours that has the smoothest surface with minimal grain size. That demonstrates progressive grain size reduction and surface flattening with increasing annealing temperature.

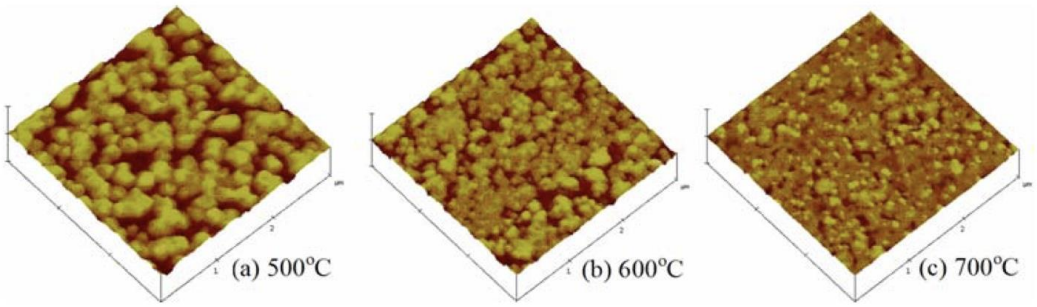

Figure 1.3.1. - The surface morphology of the *a*-GeO_2 thin films on various annealing temperatures from AFM images of [16] show a reduction in surface roughness with annealing.

These results show that the properties of *a*-GeO_2 thin films are strongly dependent on post-deposition thermal treatment.

Earlier work on sputtered *a*-GeO_2 films also revealed important annealing effects. As-deposited films were found to be amorphous, while thermal treatment at elevated temperatures induced recrystallization into polycrystalline *a*-GeO_2, accompanied by changes in optical absorption and structural order [14]. The disappearance of specific absorption features upon recrystallization was attributed to the elimination or reorganization of defect-related states, highlighting the close connection between structure, defects, and optical properties in *a*-GeO_2 films.

The abovementioned studies demonstrate that *a*-GeO_2 thin films are highly sensitive to annealing and that both their structural and functional properties can be substantially modified by thermal treatment. At the same time, the complex oxidation chemistry of Ge, as evidenced by the presence of multiple oxidation states and thermally driven redistribution processes, suggests that the response of *a*-GeO_2 films to annealing cannot be understood only in terms of simple structural relaxation or crystallization. Instead, chemical effects, including changes in bonding configuration and stoichiometry, must also be taken into account.

Importantly, the majority of studies have focused primarily on the influence of annealing temperature and time, while the role of the annealing atmosphere itself has received less attention. Given the chemical activity of *a*-GeO_x, it is reasonable to expect that the surrounding environment during annealing can play an important role in determining the final structural and chemical state of *a*-GeO_2 thin films.

For example, Le Yang's PhD thesis [17] demonstrates that amorphous *a*-GeO_2 thin films deposited via ion beam sputtering at elevated substrate temperatures (up to 0.83 $T_g \approx 650°C$) exhibit enhanced medium-range order, characterized by *a*-GeO_4 tetrahedra increasingly forming 6-membered rings instead of defect-prone 3-membered rings, as confirmed by Raman A_6/A_3 peak ratios rising from ~0.68 at room temperature to ~0.97. This structural evolution is more pronounced during high temperature deposition than post-annealing which correlates directly with reduced room-temperature mechanical loss (internal friction Q^{-1}), dropping 44% from $(2.98 \pm 0.27)\times10^{-4}$ at room temperature to $(1.66 \pm 0.14)\times10^{-4}$ at 0.83 T_g, plateauing at $\sim1\times10^{-4}$ after optimal annealing conditions. Pure *a*-GeO_2 achieved the second lowest $Q^{-1} \approx (0.6 \pm 0.2) \times10^{-4}$, with first lowest being *a*-SiO2, among the family of oxides that were studied [10]. Further, Yang et al. reported the vapor-deposited *a*-GeO_2 can achieve a network configuration that is glass-like when deposited near T_g

and with post-deposition annealing, consisting of an increased population of 6-membered ring populations at the expense of smaller rings [18].

1.4 *a*-44%Ti-doped GeO_2 ($GeTiO_2$ / $TiGeO_x$) mixed oxide thin films

In addition to pure *a*-GeO_2, mixed oxide systems based on titanium and *a*-GeO_x have gained a lot of attention due to their tunable structural, optical, and electrical properties. Titanium dioxide (TiO_2) itself is a widely studied oxide, used in optical coatings, sensors, and electronic devices, due to its high refractive index, chemical stability, and wide band gap. By incorporating Ge into TiO_2-based systems, it is possible to modify the electronic structure, phase stability, and microstructural evolution of the resulting films, thereby extending the range of achievable material properties.

In this work, the composition *a*-44% Ti-doped GeO_2 refers to the atomic fraction of Ti relative to the total cation content: Ti/(Ti + Ge) = 0.44. The films are produced by co-sputtering, resulting in an amorphous mixed oxide network in which Ti atoms are incorporated into the Ge-O matrix at the atomic scale. This structure differs from a physical mixture of *a*-TiO_2 and *a*-GeO_2 phases. Instead of phase separation, a homogeneous amorphous network is formed, where Ti modifies the local bonding environment. This incorporation increases resistance to crystallization and enhances structural stability of the amorphous phase.

Mixed *a*-44%Ti-doped GeO_2 thin films are often described in the literature as $GeTiO_2$ or $TiGeO_x$, reflecting the fact that their exact composition and phase structure can vary depending on deposition and annealing conditions. In such systems, annealing plays a particularly critical role, as it can drive crystallization, phase separation, and redistribution of elements within the film [19]. These processes are not only thermally activated but are also strongly influenced by the chemical stability of *a*-GeO_x and their tendency to undergo reduction or oxidation at elevated temperatures, as has been observed when adding nitrogen during the growth to a-GeO_2 [20].

A detailed study of annealing-induced structural transformations in *a*-$GeTiO_2$ thin films was reported by Stavarache et al. [21]. In that work, amorphous *a*-$GeTiO_2$ films deposited by magnetron sputtering were annealed in the temperature range from 400 °C to 700 °C. The authors observed that films annealed at lower temperatures remained amorphous, while higher annealing temperatures led to crystallization and the formation of complex multiphase structures. In particular, the appearance of a *a*-$(TiGe)O_2$ rutile-type structure, *a*-TiO_2 anatase phases, and *a*-GeO_2 crystallites was reported, depending on the annealing temperature and film composition. At the highest annealing temperatures, diffusion of Ge toward the film surface and partial loss of Ge due to the formation of volatile *a*-GeO species were observed [21].

These findings highlight several important aspects of *a*-44%Ti-doped *a*-GeO_2 thin films. First, the structural state of the films is highly sensitive to annealing temperature, with transitions from amorphous to crystalline and from single-phase to multi-phase structures occurring over a relatively narrow temperature range. Second, the presence of Ge introduces additional complexity due to its multiple oxidation states and the possibility of Ge diffusion and segregation. Third, annealing-induced structural changes are closely correlated with modifications of functional properties such as optical transmittance and electrical conductivity, emphasizing the strong coupling between structure, chemistry, and performance in these materials [21].

From the perspective of thin film processing, these results imply that *a*-44%Ti-doped GeO_2 systems cannot be treated as simple, thermally stable mixtures of *a*-TiO_2 and *a*-GeO_2. Instead, they represent chemically and structurally dynamic materials in which annealing can trigger a sequence of transformations involving crystallization, phase separation, and chemical redistribution [21,22]. This sensitivity makes *a*-44%Ti-doped GeO_2 films an excellent model system for studying the dependency between thermal treatment, chemical environment, and thin film evolution.

Vajente, et al. in [23] and Yang, et al. in [10] exploited these properties of *a*-44%Ti-doped GeO_2 films to engineer low-loss mirror coatings for gravitational wave detectors, achieving a breakthrough with 44% Ti-doped GeO_2 mixtures. After 108 hours at 600°C, amorphous films reached mechanical loss $\varphi = (0.96 \pm 0.18)\times10^{-4}$ which is 2.5 times lower than TiO_2:Ta_2O_5, while maintaining n = 1.88 and absorption of less than 3 ppm at 1064 nm. *a*-44%Ti-doped GeO_2/SiO_2 multilayer designs for Advanced LIGO+ end test masses, which are 40 kg fused silica mirrors positioned at the far ends of LIGO's 4 km interferometer arms, are predicted to achieve ow thermal noise, and extremely low absorption loss at λ=1064 nm. Efforts are under way to demonstrate mirror coatings with the same design as current 25%TiO_2:Ta_2O_5/SiO_2 and achieve the predicted performance [24].

1.5 Role of annealing atmosphere in oxide thin films

While temperature and annealing time are commonly considered the primary parameters of controlling post-deposition heat treatment, the chemical nature of the annealing atmosphere can be equally important. In many practical cases, annealing is performed in ambient air or in nominally inert environments, and the atmosphere is treated as a passive background. However, from a physicochemical point of view, the annealing environment can actively participate in reactions that modify the film's composition, defect structure, and surface chemistry.

In oxide materials, the annealing atmosphere can influence the balance between oxidation and reduction processes, affect the concentration of oxygen vacancies and other point defects, and promote or suppress diffusion of species within the film. For example, annealing in oxygen-rich environments can lead to further oxidation and defect healing, while annealing in oxygen-poor or reducing environments can promote the formation of oxygen vacancies or suboxide phases [25].

These changes can have a strong impact on optical absorption, electrical conductivity, and chemical stability.

The importance of chemical effects during annealing is particularly evident in materials with multiple possible oxidation states or with components that can undergo thermally activated redox reactions. *a*-GeO_x represents a clear example of such behavior. As discussed earlier, Ge can exist in different oxidation states, and high-resolution photoelectron spectroscopy studies have shown that annealing can drive redistribution among these states, favoring specific bonding configurations [14]. This implies that the chemical environment during annealing can influence not only the overall oxygen content of the film, but also the detailed bonding structure and electronic state of Ge.

In the case of *a*-GeO_2 and *a*-44%Ti-doped GeO_2 thin films, this sensitivity to chemical environment is further amplified by the possibility of Ge diffusion at elevated temperatures, as reported in annealing studies of *a*-$GeTiO_2$ films [21]. Such processes are not determined by temperature alone but depend critically on the availability of reactive species in the surrounding atmosphere and on the chemical potentials of the involved elements.

1.5.1 Chemical activity of annealing environments

From a thermodynamic and kinetic perspective, the annealing atmosphere provides a reservoir of chemical species that can interact with the thin film [25]. In air or oxygen-containing environments, oxygen partial pressure plays a key role in determining the oxidation state of the film and the concentration of oxygen-related defects. For example, In $BiFeO_3$ thin films, X-Ray Photoelectron Spectroscopy (XPS) reveals that the O 1s binding energy shifts between air and argon annealing, reflecting atmosphere-controlled oxidation states (Figure 4). So, in inert

atmospheres such as argon or nitrogen, the absence of reactive oxygen can stabilize oxygen-deficient states or promote reduction processes [26].

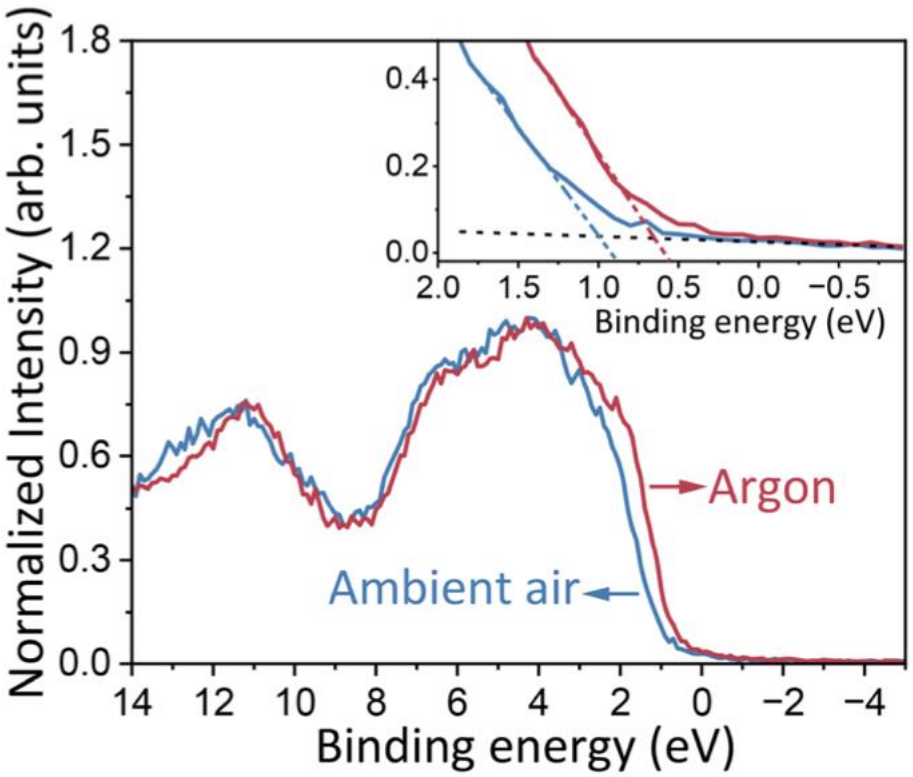

Figure 1.5.1.1. - VB-XPS spectra of BFO thin films annealed in ambient air and argon [26].

These considerations are particularly relevant for oxides containing elements with volatile suboxides or multiple stable oxidation states. Ge is known to form both *a*-GeO and *a*-GeO_2, and under certain conditions, *a*-GeO can become volatile at elevated temperatures, leading to material loss and changes in film composition. The observation of Ge loss and *a*-GeO_2 surface crystallite formation in annealed *a*-$GeTiO_2$ films provides experimental evidence for such chemically driven processes [21].

In addition, the annealing atmosphere can influence interfacial reactions between the film and the substrate, as well as the incorporation or removal of impurities such as hydrogen or hydroxyl groups as observed in chromium oxide [27]. These effects are often most noticeable near

the film surface and interfaces, but they can also propagate into the film bulk through diffusion processes, especially during long or high-temperature annealing treatments [27].

1.5.2 Role of humidity and water vapors

Among the possible components of the annealing atmosphere, water vapor plays a special role due to its ability to act as a source of both hydrogen and oxygen. In oxide thin films, the presence of water vapor can promote hydroxylation reactions and modify the local bonding [28]. For example, hydrogen-related species can passivate certain defects, while hydroxyl groups can become incorporated into the oxide network, leading to changes in vibrational spectra, density, and potentially even mechanical and electrical properties [29].

In many experimental studies, annealing is carried out in ambient air without explicit control or reporting of humidity [4,6,27]. However, from a chemical standpoint, the difference between dry air and humid air can be significant, particularly for materials that are sensitive to hydrogen or hydroxyl incorporation [30]. Given the complex oxidation chemistry of Ge and the strong annealing-induced transformations observed in *a*-GeO_2 and *a*-44%Ti-doped GeO_2 films [16,21], it is reasonable to expect that humidity can play a non-negligible role in determining the outcome of thermal treatment. Water plays a significant role in modifying the structural evolution of oxide thin films during annealing. The incorporation of water occurs primarily through the formation of hydroxyl groups and molecular species, which alter the local bonding configuration of the oxide network.

These interactions weaken the network by breaking bridging bonds and introducing non-bridging oxygen species, facilitating atomic rearrangement. As a result, the presence of water effectively lowers the crystallization threshold of amorphous films.

At the same time, annealing promotes dehydration, leading to a competing balance between water removal and re-incorporation. Therefore, the structural evolution of the films is governed not only by temperature, but also by the dynamic interaction between dehydration and water-assisted network modification [25].

Despite this, systematic investigations that directly compare annealing in dry or ambient conditions with annealing in high-humidity environments for *a*-GeO_2 and *a*-44%Ti-doped GeO_2 thin films are lacking. Most available studies focus on temperature-driven effects or on annealing in a single, fixed atmosphere, making it difficult to separate purely thermal effects from chemically induced changes related to the annealing environment.

This lack of comparative data motivates a more detailed and controlled study of humidity assisted annealing, in which the influence of water vapor is isolated and examined in parallel with conventional ambient annealing under otherwise identical thermal conditions.

1.6 Characterization methods for structural and chemical analysis of oxide thin films

A comprehensive understanding of annealing-induced changes in oxide thin films requires the use of complementary characterization techniques capable of probing different aspects of the material. Since annealing can simultaneously affect crystal structure, chemical bonding, surface composition, and morphology, no single method is sufficient to capture the full picture. Instead, a combination of structural, spectroscopic, and microscopic techniques is necessary.

Powder X-ray diffraction (PXRD) is one of the most widely used tools for investigating the structural state of thin films [31]. It provides information about whether a film is amorphous or crystalline, identifies crystalline phases, and allows the detection of phase transformations induced by annealing. In the context of *a*-GeO_2 and *a*-44%Ti-doped GeO_2 thin films, PXRD is particularly useful for monitoring the amorphous-to-crystalline transition observed in *a*-GeO_2 films after

annealing [9] and for identifying the complex multiphase structures that can form in annealed *a*-$GeTiO_2$ films, including rutile-type *a*- $(TiGe)O_2$ and *a*-GeO_2 crystallites [21]. Changes in peak positions, widths, and intensities also provide insight into crystallite size, structural ordering, and possible strain effects.

While PXRD probes long-range structural order, spectroscopic techniques are required to investigate local bonding environments and chemical structure. Fourier transform infrared spectroscopy (FT-IR) is a powerful method for studying vibrational modes associated with specific chemical bonds in oxide networks [31]. In oxide thin films, FT-IR can reveal information about metal–oxygen stretching and bending modes and the presence of hydroxyl groups or other hydrogen-related species. This is particularly relevant for the present work, as the incorporation of hydroxyl groups or changes in Ge-O and Ti-O bonding configurations may occur during annealing, especially in humid environments. FT-IR therefore provides a sensitive probe of chemically driven changes that may not be directly visible in diffraction data.

Optical and morphological inspection methods are necessary to assess the macroscopic and microscopic uniformity of the films. Nomarski (differential interference contrast) microscopy provides a sensitive means of visualizing surface topography, defects, inhomogeneities, and stress-related features in thin films. Although it does not offer atomic-scale resolution, it is highly useful for detecting annealing-induced surface changes such as cracking, delamination, roughening, or the formation of large-scale morphological features that may be associated with crystallization, densification, or chemical degradation processes [32].

The combined use of PXRD, FT-IR and Nomarski microscopy provides a comprehensive and complementary characterization. Together, these techniques enable the correlation of structural transformations, chemical modifications, and morphological changes induced by annealing,

allowing a more complete understanding of how both temperature and atmosphere influence the evolution of *a*-GeO_2 and *a*-44%Ti-doped GeO_2 thin films.

1.7 Motivation of this work

The processing of sputtering of oxide thin films and post-deposition annealing is a well-established and widely used approach for tailoring their structural, chemical, and functional properties. Numerous studies have demonstrated that annealing temperature and time strongly influence film densification, defect concentration, crystallization behavior, and phase stability [4,10,11]. As a result, thermal treatment is routinely employed as a key step in the fabrication of oxide coatings for optical, electronic, and protective applications.

However, in most cases, the annealing atmosphere is either fixed or barely specified, most often as “ambient air” or a nominally inert environment [30]. In such cases, the chemical composition of the atmosphere, and particularly the presence of reactive species such as water vapor, is implicitly assumed to play a secondary role compared to temperature. This assumption is not always justified, especially for oxide systems with complex chemistry and multiple possible oxidation states.

a-GeO_2 and *a*-44%Ti-doped GeO_2 mixed oxide thin films represent a class of materials for which the chemical environment during annealing is expected to be especially important. As discussed in the previous sections, *a*-GeO_x exhibit multiple oxidation states and a pronounced sensitivity to thermal and chemical processing, as evidenced by spectroscopic studies of Ge oxidation and annealing-driven redistribution of oxidation states [33]. In thin film form, *a*-GeO_2 has been shown to undergo significant structural and morphological changes upon annealing, including recrystallization and defect-related transformations [17].

In the work of Le et. al [18, 23] authors investigated sputtered *a*-GeO_2 and *a*-44%Ti-doped GeO_2 mixed oxide thin films annealed in ambient air at temperatures ranging from 300-600°C for 2-10 hours without humidity or gas flow control. PXRD revealed progressive crystallization in pure *a*-GeO_2 films above 500°C, evidenced by emerging peaks at $2\theta \approx 22°$ corresponding to the hexagonal phase [18]. In *a*-44%Ti-doped GeO_2 alloys the crystallization temperature increased with respect to that of *a*-GeO2 [23]. As it will be shown in this work, FT-IR spectra confirmed annealing changes in local bonding, including weakening of OH-related modes near 3400 cm^{-1} and shifting of asymmetric Ge-O stretches (850-950 cm^{-1}), indicates hydrogen desorption and network densification under uncontrolled air exposure. Nomarski microscopy shown the stress-induced micro cracking in air-annealed *a*-GeO_2 films post 500°C annealing.

From abovementioned, *a*-44%Ti-doped GeO_2 films exhibit complex annealing-induced behavior, including crystallization, phase separation, diffusion of Ge, and even partial loss of Ge at elevated temperatures [17,34,35]. These observations clearly indicate that annealing of Ge-containing oxide films is not a purely structural relaxation process, but involves chemically driven transformations that can, in principle, be strongly influenced by the surrounding atmosphere [30].

Water vapor is a particularly important component of the annealing environment because it can act as a source of both hydrogen and oxygen and can participate directly in chemical reactions at the film surface and within the near-surface region [28]. The presence of water vapor can promote hydroxylation, modify local bonding configurations, and alter oxidation [13]. Despite these chemical effects, humidity is rarely treated as an independent and controlled parameter in annealing studies of *a*-GeO_2 and *a*-44%Ti-doped GeO_2 thin films. Instead, it is often either uncontrolled or simply not reported, making it difficult to assess its true impact on film evolution.

This situation leads to an important and practically relevant gap in current understanding. If two films are annealed at the same temperature and for the same duration, but in atmospheres

with significantly different humidity levels, there is no guarantee that their structural and chemical states will be identical. For materials as chemically sensitive as *a*-GeO_2 and *a*-44%Ti-doped GeO_2, even moderate differences in the chemical environment may result in measurable differences in phase composition, bonding structure, defect population, and surface morphology. From the perspective of thin film processing and application, this lack of clarity represents a serious limitation, as it undermines the reproducibility and predictability of annealing treatments.

The central motivation of the present work is to move beyond a purely temperature-centered view of annealing and to explicitly investigate the role of the annealing atmosphere, with particular emphasis on the influence of humidity.

To achieve this goal, *a*-GeO_2 and *a*-44%Ti-doped GeO_2 thin films were deposited using ion-beam-based deposition techniques and subsequently subjected to controlled annealing treatments in two different environments: conventional ambient air and a high-humidity atmosphere. The use of identical thermal schedules for both environments allows a direct comparison of the resulting films and enables the specific influence of humidity to be isolated. Structural, chemical, and morphological changes induced by annealing are investigated using a combination of complementary characterization methods, including powder X-ray diffraction (PXRD), Fourier transform infrared spectroscopy (FT-IR), and Nomarski microscopy.

This work aims to provide a detailed characterization of annealing-induced structural transformations in *a*-GeO_2 and *a*-44%Ti-doped GeO_2 thin films, including amorphous-to-crystalline transitions and phase evolution. Also, it aims to clarify how the chemical bonding state and surface composition of these films change as a function of annealing atmosphere, with particular attention to oxidation states, hydroxyl incorporation, and stoichiometry variations. Third, it examines the morphological consequences of annealing under different environments, including the development of surface inhomogeneities, defects, or stress-related features.

By addressing these points in a systematic and comparative manner, this thesis aims to establish a clearer and more physically grounded understanding of how humidity influences the annealing of *a*-GeO_2 and *a*-44%Ti-doped GeO_2 thin films. The results are expected to contribute not only to the fundamental understanding of thermo-chemical processes in Ge-based oxides, but also to the development of more reliable and controllable processing strategies for oxide thin films, in which both temperature and atmosphere are treated as equally important parameters.

This work investigated the effect of annealing environment on the stability of oxide thin films deposited. The results show that *a*-GeO_2 thin films crystallize earlier when annealed under high humidity compared to ambient conditions, indicating that the presence of water promotes structural transformation in *a*-GeO_2 coatings. *a*-44%Ti-doped GeO_2 films remain amorphous after annealing at 600 °C in high humidity, demonstrating that Ti incorporation improves the stability of the amorphous network.

Additional experiments on SiO_2, Al_2O_3, and multilayer stacks ($SiO_2/GeO_2/SiO_2$, SiO_2/TiGeO/SiO_2, $Al_2O_3/GeO_2/Al_2O_3$, and Al_2O_3/TiGeO/Al_2O_3) showed significant surface degradation after humid annealing. FTIR measurements confirmed increased O-H absorption associated with water incorporation, while Nomarski microscopy showed bubbling and delamination features on the film surface.

Overall, the results demonstrate that humidity during annealing strongly affects the structural stability of *a*-GeO_2-based coatings, while Ti doping improves resistance to moisture-induced crystallization.

Following Chapter 2 describes the experimental methodology employed in this work, including thin film deposition using Laboratory Alloy and Nanolayer System (LANS) biased target ion beam deposition and Veeco Spector gridded ion beam sputtering systems (Sections 2.1-2.2), followed by controlled annealing in ambient air and high-humidity conditions using a custom

muffle furnace setup with humidity control (Section 2.3). Comprehensive pre- and post-annealing characterization includes PXRD for crystallization assessment (Section 2.4), FT-IR spectroscopy for local bonding and water content analysis (Section 2.5), and Nomarski microscopy for surface morphology evolution (Section 2.6).

Despite the widespread use of annealing to improve optical properties of oxide coatings, the role of humidity during annealing remains poorly understood. In particular, the interaction between water incorporation, structural stability, and crystallization behavior in *a*-GeO_2-based thin films has not been systematically studied.

CHAPTER 2 EXPERIMENTAL

In this work the initial samples of interest were deposited using two different systems - Laboratory Alloy and Nanolayer System (LANS) and Veeco Spector. Sections 2.1 and 2.2 cover design and the principles of this deposition system's operation.

Deposited samples were later annealed at different temperatures and humidity conditions using a set up developed in the lab. Section 2.3 covers the annealing setup that includes muffle furnace (MTI KSL1200XM) and humidifying system. Before and after the annealing all the samples were examined for crystallization by means of Bruker D8 Discover DaVinci - PXRD (Powder X-Ray Diffraction) described in section 2.4.

To gain deeper understanding of how the water content in the deposited film was changed under different annealing conditions the following measuring techniques described in sections 2.5-2.6 were implemented.

For Infrared spectroscopy we were using Nicolet iS-50 FT-IR Fourier Transform Infrared Spectrometer with a single pass ATR (diamond and ZnSe crystals) - FTIR (section 2.5) for measuring the sample absorbance at different frequencies. The surfaces of the samples were visually investigated using the Nomarski microscope to follow the changes on the deposited surface (section 2.6).

It is worth mentioning that all the abovementioned measuring techniques were implemented before and after the annealing in both ambient and high humidity conditions.

2.1 Laboratory Alloy and Nanolayer System (LANS)

The Laboratory Alloy and Nanolayer System (LANS) is a thin-film deposition based on biased target ion beam deposition (BTD) [35-37]. This instrument allows the sequential deposition of six different materials or the simultaneous deposition of two or three different materials. The system is shown in the picture below.

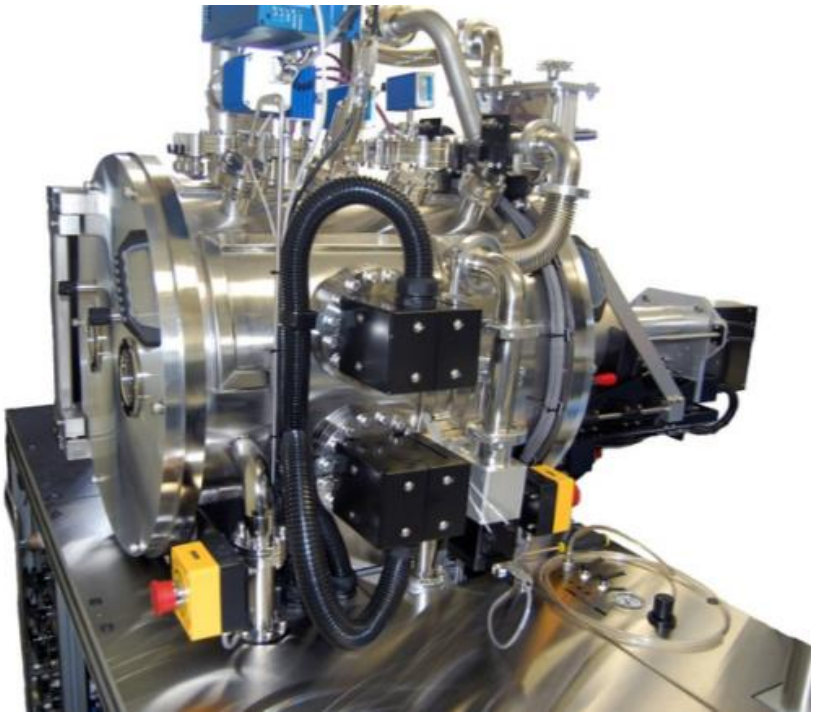

Figure 2.1.1. - LANS depositing system.

The LANS system has independent adjustment of key deposition parameters, such as control of target voltage and current, ion beam energy, ion current density, deposition rate, materials used for deposition (targets), pulse width and working gas pressure. This level of control makes it possible to tune the film density, thickness and composition [38,39]. Substrates are mounted on a holder with controlled positioning, ensuring uniform material flux over the sample surface. The instrument allows one to deposit both single layer, multilayer materials and to create oxide mixtures.

The biased target deposition (BTD) system uses a low energy ion source, kinetic energy typically < 25 eV to create a plume of noble gas ions which is directed toward a negatively biased target. The ions are attracted to the targets by applying a negative bias (300-1200 eV). When the energetic ions impact the target surface, momentum transfer causes atoms to be ejected from the target material. These sputtered atoms propagate through the vacuum chamber and condense on the substrate surface, forming a thin film. A schematic of the process is shown in Figure 2.1.2.

The deposition process is performed under high-vacuum conditions, with the chamber pressure typically maintained in the 10^{-4}-10^{-2} Torr range during operation. The ion beam energy, ion current density, target bias voltage, and working gas pressure can be independently controlled, allowing precise tuning of the film growth conditions and resulting material properties such as density, composition, and surface morphology.

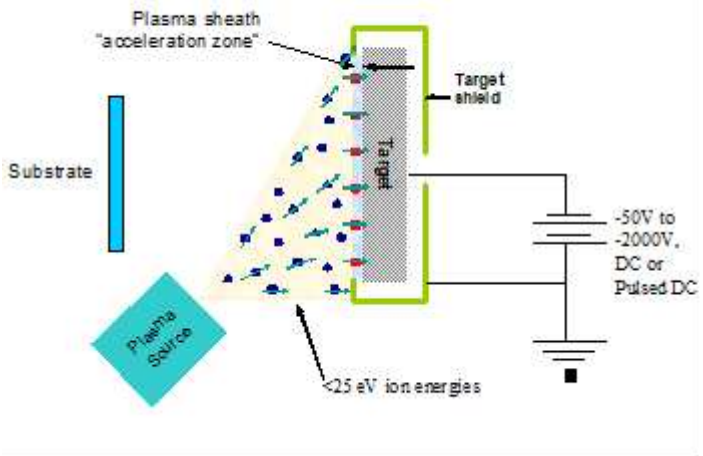

Figure 2.1.2. - Scheme of BTD sputtering.

Pulsed DC target bias is used depending on the target material and desired process. The selection of the target voltage has an important impact on film density, grain size, atomic scale mixing at thin film interfaces and the overall roughness of the growing films.

Recent work at 4Wave demonstrated the capability of BTD to co-sputter alloys and reactively deposit dielectric films from metal targets [40].

A schematic diagram of the alloy co-sputtering configuration used in the LANS deposition system is shown in Figure 2.1.3.

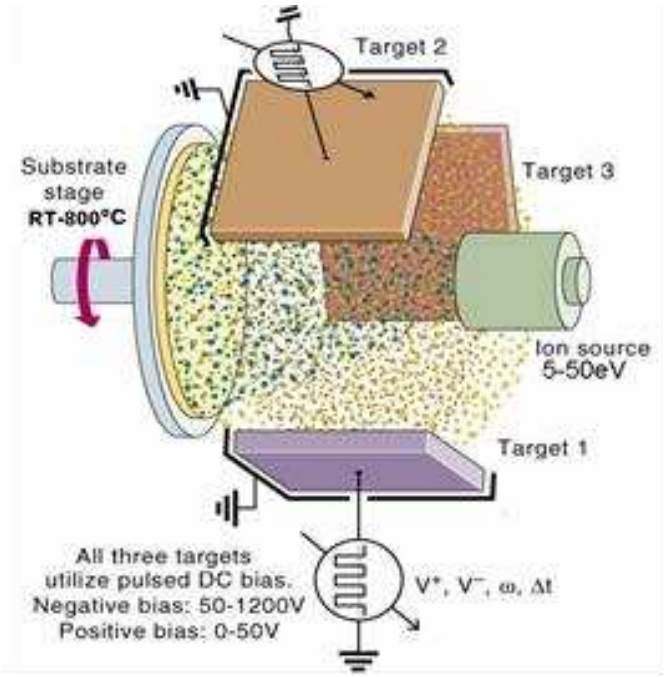

Figure 2.1.3. - Alloy co-sputtering scheme.

2.2 Veeco Spector

The Veeco Spector deposition system is a thin film coating system that uses gridded ion sources for sputtering (IBS). Gridded IBS is widely used for optical coating applications due to its ability to produce dense, smooth, and highly uniform thin films. In gridded IBS, an inert gas typically argon, is introduced into an ion source where a plasma is generated using inductively coupled radiofrequency (RF) power. Positive noble gas ions are extracted from the plasma and accelerated by a set of metallic grids with applied high voltages [36,39].

Figure 2.2.1 - Veeco Spector Chamber.

Then the accelerated ion beam is directed toward the deposition target. When energetic noble gas ions impinge on the target surface, they dislodge atoms and molecules from the target. The sputtered species propagate through the high-vacuum chamber and condense on the substrate surface, forming a thin film.

The Veeco Spector system provides independent control over key deposition parameters, including ion beam energy, ion current density, working gas pressure, reactive gas flow, and deposition rate. A schematic of the principle of operation of the Veeco Spector system is shown in Figure 2.2.2.

In this work, the Veeco Spector gridded IBS system was used to deposit oxide thin films under well-controlled conditions, providing a reference for comparison with films deposited using biased target ion beam deposition.

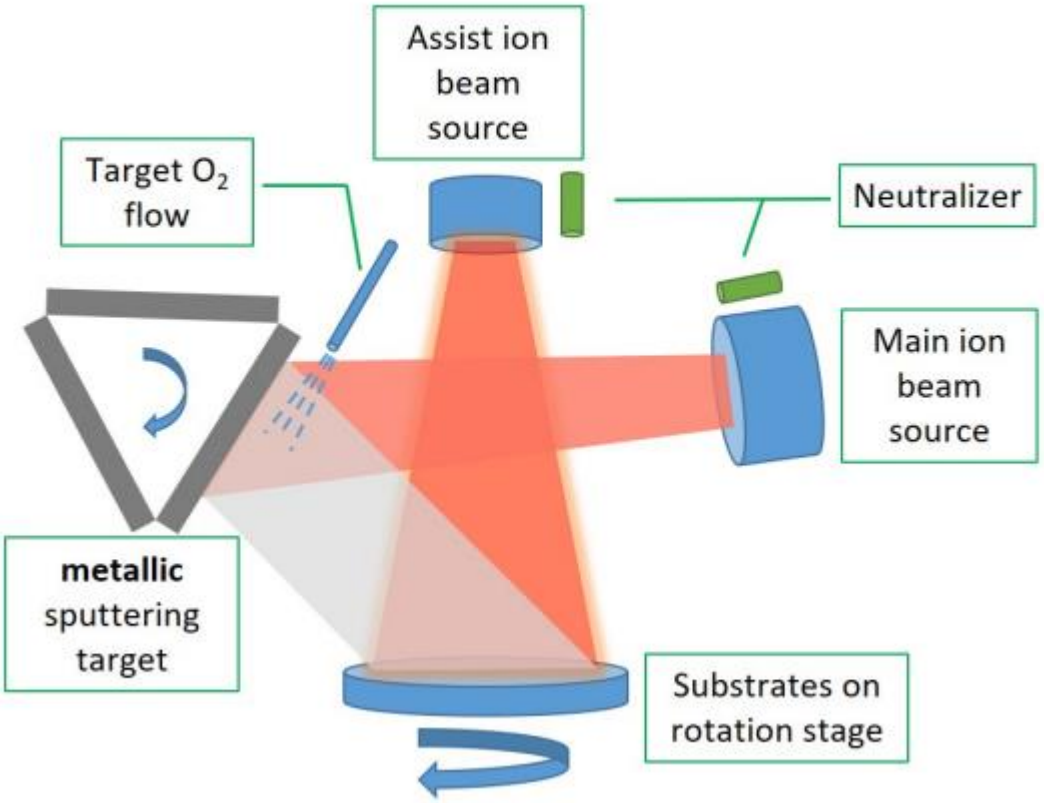

Figure 2.2.2. - Schematic of the dual ion beam sputtering deposition system fabricated by Veeco.

This system is widely used for fabricating oxide coatings as SiO_2, GeO_2, Al_2O_3, TiO_2, and mixed oxides including *a*-44%Ti-doped GeO_2. Films deposited by IBS are characterized by high density, low surface roughness, perfect thickness uniformity, and low optical absorption [35].

There are some process parameters which influence the quality and properties of the deposited films. Ion beam energy controls the kinetic energy of sputtered particles and affects film density and microstructure. Ion current density determines the sputtering rate and deposition rate, influencing film thickness and growth dynamics. Working gas pressure affects the mean free path of sputtered species. Lower pressures produce smoother films. Also, the reactive gas flow determines film stoichiometry and optical properties, while substrate temperature and rotation influence film uniformity and internal stress.

2.3 Muffle Furnace with Controlled Humidity

Annealing of the samples was performed by the setup that consists of a muffle furnace (MTI KSL1200XM) coupled to an external humidity control system. The purpose of this configuration is to control temperature and humidity during the process.

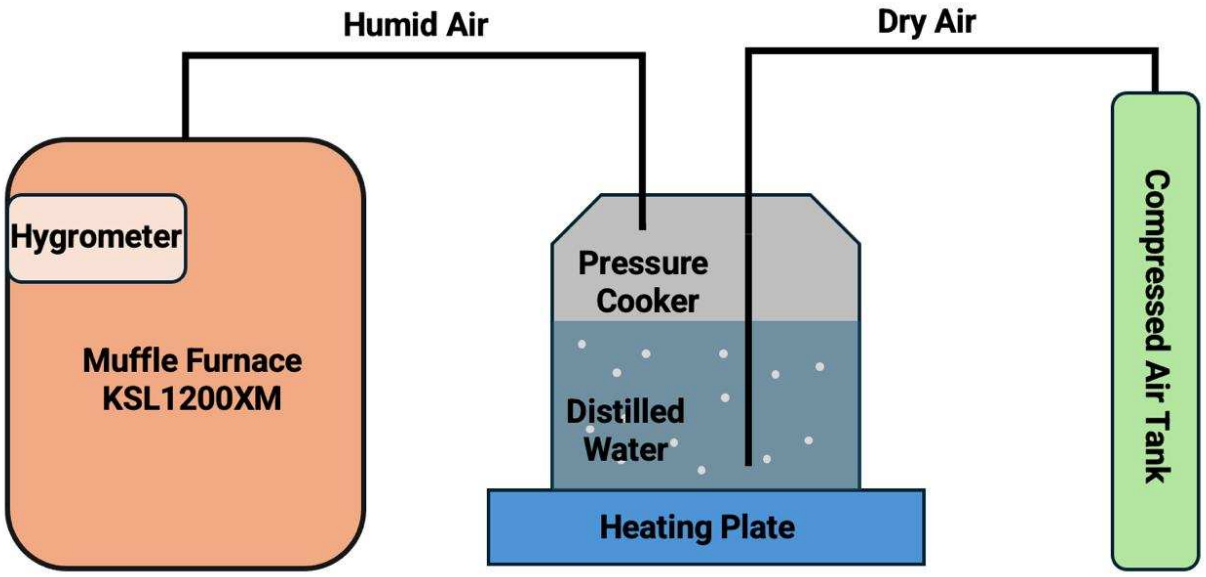

Figure 2.3.1. - Schematics of the controlled humidity annealing system.

The muffle furnace provides a uniform, high-temperature environment where the samples are annealed. Samples are placed inside the furnace chamber, where the temperature is raised to the target annealing value (550-900°C) at different annealing conditions and held for a defined duration (10 hours). The furnace atmosphere itself is not actively evacuated or sealed, instead, it is continuously exchanged with a controlled gas flow supplied from the external system [41].

Humidity control is achieved using a heated distilled water reservoir (pressure cooker) placed on a heating plate. Dry compressed air from the air tank is directed into the water reservoir, where it bubbles through heated distilled water. As a result, the air becomes saturated with water

vapor, producing a stream of humid air. The humidity inside of the furnace was controlled with a commercially available hygrometer (~94%). The humid air continuously flowed through the furnace during annealing.

2.4 Bruker D8 Discover DaVinci - PXRD (Powder X-Ray Diffraction)

The Bruker D8 Discover DaVinci is a high-resolution X-ray diffraction (XRD) system designed for structural characterization of crystalline and partially crystalline materials equipped with a Cu Kα radiation source (λ = 1.5406 Å). The instrument is based on a modular goniometer platform that enables flexible configuration for powder diffraction, thin-film analysis, and advanced scattering geometries.

In powder X-ray diffraction (PXRD), a monochromatic X-ray beam is directed onto the sample, and the diffracted intensity is recorded as a function of the scattering angle. Diffraction occurs when the Bragg condition is satisfied, allowing determination of crystallographic structure, lattice parameters, and crystallite size. PXRD is particularly well suited for identifying crystalline phases and monitoring structural changes such as crystallization induced by thermal treatment [42].

Figure 2.4.1. - PXRD System.

In the thin-film PXRD, the diffracting volume is significantly smaller than in bulk samples, which results in weaker diffraction signals and increased sensitivity to background scattering from the substrate.

The physical basis of X-ray diffraction is described by Bragg's law, which defines the condition for constructive interference of X-rays scattered by parallel atomic planes in a crystalline material:

$$n\lambda = 2d\sin\ \theta \qquad (1)$$

Where n is the order of diffraction, λ is the wavelength of the incident X-ray radiation, d is the interplanar spacing of the crystal lattice, and θ is the angle between the incident beam and the diffracting planes.

This relationship allows determination of lattice spacing and identification of crystalline phases by comparing measured peak positions to reference databases [43].

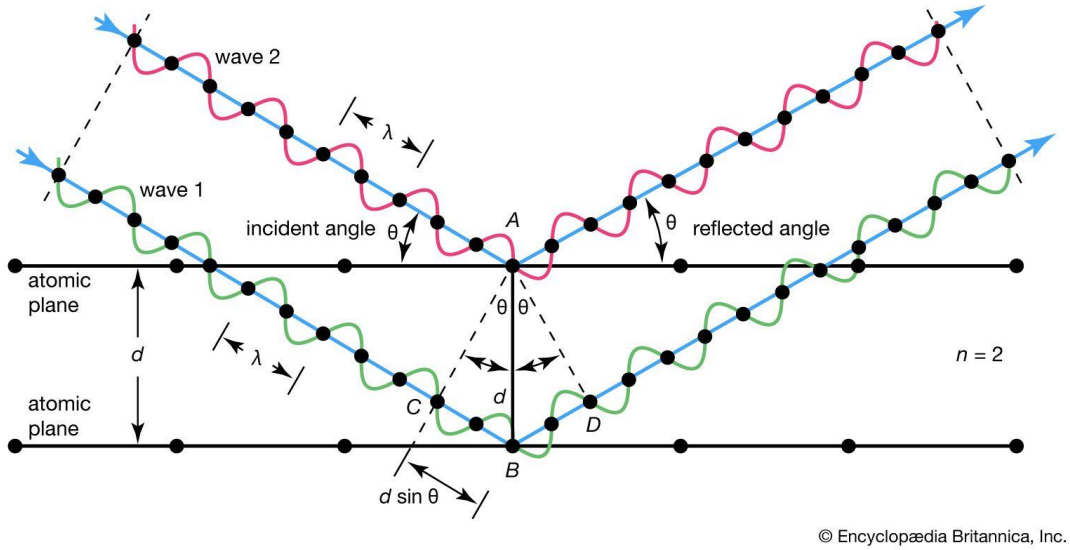

Figure 2.4.2. - Bragg's law condition satisfied in a family of crystalline planes separated by an inter-atomic distance d.

When the Bragg condition is satisfied, scattered waves from successive lattice planes interfere constructively, producing a diffraction peak at a characteristic angle 2θ.

For thin films, diffraction peak positions provide information on lattice parameters and possible strain, while peak intensities and widths reflect the degree of crystallinity and coherent domain size. Amorphous films only produce broad background features rather than sharp diffraction peaks. In a conventional θ-2θ geometry, the incident angle θ and the detector angle 2θ are coupled. As the sample rotates by θ, the detector simultaneously moves by 2θ.

In thin films, this geometry is particularly useful for detecting crystallization because newly formed crystallites tend to align with respect to the substrate.

In this work, PXRD measurements were performed before and after annealing to investigate structural evolution of the deposited films. Changes in the diffraction peak intensity, position, and

width were used to assess the onset of crystallization and phase formation under different thermal and humidity conditions.

A typical PXRD pattern obtained from a thin film sample is shown in 2.4.3. In a θ-2θ scan the measured diffraction intensity is plotted as a function of the scattering angle 2θ. Crystalline materials produce sharp diffraction peaks that satisfy Bragg's law, while amorphous materials produce only broad diffuse features.

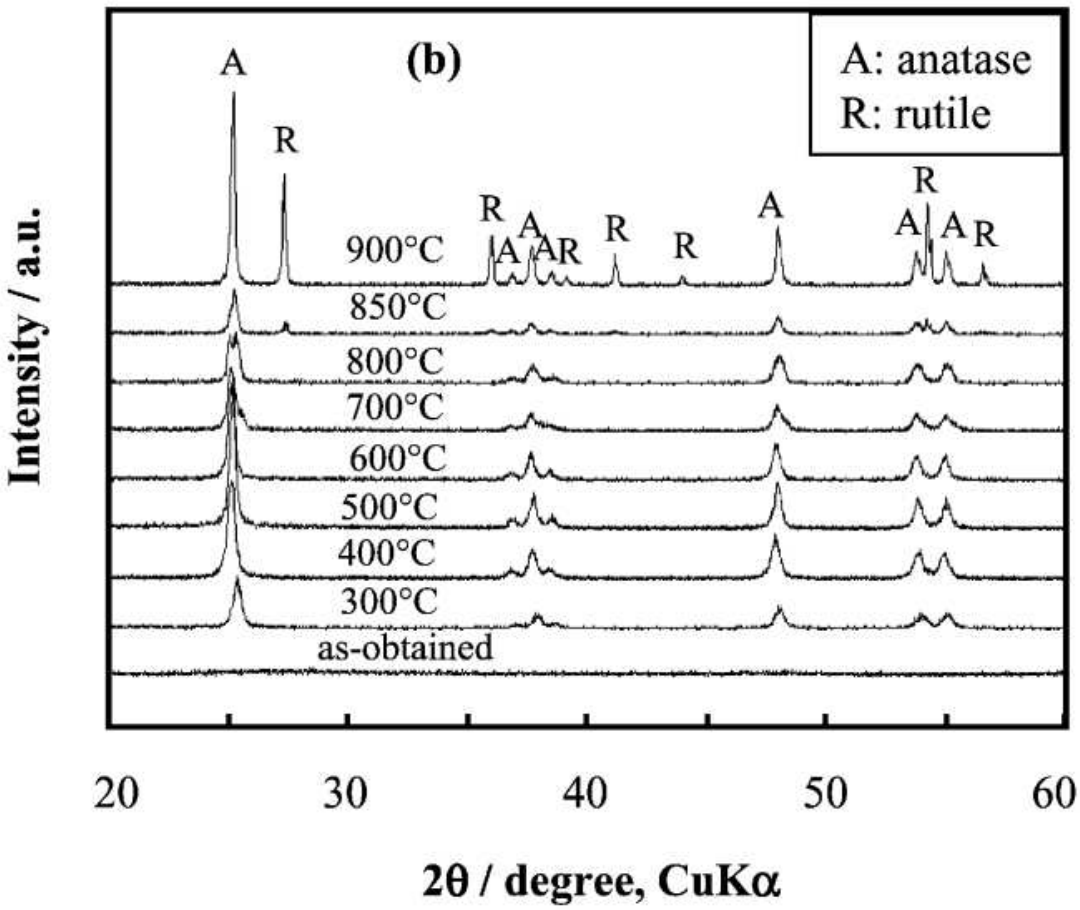

Figure 2.4.3. - XRD profiles of the thin film are annealed at different temperatures from which the onset of crystallization can be determined [44].

Although grazing incidence X-ray diffraction (GI-XRD) is preferred for thin-film analysis due to its enhanced surface sensitivity, the GI-XRD configuration was not available during the period of this study.

In GI-XRD, the incident angle is fixed at small value (<1°), which reduces X-ray penetration depth and increases sensitivity to the thin film layer. However, for the film thickness investigated in this work, the θ-2θ PXRD configuration provided sufficient sensitivity to detect crystallization onset and phase evolution after annealing.

2.5 Fourier transform infrared (FT-IR) spectroscopy

Fourier transform infrared (FT-IR) spectroscopy measurements were performed using the Nicolet iS-50 FT-IR spectrometer, manufactured by Thermo Fisher Scientific, and equipped with a single-pass attenuated total reflection (ATR).

FT-IR spectroscopy is based on the interaction of infrared radiation with matter, where absorption occurs when the frequency of the incident radiation matches the vibrational modes of the bonds. FTIR is sensitive to short-range order and is therefore well suited for detecting molecular species such as hydroxyl groups and adsorbed or incorporated water [45,46].

The Nicolet iS-50 employs a Michelson interferometer to generate an interferogram containing information from all infrared frequencies simultaneously. A Fourier transform is applied to convert the interferogram into an intensity-versus-wavenumber spectrum. This approach provides high spectral resolution, excellent signal-to-noise ratio, and reproducible spectral calibration.

Figure 2.5.1. - Nicolet iS-50 FT-IR spectrometer.

In this work, FT-IR measurements were carried out using single-pass ATR geometry. In ATR, the infrared beam is directed into a high-refractive-index crystal and undergoes total internal reflection at the crystal to sample interface. An evanescent electromagnetic field penetrates a short distance into the sample, typically of the order of hundreds of nanometers to a few micrometers, depending on wavelength, angle of incidence, and refractive indices.

Absorption of the evanescent field by the sample results in attenuation of specific infrared frequencies corresponding to vibrational modes of the material. Because the penetration depth is limited, ATR-FTIR provides surface and near surface information, making it well suited for probing thin films without requiring substrate subtraction or transmission through the sample.

The penetration depth d_p of the evanescent wave is defined as the distance at which the electric field amplitude decreases to $1/e$ of its value at the interface and is given by

$$d_p = \frac{\lambda}{2\pi n_1 \sqrt{\sin^2\theta - \left(\frac{n_2}{n_1}\right)^2}} \qquad (2)$$

Where λ is the wavelength of the infrared radiation, n_1 is the refractive index of the ATR crystal, n_2 is the refractive index of the sample, and θ is the angle of incidence at the crystal-sample interface.

FTIR spectroscopy was employed to investigate changes in chemical bonding and water content in the films deposited before and after annealing under ambient and high-humidity conditions. Absorption bands associated with O-H stretching were analyzed to assess water incorporation and bonding configuration.

A FTIR spectrum of the deposited oxide films is shown in Figure 2.5.2.

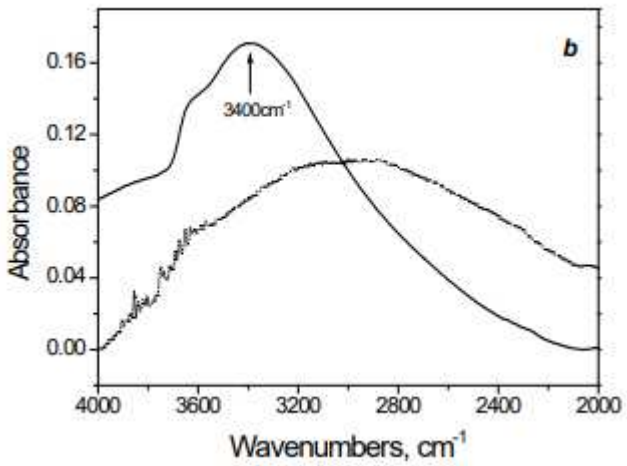

Figure 2.5.2. - The FTIR spectra of electron beam evaporated *a*-SiO_2 (solid line) and thermally grown dioxide (dotted line) in the range O-H vibrations [47].

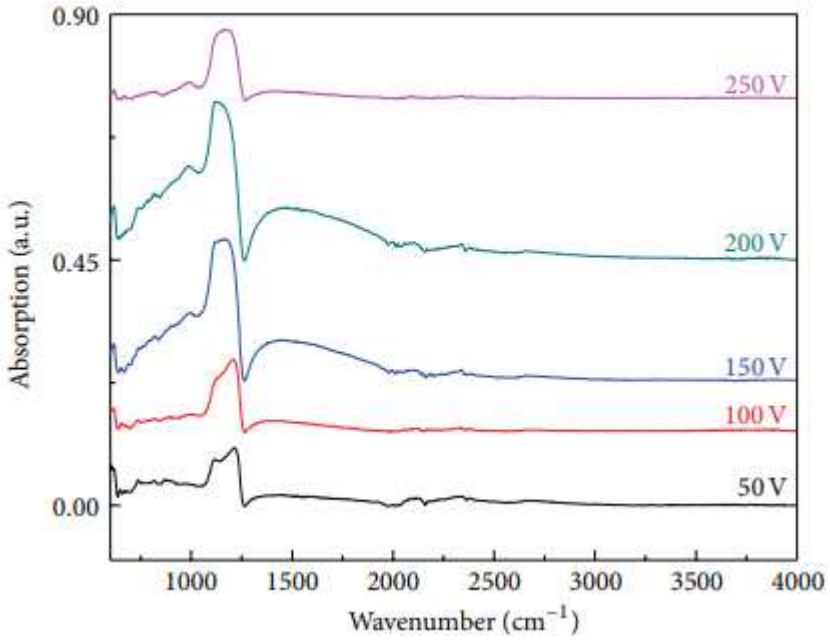

Figure 2.5.3. - ATR-FTIR spectra of anodic SiO_2 thin films, illustrating typical vibrational regions of oxide films, including water-related bands H-O-H [48].

The characteristic FTIR spectral regions related to water incorporation in oxide thin films are illustrated in Figures 2.5.2 and 2.5.3. In oxide materials, the presence of hydroxyl groups and molecular water identified by two main absorption features O-H (3000-3700 cm^{-1} originates from hydroxyl groups and hydrogen-bonded water) and H-O-H (~1630 cm^{-1} associated with molecular water present in oxide films or adsorbed on oxide surfaces).

Changes in the intensity or shape of these absorption bands after annealing were used to evaluate the effect of thermal treatment and humidity on the bonding environment in the deposited coatings.

2.6 Nomarski Microscopy

The surface morphology of the deposited films was examined using Nomarski microscope. This technique is an optical imaging method designed to enhance contrast in transparent or weakly

reflecting samples by converting small variations in surface height and refractive index into intensity differences [49,50].

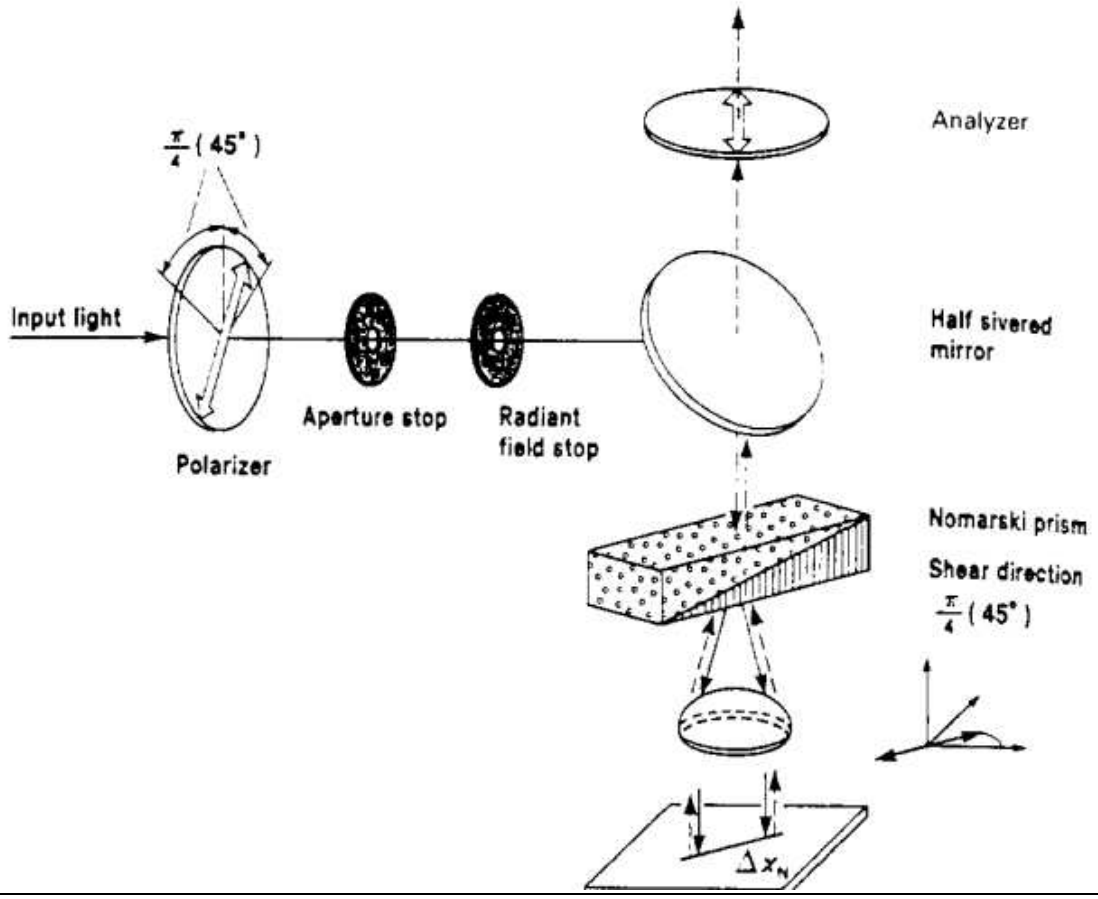

Figure 2.6.1. - Nomarski microscope system [51].

Nomarski microscopy operates by splitting a linearly polarized light beam into two laterally displaced, mutually coherent beams using Nomarski prism. These two beams traverse closely spaced regions of the sample surface and accumulate different optical path lengths depending on local height variations or refractive index gradients. After reflection from the sample, the beams are recombined, producing constructive or destructive interference that results in contrast proportional to the local gradient of the optical path difference.

As a result, Nomarski microscopy is particularly sensitive to surface topography changes, such as roughness variations, cracks, blisters, and delamination. For example, Figure 2.6.2. shows the Nomarski microscopy of grown SiC thin film from Astuti et. al. [52].

In this work, Nomarski microscopy was used as a qualitative, non-destructive method to visually assess surface changes in the films before and after annealing. Particular attention was paid to the appearance of annealing induced defects, surface roughening, and macroscopic structural inhomogeneities. Comparison of images acquired under identical imaging conditions allowed identification of surface modifications associated with thermal treatment and exposure to different humidity environments.

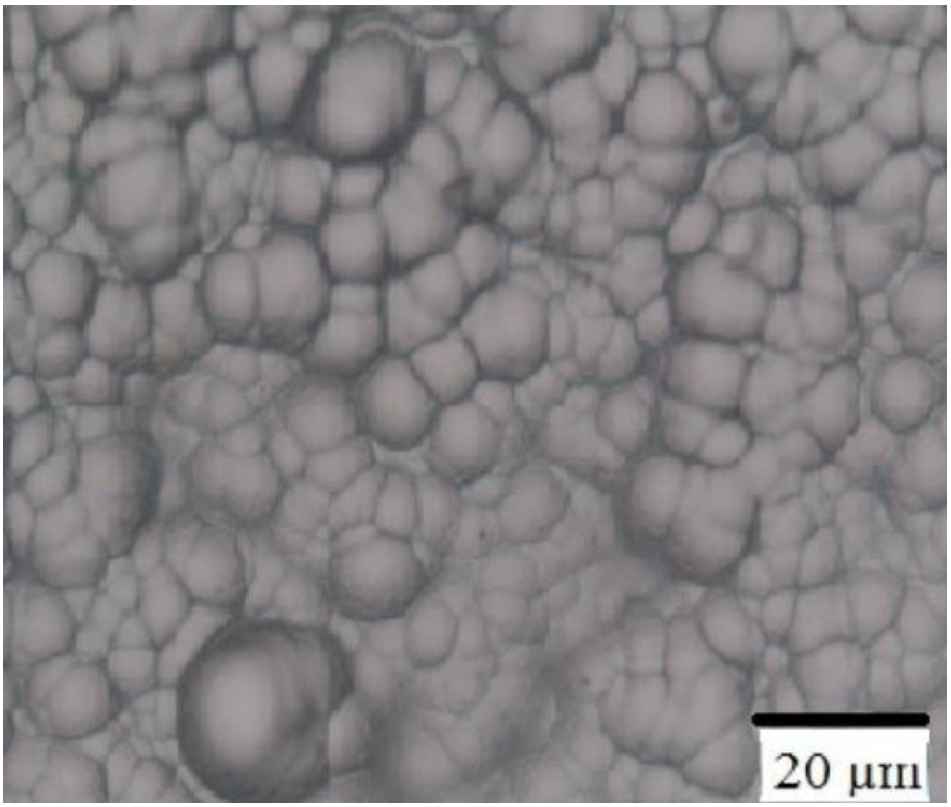

Figure 2.6.2. - Nomarski photo of grown SiC thin film on graphene/SiO2/Si substrate [52].

CHAPTER 3 RESULTS

3.1. Motivation: Mechanical Loss and Structural Order in *a*-GeO_2-Based Thin Films

The reduction of mechanical loss in amorphous oxide thin films has critical importance for optical coatings for gravitational wave interferometers as the thermal noise in the coatings limit the detector's sensitivity. According to the fluctuation-dissipation theorem, the mechanical loss angle Q^{-1} directly governs thermally driven displacement fluctuations in dielectric mirror coatings. From abovementioned, identification of amorphous materials with low internal friction while maintaining favorable optical properties remains a central objective in the research for coatings for gravitational wave detectors.

Among the family of amorphous oxides, *a*-SiO_2 has the lowest mechanical loss. *a*-SiO_2 is a glass former, consisting of tetrahedrally coordinated Si-O bonds. Experiments by Yang et al. [18] demonstrated that ion-beam sputtered *a*-GeO_2 can also achieve remarkably low room-temperature mechanical loss. Similarly to *a*-SiO_2, this material is also a glass former, in which the cation is tetrahedrally coordinated to the O atoms. In Yang's study, *a*-GeO_2 films deposited at elevated substrate temperatures near $0.83T_g$ exhibited enhanced medium-range structural organization, characterized by a large population of six-membered *a*-GeO_4 rings. From the Raman spectroscopy signal corresponding to six-member rings A_6 band (~430 cm^{-1}), it was shown that depositing the thin films at a substrate temperature $T_{sub}=0.8T_g$, (T_g:glass transition temperature) and with post-deposition thermal annealing the population of six member rings increased.

This structural reorganization was directly correlated with mechanical loss reduction. Films deposited at room temperature exhibited $Q^{-1} \approx 3 \times 10^{-4}$, whereas films deposited near $0.83\ T_g$ showed a reduction of approximately 44%.

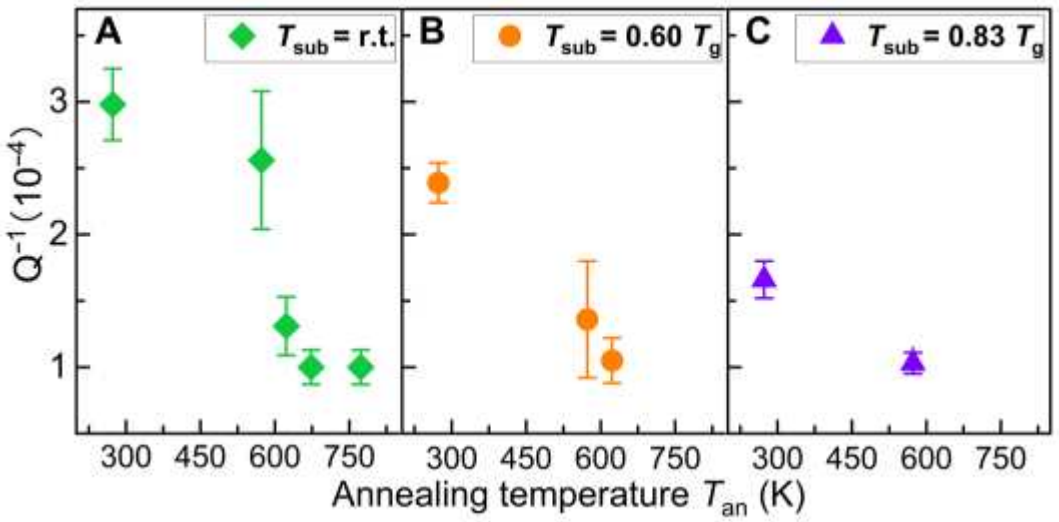

Figure 3.1.1 - Room temperature internal friction Q^{-1} of *a*-GeO_2 thin films deposited at different temperatures. (A) T_{sub} = room temperature (green), (B) T_{sub} = 0.60 T_g (orange), and (C) T_{sub} = 0.83 T_g (purple). The T_{an} to reach the lowest room temperature internal friction is T_{an} = 673 K, T_{an} = 623 K, and T_{an} = 573 K for samples deposited at T_{sub} = room temperature (green), T_{sub} = 0.60 T_g (orange), and T_{sub} = 0.83 T_g (purple), respectively [18].

After optimized annealing, all *a*-GeO_2 films converged toward a minimum loss level near 1×10^{-4}, although the annealing temperature required to reach this value depended strongly on the initial deposition temperature. Films deposited at elevated T_{sub} required lower annealing temperatures to achieve minimum mechanical loss, demonstrating increased efficiency of structural relaxation during growth.

This research established a direct relationship between structural ordering at medium range (~2nm) and elastic energy dissipation or mechanical loss. In *a*-GeO_2 the larger population of six member rings formed by Ge-O corner-shared links in the as deposited thin film coupled with the structural relaxation that occurs with annealing that further increases the population of large (>4) rings is central to achieving such low values of mechanical loss [57].

Building upon this understanding, a novel alloy of *a-44%* TiO_2-doped GeO_2 alloys was demonstrated by the CSU group [23]. For a composition of *a*-44% TiO_2:GeO_2, and an optimized annealing at 600 °C for 100 hours yielded a thin film with a mechanical loss of

$$Q^{-1} = 0.98 \times 10^{-4}.$$

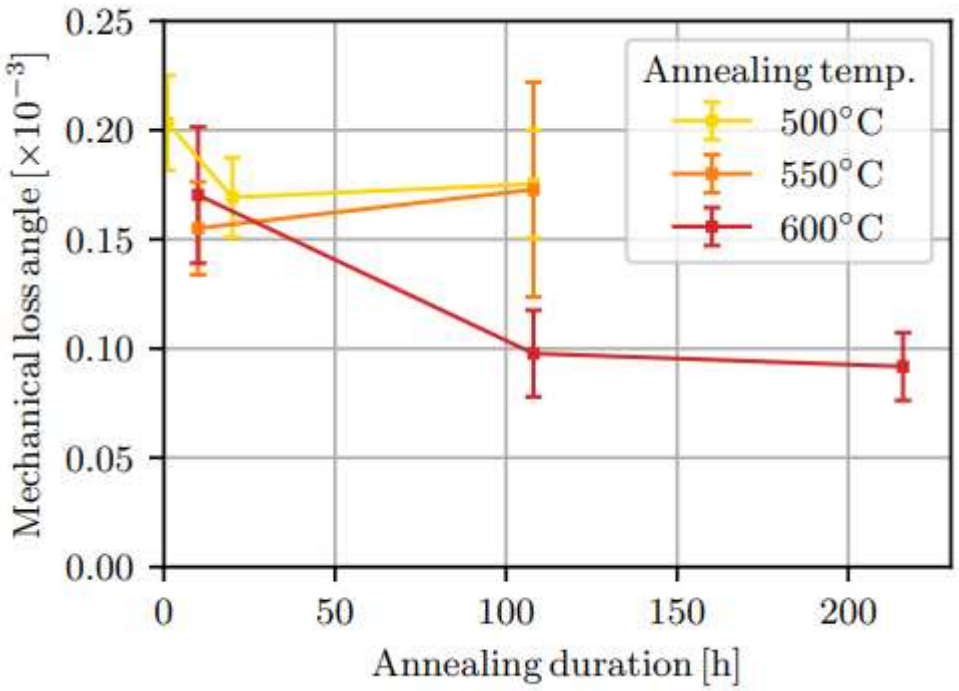

Figure 3.1.2. - Effect of the annealing duration on the measured loss angle for the 44% TiO_2:GeO_2 film [23].

The lowest value demonstrated to date in a high index amorphous oxide material (Figure 3.1.2.). As shown in Table 3.1. and Fig. 3.1.3., the refractive index and absorption loss at 1064 nm wavelength are modified with the content of TiO_2 into GeO_2. Experiments showed that the optimum concentration of TiO_2 was 44%. This alloy with a refractive index of 1.89 combines low mechanical loss with an absorption loss of 2.3 ppm at 1064 nm (for a layer ~130 nm thick). Further calculations showed, this material, when incorporated into the design of high reflectivity

mirrors with the same design of coatings in the advanced LIGO (aLIGO) detector, could reach a 2x reduction in coating thermal noise [23].

Table 3.1.1. - Absorption at 1 µm measured at quarter-wave layer thickness (QWL) for *a*-44%Ti-doped GeO_2 coatings with different Ti/(Ti+Ge) ratios.

Ti/(Ti+Ge)	abs. at 1 µm (QWL)
0	< 1 ppm
27	1.5
44	2.3

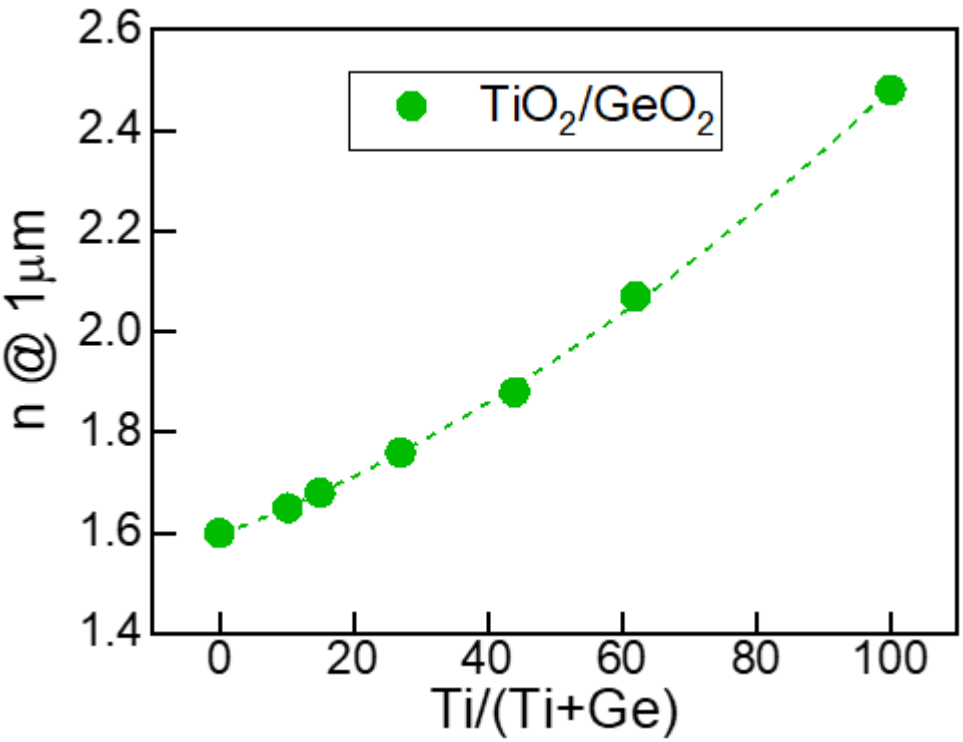

Figure 3.1.3. - Refractive index at 1 µm as a function of Ti concentration expressed as Ti/(Ti+Ge) for *a*-44%Ti-doped GeO_2 coatings [24].

High-reflectivity coatings based on *a*-44%Ti-doped GeO_2 have been demonstrated by A. Davenport et al. [24]. These coatings exhibit outstanding optical quality in the as-deposited state,

as shown in Figure 3.1.4. However, when annealed at 600 °C for extended periods the coatings were observed to develop bubble defects, which are interpreted as a sign of compressive failure in the multilayer structure. An example of this behavior is shown in Figure 3.1.4. presented below.

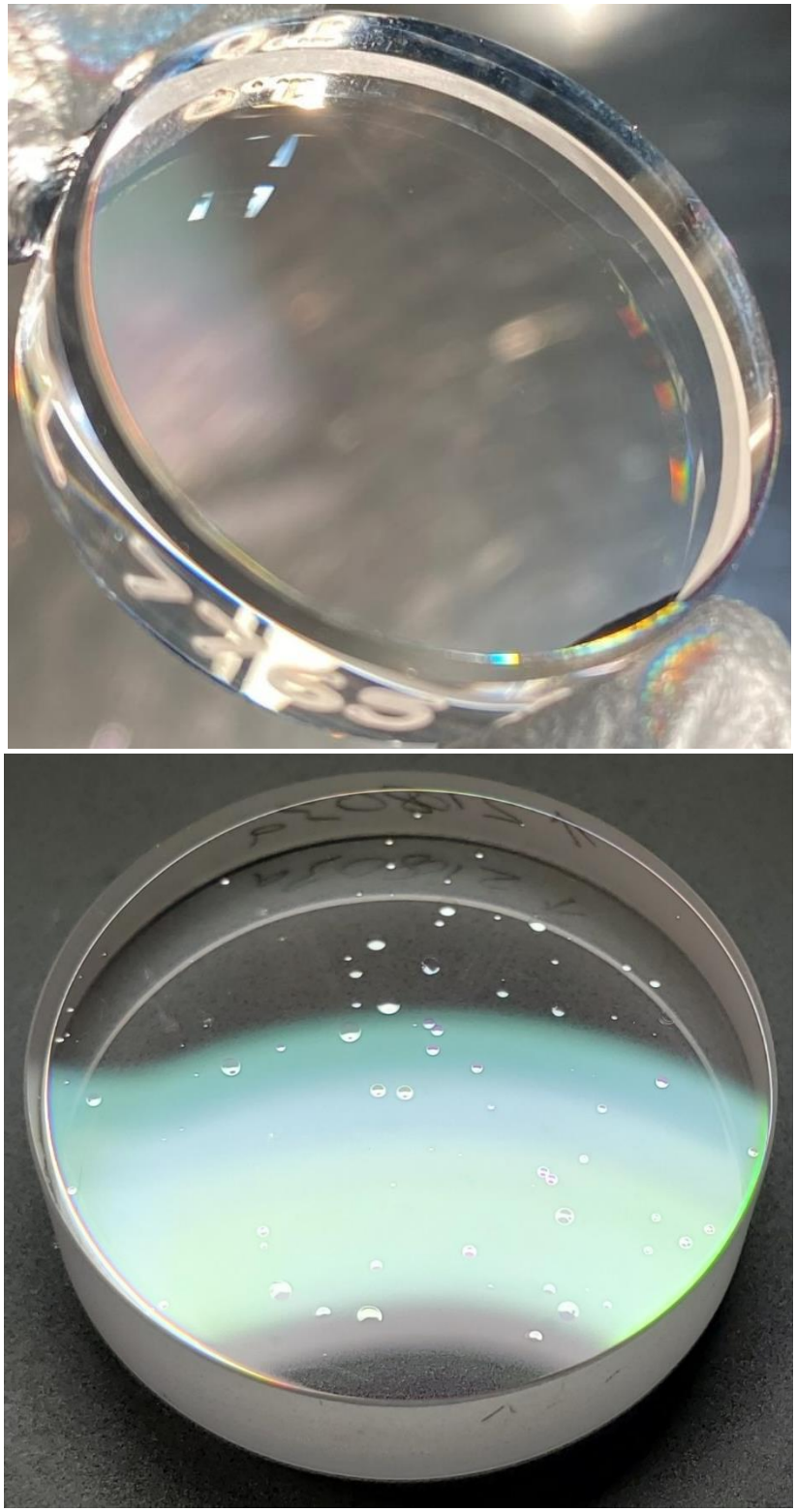

Figure 3.1.4. - Pictures of TiO_2:GeO_2 high-reflectivity (HR) coatings before and after thermal annealing at 600 °C for 10 hours. The annealed sample shows visible surface changes.

In a study conducted by A. Davenport, it was shown that the base pressure of the deposition chamber prior to the growth of the high-reflectivity (HR) coating plays a critical role in the formation of bubbles during annealing [24]. A. Davenport demonstrated that when the chamber base pressure was below 1.5×10^{-7}Torr, the corresponding water partial pressure was reduced to approximately 0.75×10^{-7}Torr.

Furthermore, during the deposition of the HR coating at a substrate temperature of 200 °C, the water partial pressure remained low, with measured values of 6×10^{-5}Torr during deposition of the *a*-44%Ti-doped GeO_2 and 4×10^{-6}Torr during deposition of the SiO_2 layers. HR coatings deposited at these conditions did not show the bubble formation, even after annealing at 600 °C for 100 hours at humidity conditions found in the laboratory at CSU. These results suggest that H_2O or O-H incorporation during deposition or annealing plays an important role in the structural stability of these coatings.

Understanding and quantifying the variations in H_2O and O-H contents with annealing in *a*-GeO_2 and amorphous *a*-44%Ti-doped GeO_2 thin film coating materials motivates the proposed work. Experiments were conducted to investigate the influence of the annealing atmosphere on the structural and optical properties of *a*-GeO_2 and amorphous *a*-44%Ti-doped GeO_2 thin films, as well as multilayer coatings *a*-44%Ti-doped GeO_2 sandwiched with *a*-SiO_2 and *a*-Al_2O_3 layers.

In the following sections, results are presented for the investigation of the crystallization behavior of *a*-GeO_2 and *a*-44%Ti-doped GeO_2 films after they were annealed under two different humidity conditions: standard laboratory conditions in Fort Collins, CO, and relative humidity that was increased to approximately 94%.

Since *a*-GeO_2 is hygroscopic, exposure to high humidity during annealing may lead water to incorporate into the coating structure. The presence of water in *a*-GeO_2 materials can modify the bonding network and promote structural rearrangement, potentially decreasing the crystallization temperature of the film.

This was observed in sol-gel a-GeO_2 thin films [16]. The incorporation of TiO_2 into the *a*-44%Ti-doped GeO_2 modifies the atomic network structure, therefore, it is not known whether or not, H_2O or OH could be incorporated into the films during the annealing process.

To investigate the incorporation of water and possible modifications to the amorphous network, Fourier Transform Infrared (FTIR) spectroscopy was performed on the films before and after both annealing conditions: ambient and high humidity. Particular attention was paid to the spectral regions associated with hydroxyl groups and molecular water.

The FTIR spectra of the amorphous films showed the presence of a broad absorption band in the region between approximately 3200-3600 cm^{-1}, which corresponds to O-H stretching vibrations. This band is characteristic of hydroxyl groups incorporated into oxide networks or of absorbed water within the film. A weaker absorption peak observed near ~1630 cm^{-1}, which corresponds to the H-O-H bending mode of molecular water [58] was also monitored. The presence and relative intensity of these bands provide information about water incorporation in the films during the annealing.

The comparison between spectra obtained after ambient annealing and humid annealing therefore provides insight into how humidity affects the incorporation of hydroxyl species and molecular water in the films.

Results are also on optical microscopy observations performed to examine possible surface modifications of the coatings after annealing, including the formation of defects such as bubbles or surface roughness changes.

3.2. Crystallization vs water content during annealing - *a*-GeO_2

The crystallization behavior of the deposited a-GeO_2 films during annealing was investigated using powder X-ray diffraction (PXRD), described in Chapter 2. The measurements were performed using Cu Kα radiation (λ = 1.5406 Å). The phase identification of the diffraction peaks was performed using DIFFRAC.EVA software and comparison with reference diffraction patterns from the ICDD Powder Diffraction File (PDF) database [59]. To interpret the diffraction patterns of the coated samples, the diffraction signal of the fused silica (SiO_2) substrate was measured separately.

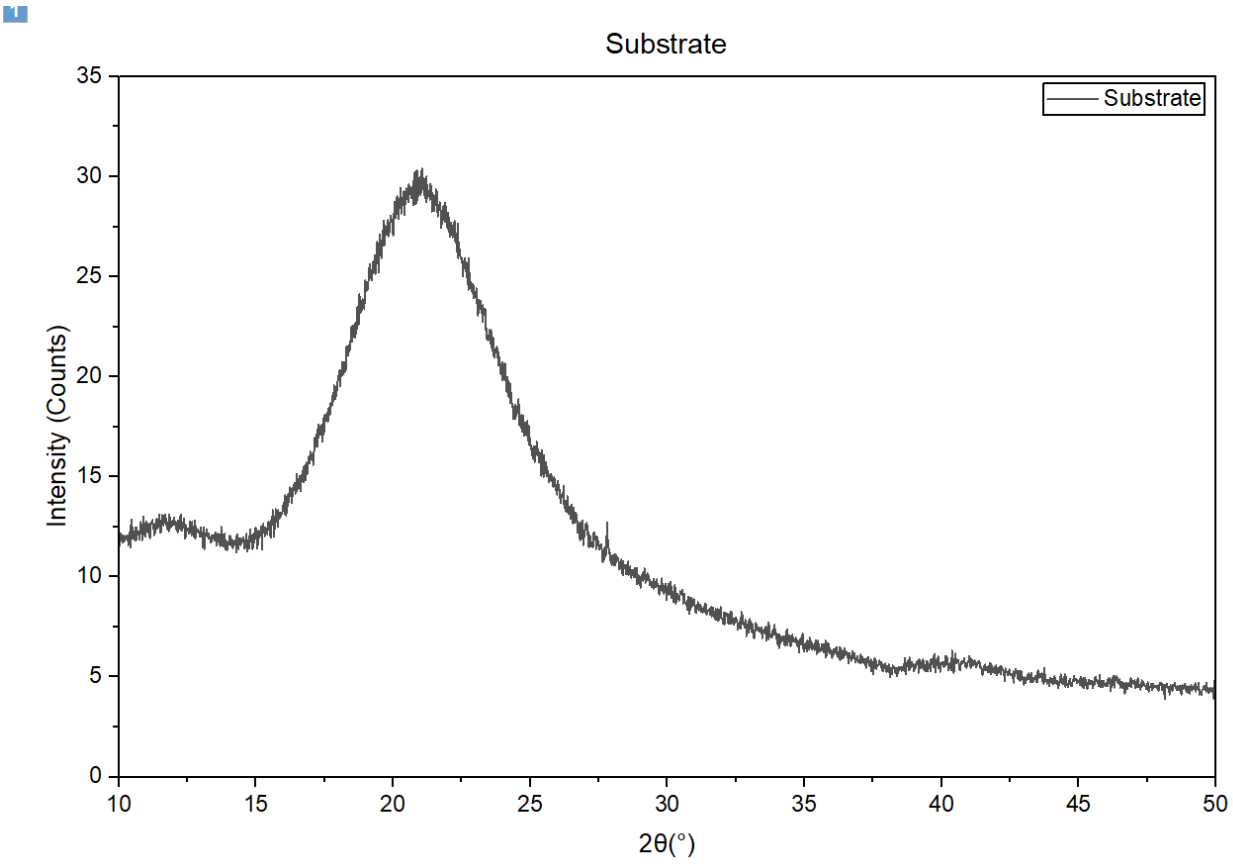

Figure 3.2.1. - PXRD spectrum of the fused silica substrate.

The PXRD spectrum of the substrate shows a broad diffuse halo centered near ~21-22° (2θ), which is characteristic of amorphous *a*-SiO_2 (Figure 3.2.1.). No sharp diffraction peaks are present, confirming that the substrate does not contain crystalline phases. Because the deposited *a*-GeO_2 films are relatively thin (~500 nm), the diffraction signal from the substrate plays a vital role to the measured diffraction patterns.

The PXRD spectrum of the as-deposited *a*-GeO_2 film is shown on Figure 3.2.2.

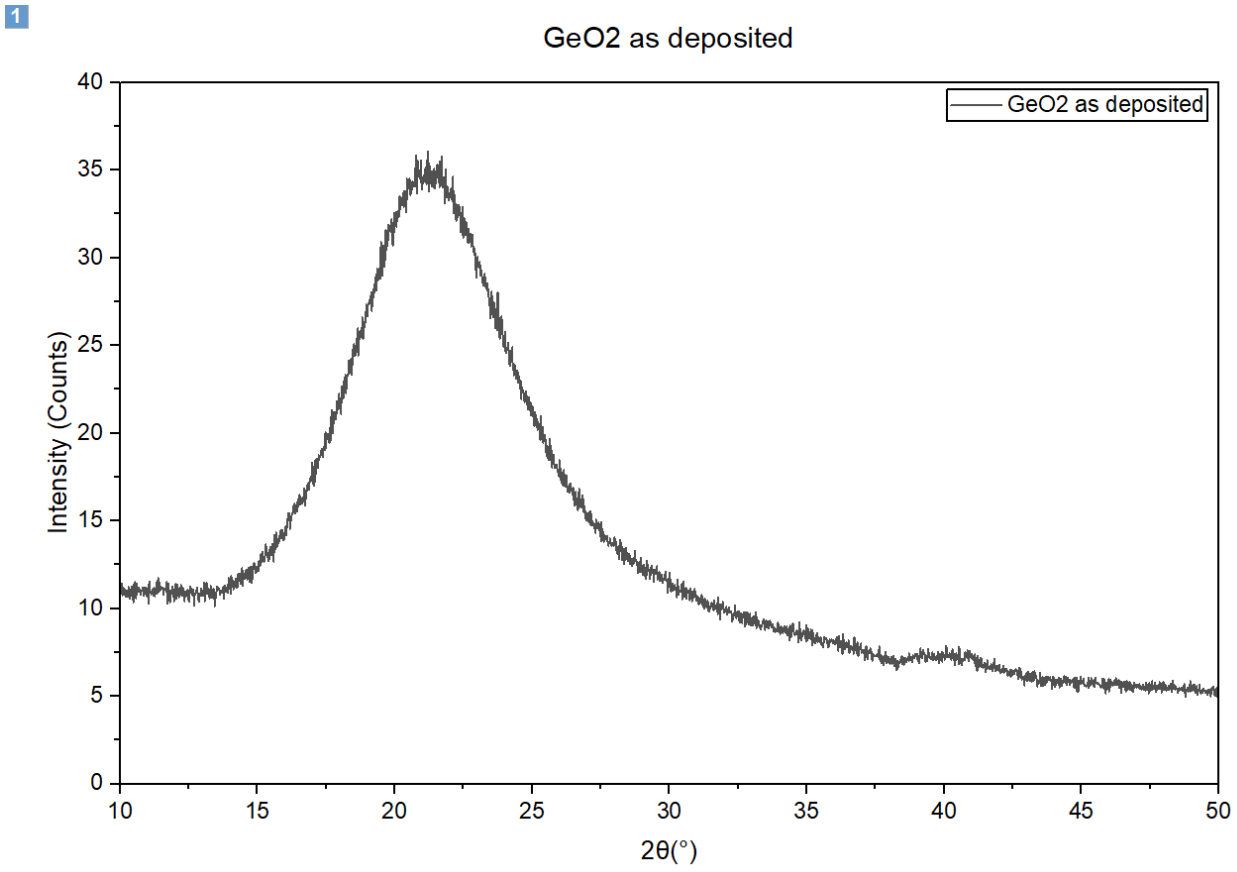

Figure 3.2.2. - PXRD spectrum of as-deposited GeO_2 film.

The diffraction pattern on Figure 3.2.2. shows the same broad halo near ~21° as then substrate spectrum, and no additional sharp diffraction peaks are observed. That indicates that the deposited thin film is amorphous *a*-GeO_2.

After annealing at 600°C for 10 hours at ambient conditions, the diffraction pattern remains mostly unchanged (Figure 3.2.3.).

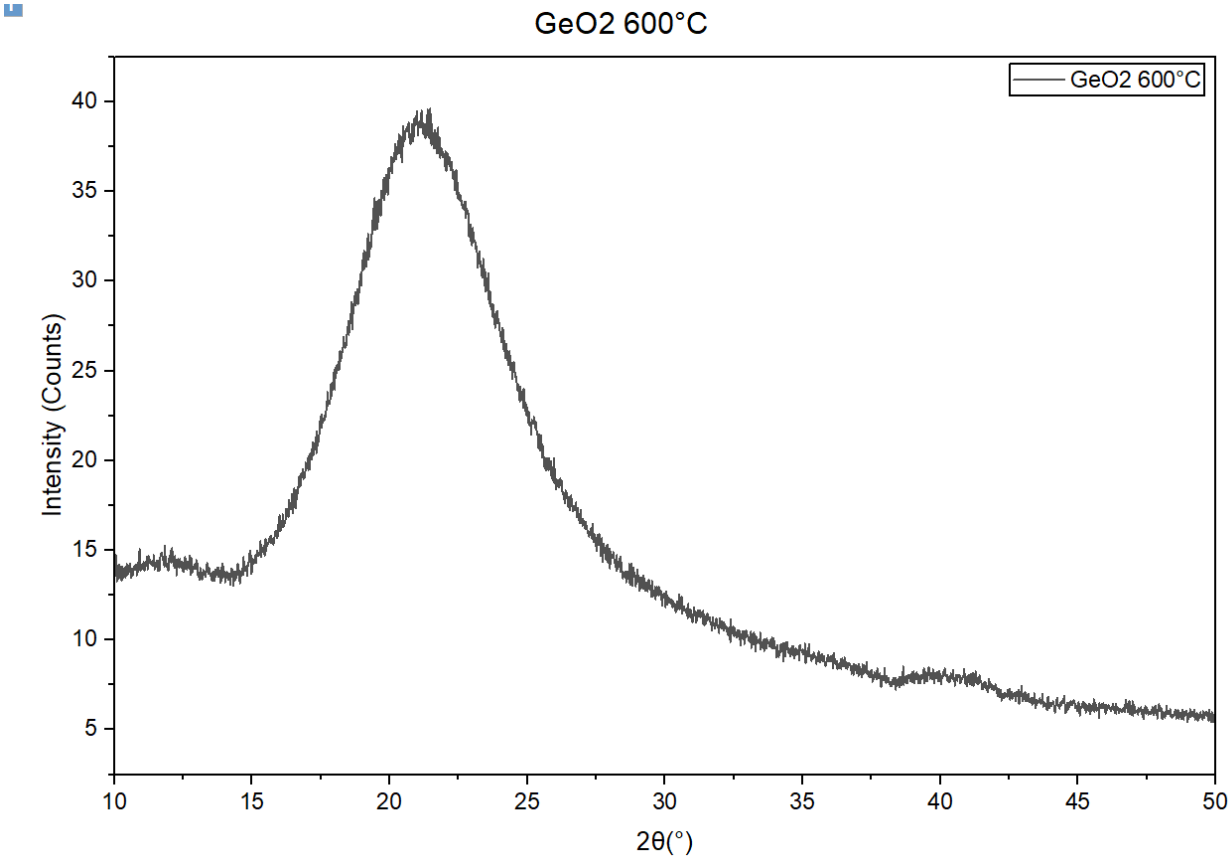

Figure 3.2.3. - PXRD spectrum of *a*-GeO_2 annealed at 600 °C.

The lack of additional diffraction peaks indicates that the film remains amorphous at this temperature. At higher annealing temperatures (750 - 800 °C for 10 h), a weak diffraction feature begins to appear near ~26-27° (2θ). This peak corresponds to the (101) reflection of crystalline α-quartz-type GeO_2, indicating the onset of crystallization in the film (Figure 3.2.4.).

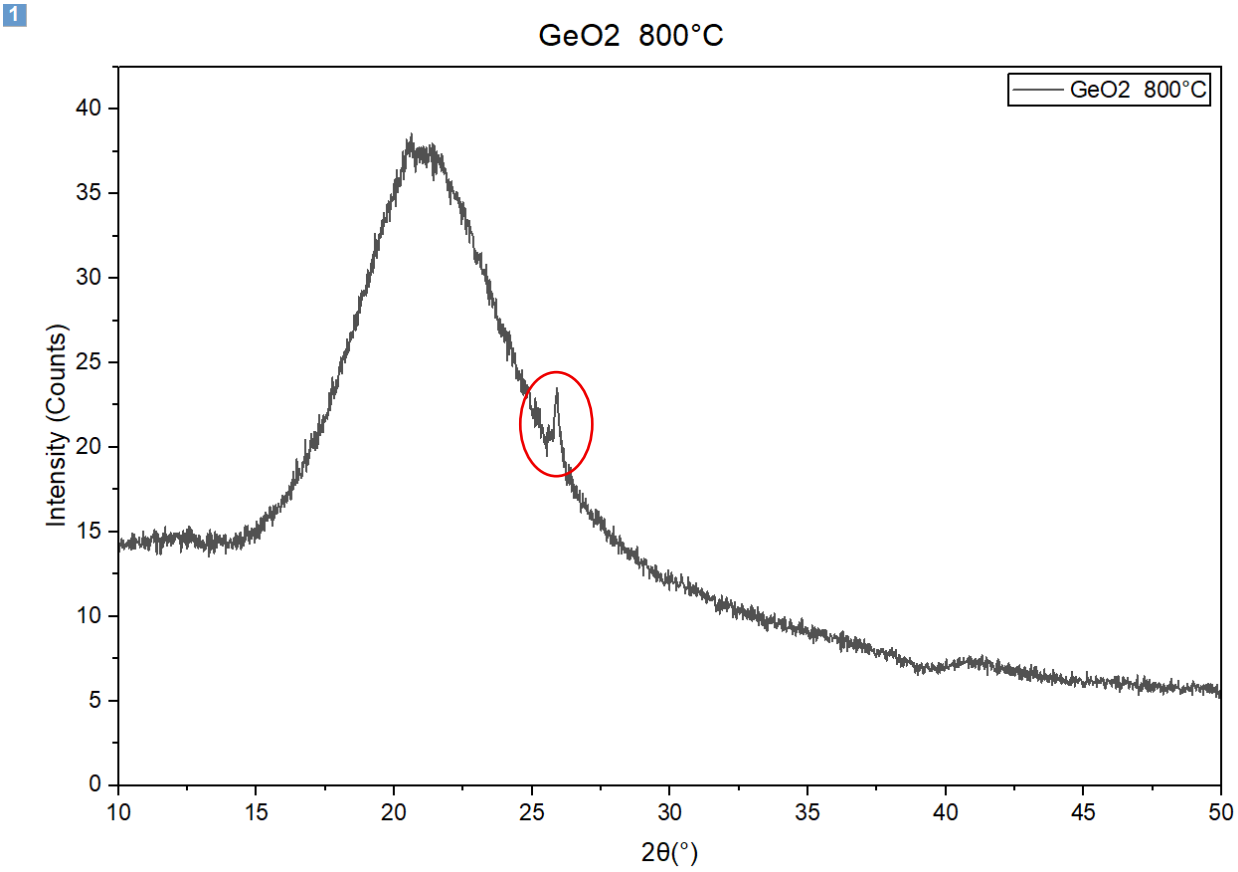

Figure 3.2.4. - PXRD spectrum of *a*-GeO_2 annealed at 800 °C.

To identify the possible formation of crystalline phases during annealing, the expected diffraction peak positions of crystalline *a*-GeO_2 were taken from the ICDD Powder Diffraction File database. The main reflections of *a*-GeO_2 are summarized in Table 3.2.1.

Table 3.2.1. - Main PXRD peaks of crystalline *a*-GeO_2.

Phase	2θ (deg)	Plane (hkl)
a-GeO_2	~21.2	(100)
a-GeO_2	~26.5	(101)
a-GeO_2	~36.3	(110)
a-GeO_2	~39.4	(102)

These results indicate that *a*-GeO_2 films remain amorphous at ambient conditions, while crystallization begins at annealing temperatures > 800 °C.

To investigate the influence of water during the annealing, *a*-GeO_2 films were annealed at 600°C for 10 hours under high humidity conditions (~94% relative humidity).

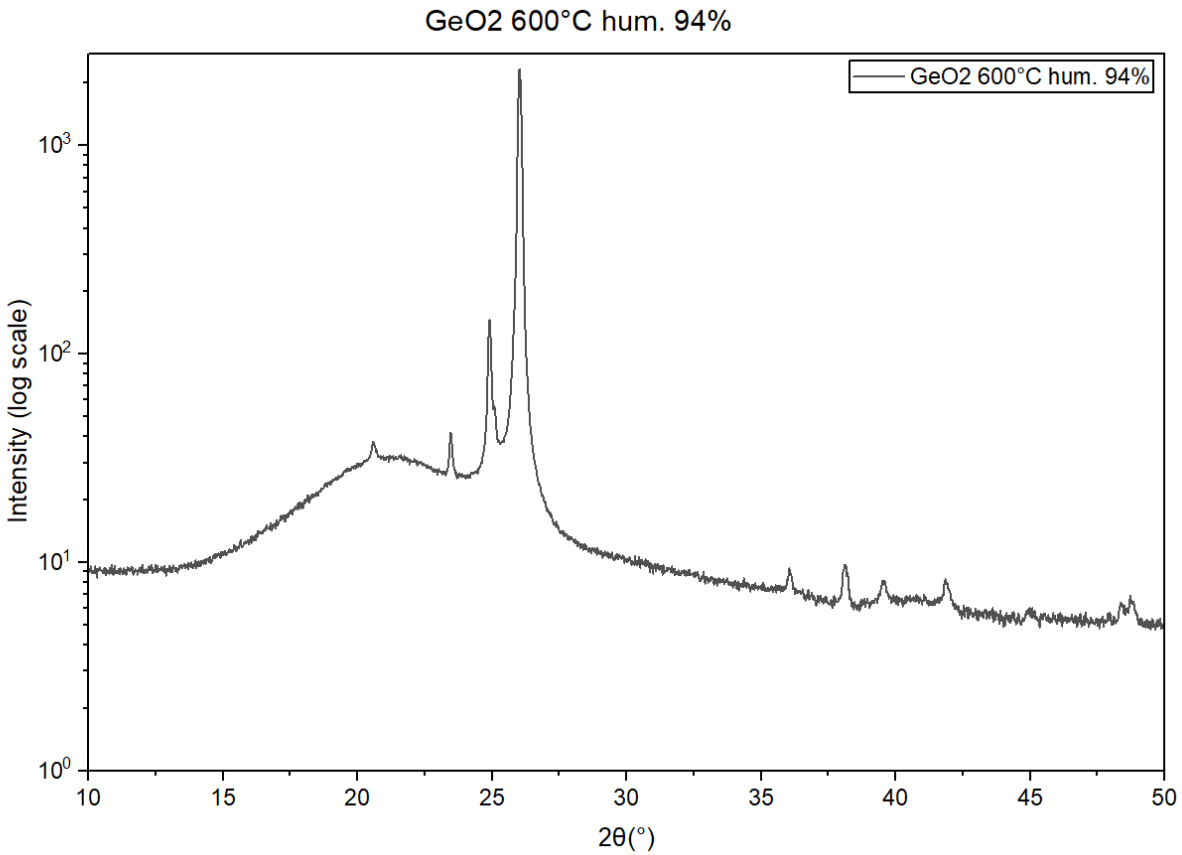

Figure 3.2.5. - PXRD spectrum of *a*-GeO_2 film annealed at 600 °C under high humidity plotted in logarithmic scale.

In this case the a-GeO2 thin film PXRD spectrum showed a sharp diffraction peak appears near $2\theta \approx 26.5°$. This peak corresponds to the (101) reflection of crystalline *a*-GeO_2. The appearance of this reflection shows the formation of crystalline *a*-GeO_2 during annealing under humid conditions. A smaller peak which is located near to the main peak is attributed to instrumental artifacts related to residual Cu Kβ radiation from the X-ray source. This feature does not correspond to any crystalline phase present in the film.

These results show that content of H_2O and O-H in the *a*-GeO_2 films may facilitate the early crystallization of the films, as indicated by the appearance of the α-GeO_2 (101) diffraction peak.

It is important to examine whether the diffraction peaks observed after humid annealing could be from the crystallization of metallic Ge. Crystalline Ge has a diamond cubic structure and exhibits well-known diffraction peaks in X-ray diffraction patterns. The diffraction peaks for crystalline Ge are listed in Table 3.2.2.

Table 3.2.2. - Main PXRD peaks of crystalline Ge.

Crystal plane (hkl)	2θ (°)
Ge (111)	~27.3°
Ge (220)	~45.3°
Ge (311)	~53.7°
Ge (400)	~65.9°

If crystallization of metallic Ge occurred in the films, pronounced diffraction peaks would be expected at approximately 27°, 45°, and 54° in the PXRD patterns.

The PXRD spectrum of the *a*-GeO_2 film annealed at 600 °C under high humidity shows a dominant diffraction peak centered at 2θ = 26.5°. This position does not coincide with the main Ge (111) reflection expected near 27.3°. In addition, no diffraction peaks are observed at the other angular positions of crystalline Ge listed in Table 3.2.2. Because of the very high intensity of the peak near 26°, a weak Ge contribution cannot be completely ruled out from this scan alone. A more precise assessment would necessarily subtract the dominant peak contribution or short-range scans around the expected Ge peak positions.

To investigate the effect of humidity on the surface morphology of the *a*-GeO_2 films during annealing, optical microscopy was used for samples annealed at 600 °C under both ambient and high humidity (~94 % RH) conditions.

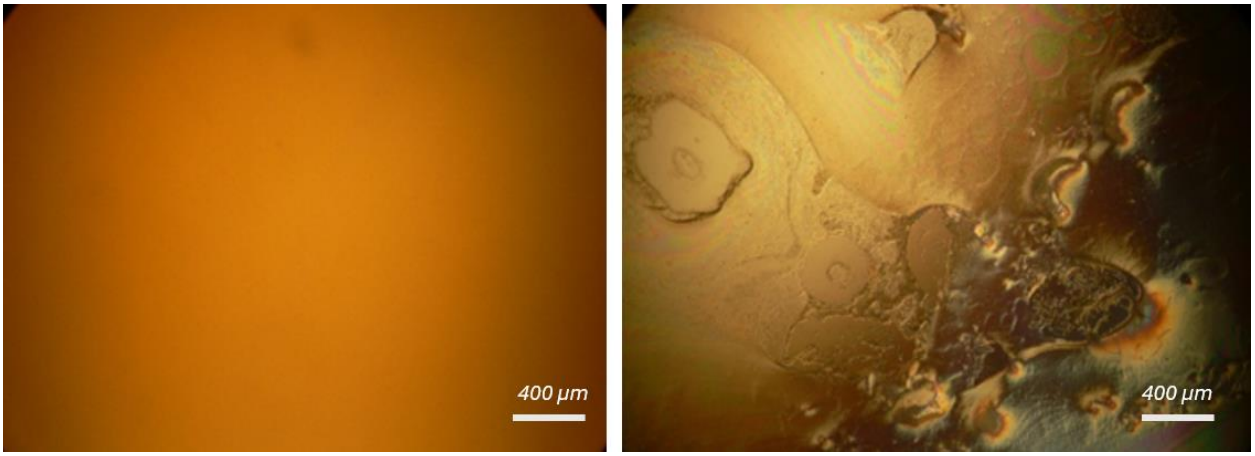

Figure 3.2.6. - Optical microscopy images of *a*-GeO_2 thin films after annealing at 600 °C. (a) *a*-GeO_2 film annealed at 600 °C under ambient conditions. (b) *a*-GeO_2 film annealed at 600 °C under high humidity (~94 % RH).

The optical microscopy images show a difference in surface morphology between the samples annealed under dry and humid conditions. The *a*-GeO_2 film annealed at 600 °C under ambient conditions shows smooth and uniform surface with no visible structural features. This indicates that dry annealing does not change the morphology of the film. But the film annealed at 600 °C under high humidity exhibits circular patterns across the surface. The observed patterns are consistent with nucleation and growth of crystalline regions or localized densification of the oxide network.

An additional experiment was performed where the furnace was preheated to 100 °C prior to the humid annealing process. In this experiment, the *a*-GeO_2 film was placed into the oven that was already reached 100 °C, after that the temperature was increased to 600 °C under high humidity conditions (~94 % RH) for 10 hours.

Optical microscopy images of the film after annealing show the formation of large textured regions and irregular surface features, indicating significant structural modification during the humid annealing process.

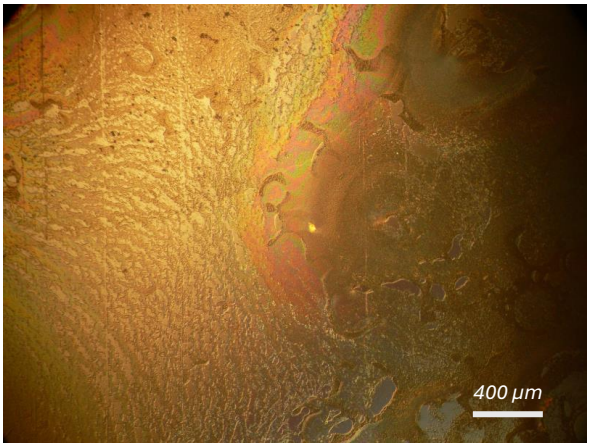

Figure 3.2.7. - Optical microscopy images of *a*-GeO_2 film annealed at 600 °C under high humidity with furnace preheated to 100 °C.

The PXRD spectrum of this sample is shown in Figure 3.2.8. A strong diffraction peak appears near $2\theta \approx 26.5°$, with several weaker reflections at higher diffraction angles.

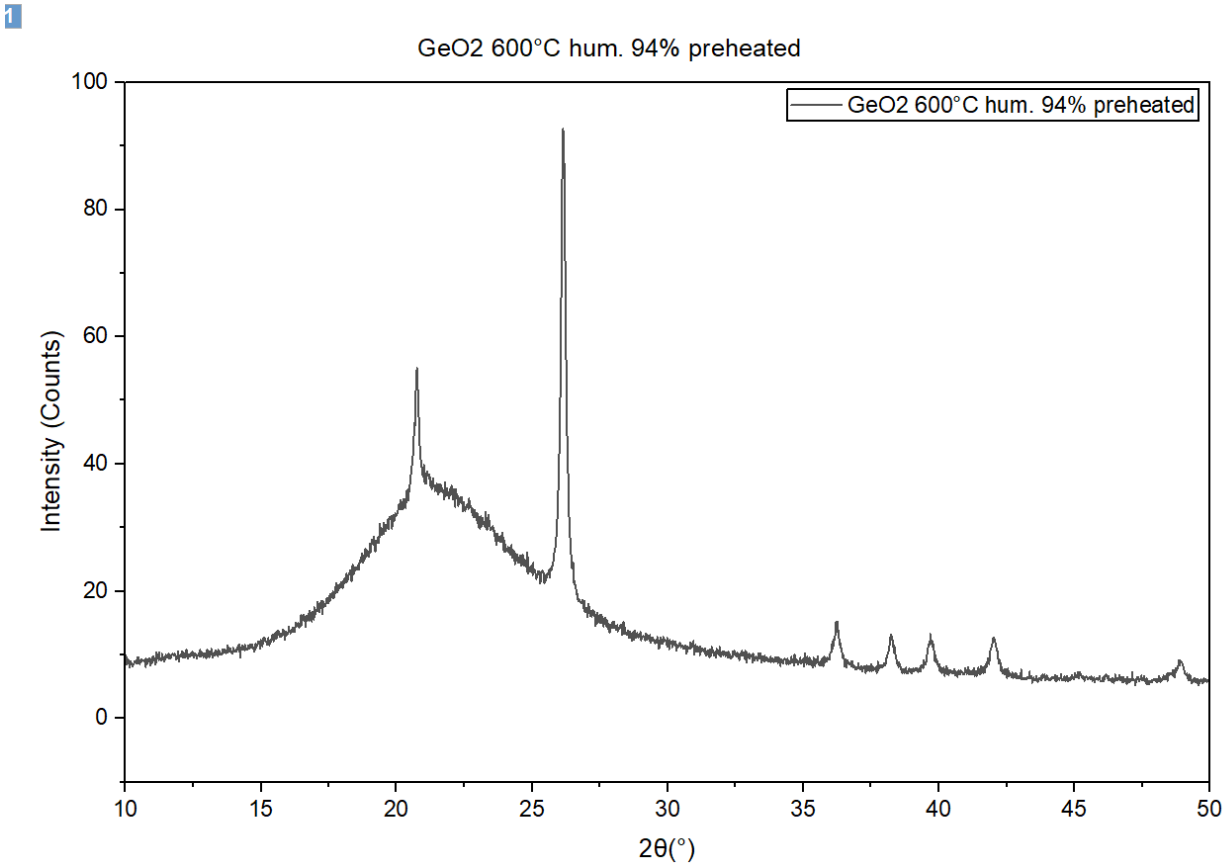

Figure 3.2.8. - PXRD spectrum of *a*-GeO_2 film annealed at 600 °C under high humidity with furnace preheated to 100 °C.

The position of the dominant peak near $2\theta \approx 26.5°$ corresponds to the (101) reflection of crystalline *a*-GeO_2. The broad diffuse background remains visible, which means that the film consists of a mixture of amorphous and partially crystallized regions.

The diffraction pattern does not show the characteristic peaks of crystalline Ge, such as the reflections near $2\theta \approx 27.3°$, 45.3°, and 53.7°. Therefore, the observed crystallization is attributed to the formation of crystalline *a*-GeO_2.

The enhanced crystallization observed in this experiment suggests that the initial thermal conditions prior to annealing influence the interaction between water vapor and the oxide

network. Preheating the furnace may modify the adsorption and diffusion behavior of water molecules within the *a*-GeO_2 film, facilitating the formation of Ge-OH groups.

3.3. Analysis of H2O and O-H penetration in a-GeO_2 by FTIR spectroscopy

To investigate the incorporation of water and hydroxyl groups in the *a*-GeO_2 films, FTIR spectroscopy was performed before and after annealing. The FTIR spectrum exhibits a broad absorption band centered near ~3400 cm^{-1}, which corresponds to O-H stretching vibrations associated with hydroxyl groups incorporated in the oxide network (Figure 3.3.1.).

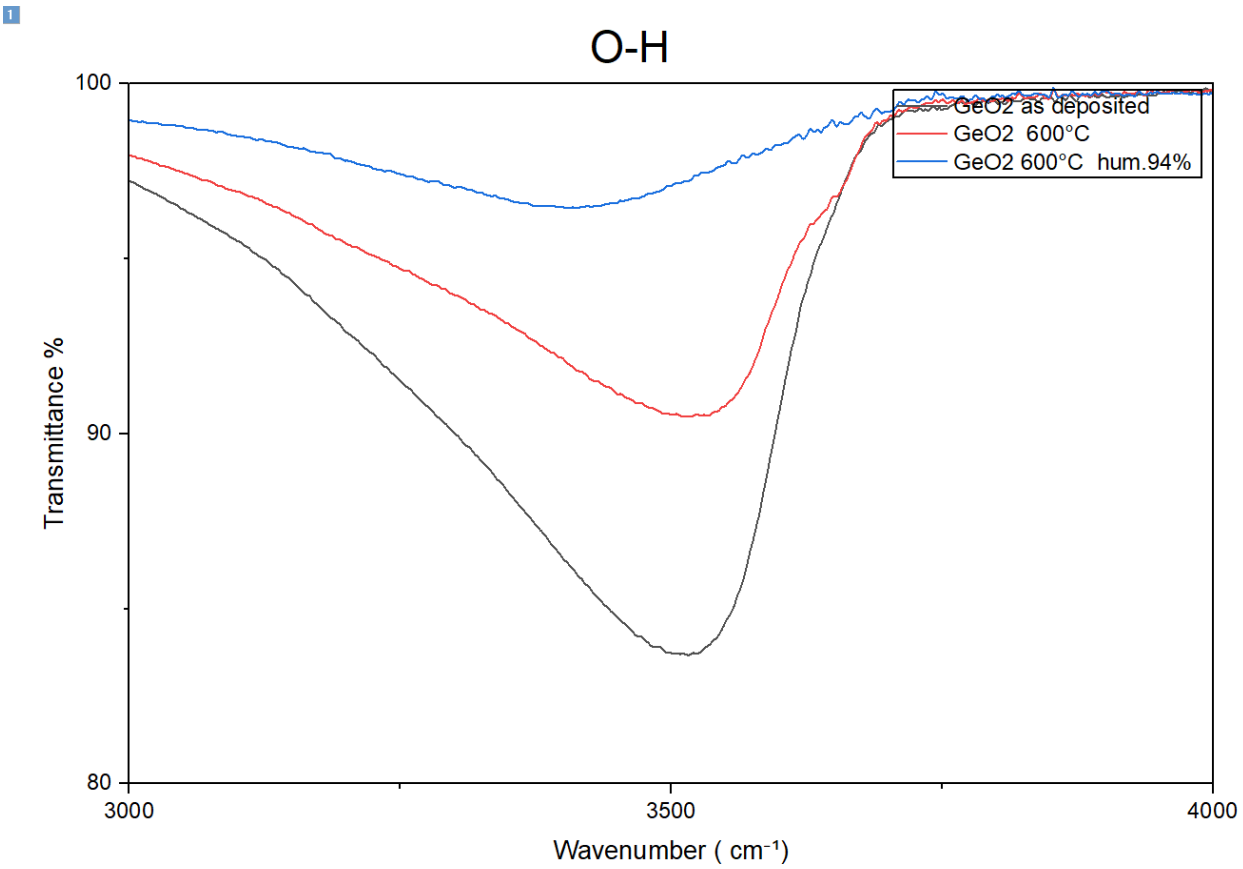

Figure 3.3.1. - FTIR spectra of *a*-GeO_2 films (as-deposited, 600 °C annealed, and 600 °C humid annealed).

The as deposited film shows the strongest O-H absorption band, indicating the presence of hydroxyl groups incorporated into the *a*-GeO_2 network during deposition. After annealing at 600

°C, the intensity of the O-H band decreases significantly, indicating partial removal of hydroxyl species during thermal treatment. The sample annealed at 600 °C under high-humidity conditions (~94 % RH) shows a similar profile with an intensity in the O-H band which is the lowest among the three curves. This suggests that at 600 °C thermal dehydration dominates and the *a*-GeO_2 network becomes progressively more dense during annealing.

The FTIR spectra in the H-O-H bending region (~1630 cm^{-1}) of the as-deposited, and annealed samples show only minor variations between the samples (Figure 3.3.2.).

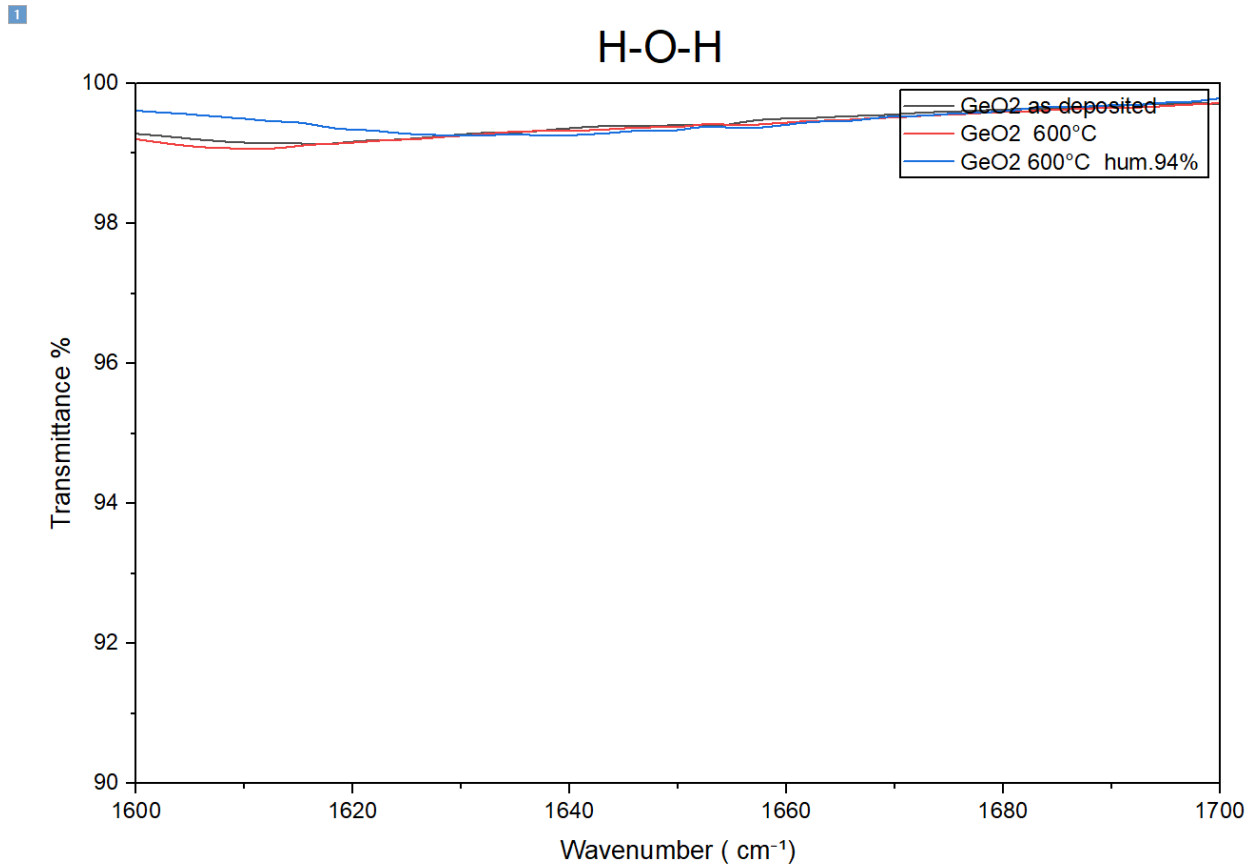

Figure 3.3.2. - FTIR spectra in the H-O-H bending region.

The relatively weak intensity of this band indicates that molecular water is not significantly trapped within the films, and that hydrogen is primarily present in the form of hydroxyl groups bonded to the *a*-GeO_2 network.

The FTIR measurements indicate that the as-deposited films contain hydroxyl groups, which correspond to non-bridging oxygen sites formed through interaction of the oxide network with water.

PXRD measurements show that despite this structural relaxation, the films remain amorphous up to 600 °C, while crystallization begins only at higher temperatures. These observations suggest that dehydration and network densification precede the crystallization process in *a*-GeO_2 thin films.

3.4. Crystallization vs Water Content During Annealing in *a*-44%Ti-doped GeO_2

Pure *a*-GeO_2 thin films are crystallizing relatively easily during the thermal annealing in a high humidity environment, which can lead to increasing optical scattering and degradation of the coating. One strategy for improving the thermal stability of *a*-GeO_2 films is alloying that material with *a*-TiO_2. Previous studies have shown that the incorporation of Ti into an oxide glass network can modify the local structure and suppress crystallization.

Based on the above findings, in this work thin films with a composition of *a*-44% Ti-doped GeO_2 were deposited by ion beam sputtering using the bias target deposition system and studied under the same annealing conditions as the *a*-GeO_2 films. The primary goal was to determine whether Ti incorporation suppresses crystallization and how humidity during annealing influences the structural stability of the alloy films.

The crystallization behavior of the *a*-44%Ti-doped GeO_2 thin films during annealing was investigated using the same systems as for *a*-GeO_2.

The PXRD spectrum of the as-deposited *a*-44%Ti-doped GeO_2 film is shown in Figure 3.4.1.

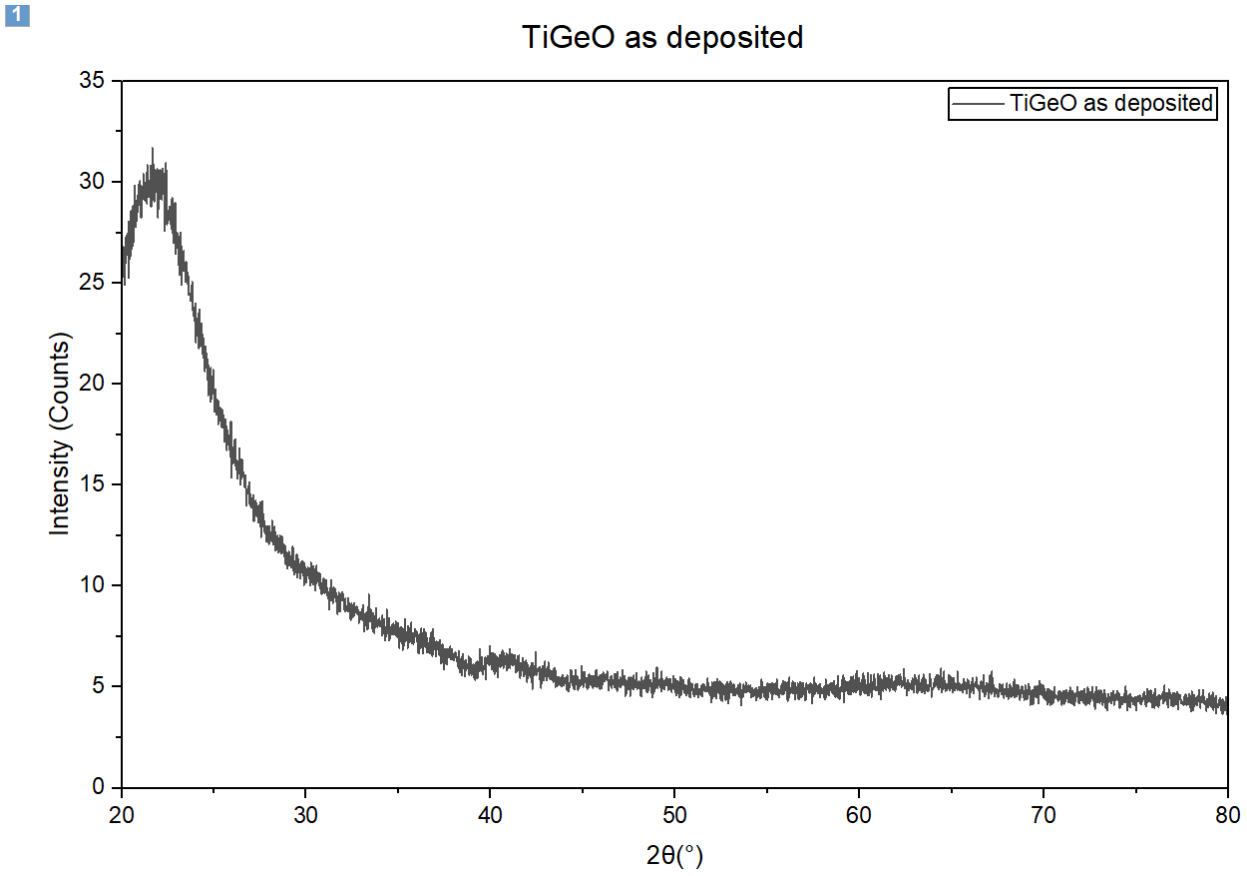

Figure 3.4.1. - PXRD spectrum of as-deposited *a*-44%Ti-doped GeO_2 film.

The diffraction pattern shows a broad diffuse halo centered near ~21–22° (2θ), which is as in the case of a-GeO_2 coatings is a characteristic of an amorphous oxide deposited on a fused silica substrate. No sharp diffraction peaks are observed, indicating that the deposited film is fully amorphous prior to annealing.

In *a*-44%Ti-doped GeO_2 coatings, crystallization at elevated temperatures is typically associated with the formation of *a*-TiO_2 crystalline phases. The main diffraction peaks of *a*-TiO_2 obtained from the ICDD Powder Diffraction File database are summarized in Table 3.4.1.

Table 3.4.1. - Main PXRD reflections of anatase TiO_2 (ICDD PDF 71-1166).

Phase	2θ (deg)	Plane (hkl)
Anatase TiO_2	~25.3	(101)
Anatase TiO_2	~37.8	(004)
Anatase TiO_2	~48.0	(200)
Anatase TiO_2	~53.9	(105)

These reference peak positions were used to identify the possible formation of crystalline *a*-TiO_2 phases during annealing.

The PXRD pattern of the *a*-44%Ti-doped GeO_2 film annealed at 600°C under ambient conditions is shown in Figure 3.4.2.

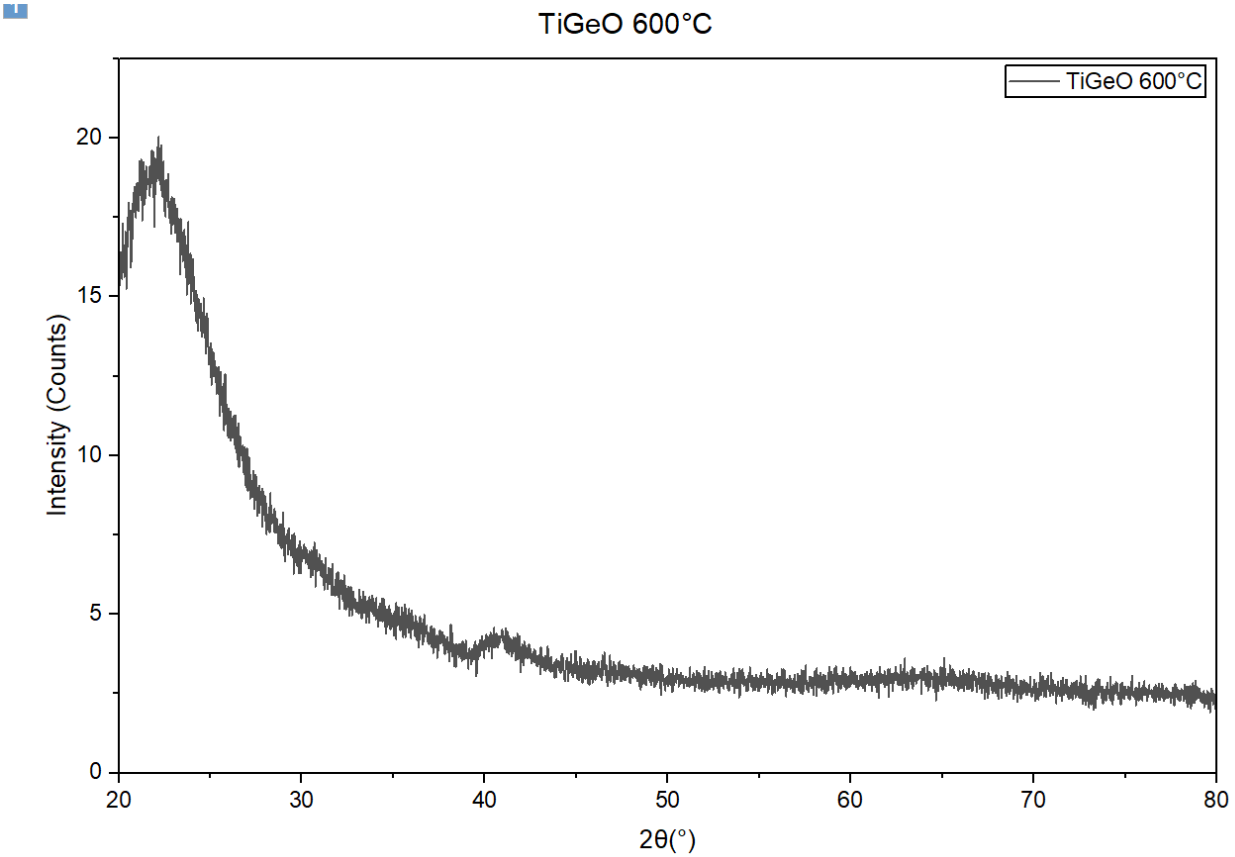

Figure 3.4.2. - PXRD spectrum of *a*-44%Ti-doped GeO_2 film annealed at 600 °C.

The material remains amorphous. No diffraction peaks corresponding to crystalline phases are observed. In particular, none of the reflections associated with anatase *a*-TiO_2 listed in Table 3.4.1. are present.

To investigate the influence of water during annealing, *a*-44%Ti-doped GeO_2 films were also annealed at 600 °C under high humidity conditions (~94 % RH). The PXRD spectrum of this sample is shown in Figure 3.4.3.

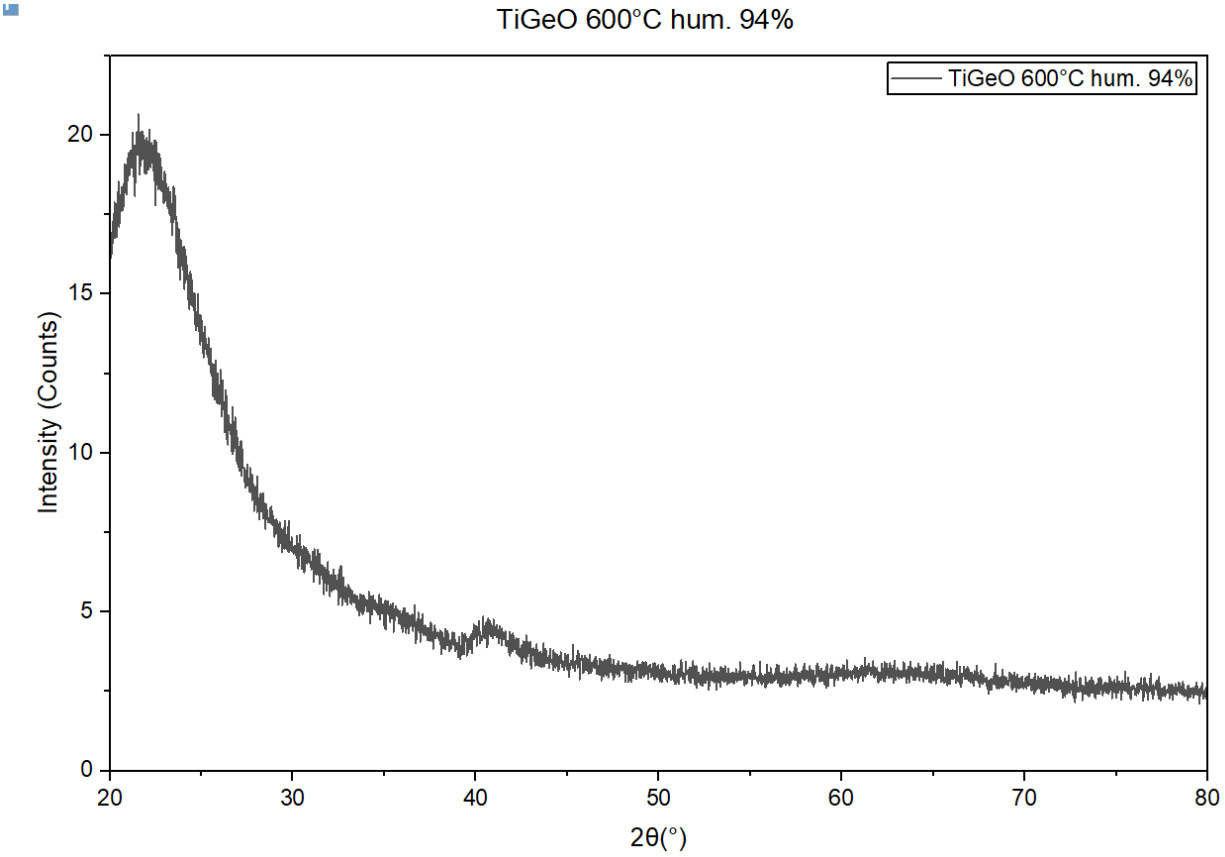

Figure 3.4.3. - PXRD spectrum of *a*-44%Ti-doped GeO_2 film annealed at 600 °C under high humidity.

The diffraction pattern shows a profile very similar to that obtained for the films annealed under ambient conditions. The pattern again is dominated by the broad amorphous of the substrate. Interestingly, there are no signs of crystallization in the PXRD spectrum. For comparison, the PXRD spectra of the as deposited, the annealed at 600 °C, and the film annealed at 600 °C under high humidity conditions are plotted together in Figure 3.4.4.

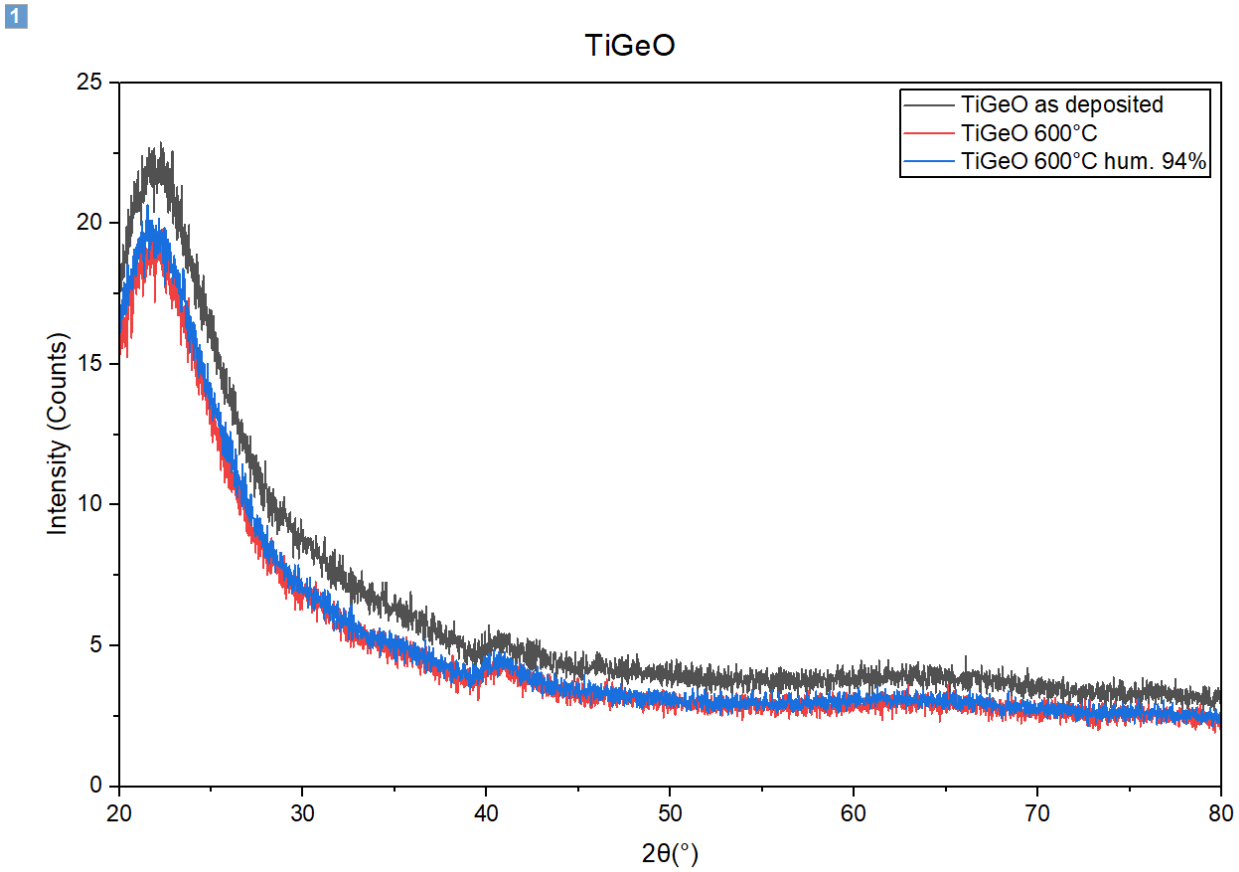

Figure 3.4.4. - Comparison of PXRD spectra for as-deposited, 600 °C annealed, and humid-annealed *a*-44%Ti-doped GeO_2 films.

The strong overlap between these spectra confirms that annealing at 600°C does not induce crystallization in the *a*-44%Ti-doped GeO_2 films, even when the annealing atmosphere contains significant humidity.

The optical microscopy images of the *a*-44%Ti-doped GeO_2 film annealed at 600 °C under dry and humid conditions are shown in Figure 3.5.5. The film annealed under ambient conditions exhibits a uniform surface with no visible features, indicating that thermal treatment at 600 °C does not significantly modify the morphology of the *a*-TiGeO film.

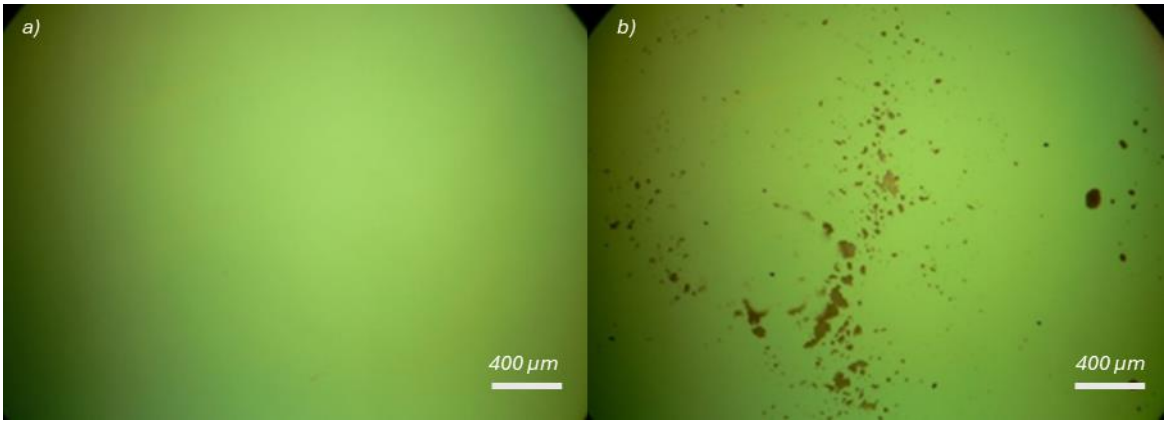

Figure 3.4.5. – Optical microscopy images of *a*-44%Ti-doped GeO_2 films after annealing at 600 °C: (a) annealed under ambient conditions; (b) annealed under high humidity (~94 % RH).

The sample annealed at 600 °C under high humidity shows the dark particles distributed on the surface. These features are most likely associated with surface contamination. Unlike the GeO_2 films, no circular domains or interference patterns are observed. This suggests that the *a*-44%Ti-doped GeO_2 layer remains more stable during humid annealing.

To further investigate the thermal stability of the *a*-44%Ti-doped GeO_2, additional samples were annealed at higher temperatures under ambient conditions. PXRD measurements were performed after annealing at 700 °C, 750 °C, and 800 °C to determine the temperature where the crystallization begins. The diffraction patterns obtained after annealing at these temperatures are shown in Figure 3.4.6.

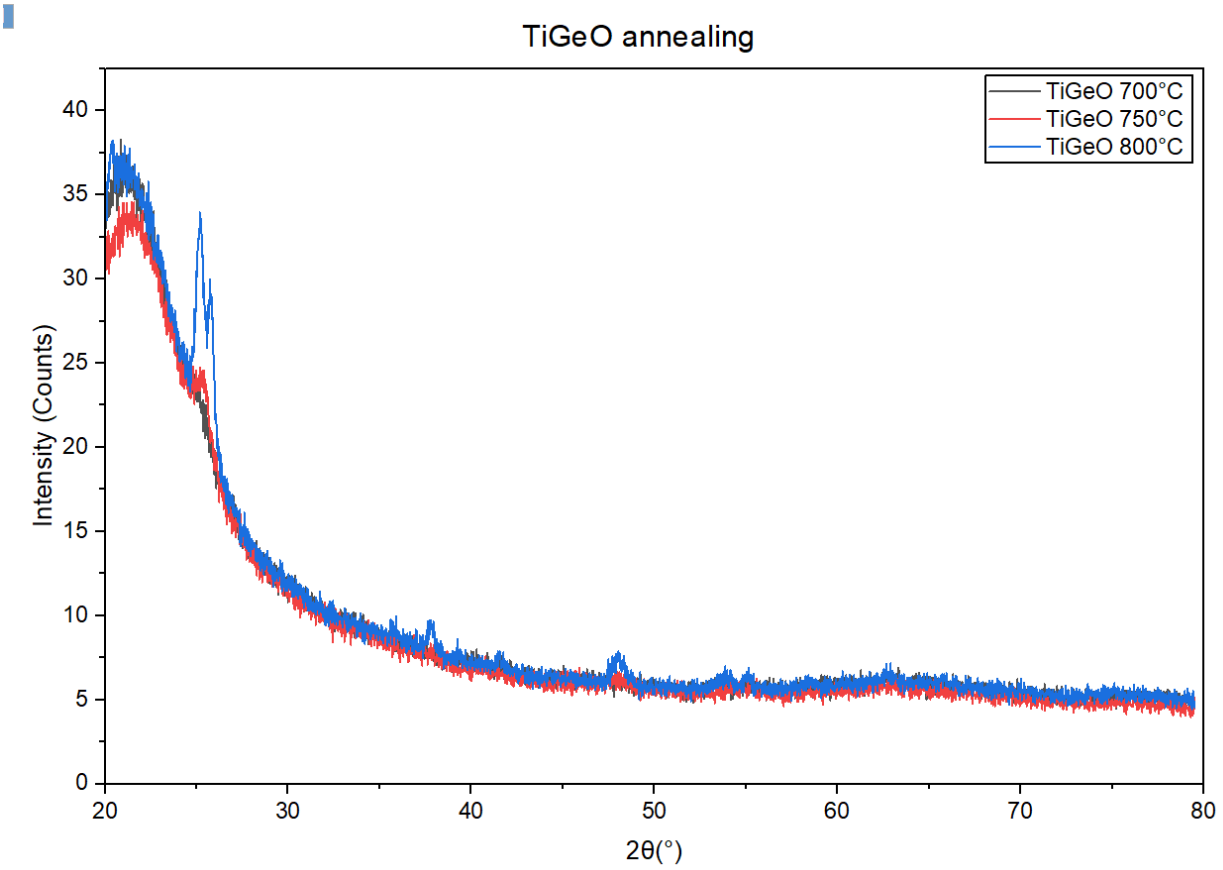

Figure 3.4.6. - PXRD patterns of 44%Ti-doped GeO_2 films annealed at 700 °C, 750 °C, and 800 °C.

The sample annealed at 700 °C exhibits a diffraction pattern similar to that observed for the films annealed at 600 °C. However, after annealing at 750 °C, the diffraction spectrum begins to show a slight distortion of the amorphous halo and the appearance of a weak shoulder near ~25° (2θ). This feature suggests the onset of crystallization and the formation of small crystalline regions within the film.

A structural change is observed for the sample annealed at 800 °C. In this case, the PXRD pattern shows a clear peak near ~25–26° (2θ) superimposed on the amorphous background. The position of this peak is consistent with the (101) reflection of anatase *a*-TiO_2, which occurs at 2θ ≈ 25.3° when measured using Cu Kα radiation. The appearance of this peak indicates that

crystalline *a*-TiO_2 phases begin to form within the *a*-44%Ti-doped GeO_2 film at high annealing temperatures.

The onset of crystallization occurs between 750 °C and 800 °C. This behavior indicates that the incorporation of *a*-TiO_2 into the *a*-GeO_2 network effectively suppresses crystallization.

3.5 FTIR results

The FTIR spectra were measured in the O-H stretching region (3000–4000 cm^{-1}) and the H-O-H bending region (~1600–1700 cm^{-1}). Figure 3.5.1. shows the FTIR spectra of the as-deposited TiGeO film, the film annealed at 600 °C under ambient conditions, and the film annealed at 600 °C under high humidity conditions (~94 % RH).

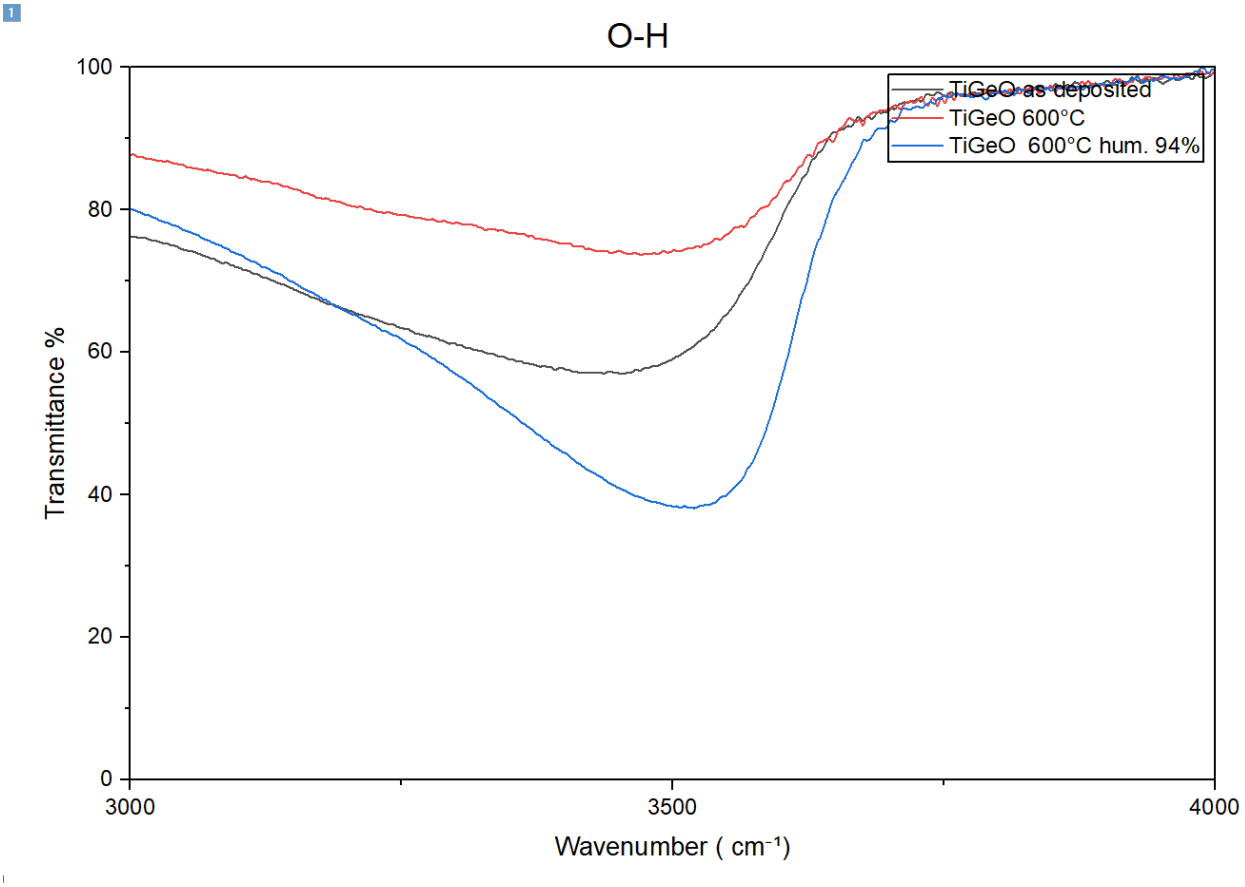

Figure 3.5.1. - FTIR spectra of *a*-44%Ti-doped GeO_2 films in the O-H stretching region.

The as-deposited *a*-TiGeO film exhibits a broad absorption band centered around ~3400-3500 cm^{-1}, which is characteristic of the O-H stretching vibration associated with hydroxyl groups in oxide networks. The hydroxyl species are commonly incorporated during thin film deposition due to residual water vapor in the vacuum system or adsorption from the ambient environment. After annealing at 600°C under ambient conditions, the intensity of the O-H absorption band decreases, indicating that thermal annealing leads to the removal of hydroxyl groups from the film. This behavior is consistent with the dehydration of the oxide network and the release of water during annealing. However, the sample annealed at 600 °C under high humidity conditions shows a stronger absorption band in the O-H stretching region. This suggests that water vapor present during annealing can be incorporated into the film structure, resulting in a higher concentration of hydroxyl groups.

After humid annealing, increase in absorption in the 3000-3700 cm^{-1} region is observed, which corresponds to O-H stretching vibrations. The presence of these bands indicates incorporation of hydroxyl groups in the oxide network. Water molecules diffusing into the film can react with bridging Ge-O-Ge bonds through a hydrolysis reaction, in which the water molecule dissociates and forms two terminal hydroxyl groups. This process breaks the oxygen bonds in the amorphous network and reduces the Ge-O structure. The formation of Ge-OH groups therefore indicates that water is incorporated into the film rather than adsorbed on the surface.

The FTIR spectra in the 1600-1700 cm^{-1} region, corresponding to the H-O-H bending vibration of molecular water, are shown in Figure 3.5.2.

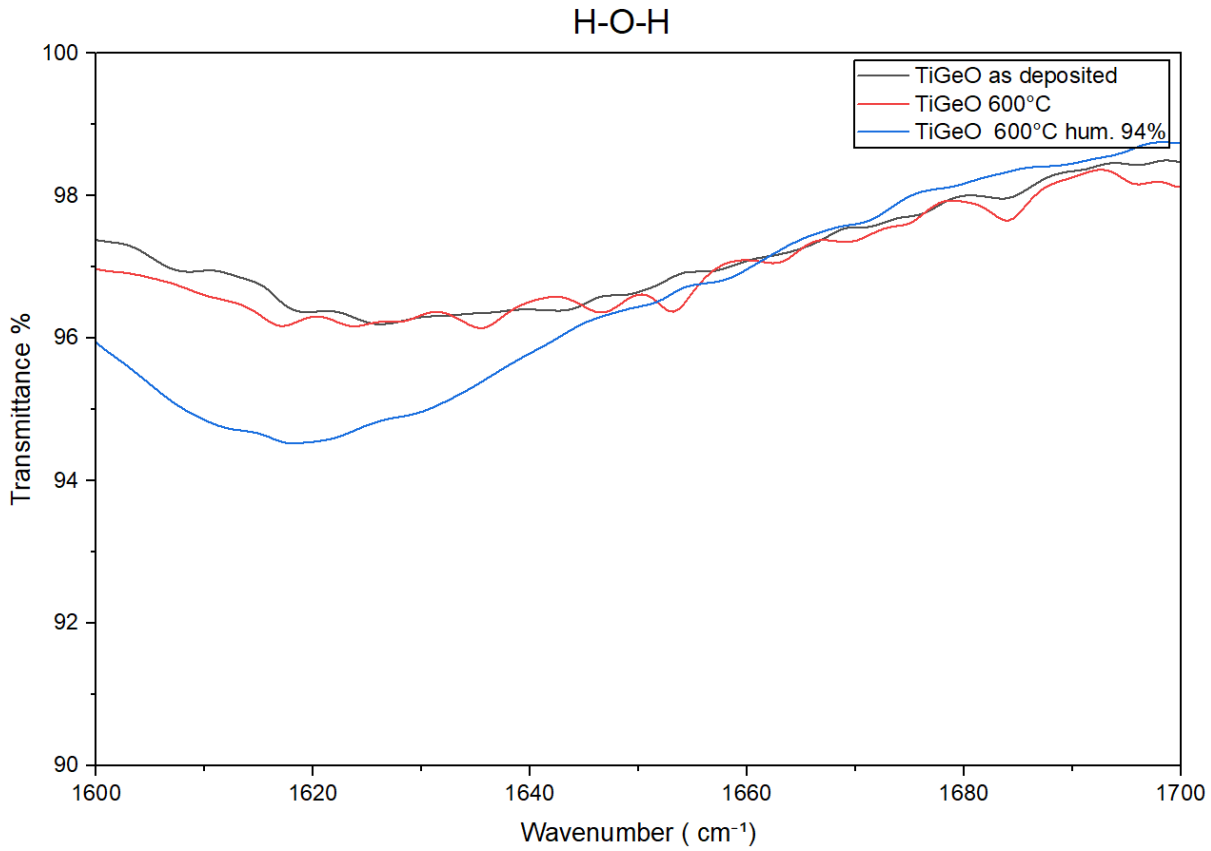

Figure 3.5.2. - FTIR spectra of *a*-44%Ti-doped GeO_2 films in the H-O-H bending region.

In this region, only a very weak spectral feature is observed for all samples. The absence of a strong absorption band near ~1630 cm^{-1} indicates that only a small amount of molecular water is present in the films.

The structural evolution of the deposited oxide coatings during annealing was investigated using a combination of PXRD and FTIR measurements. While PXRD provides information about the formation of crystalline phases and long-range ordering, FTIR spectroscopy allows the investigation of local bonding environments and hydrogen-related species in the films. Together, these techniques provide deep insight into the structural changes occurring during thermal treatment.

The PXRD measurements showed that pure *a*-GeO_2 films exhibit a tendency toward crystallization during annealing, with the appearance of diffraction features corresponding to crystalline *a*-GeO_2 phases at elevated temperatures. In contrast, the *a*-44%Ti-doped GeO_2 films remain amorphous up to temperatures of approximately 750 °C, demonstrating significantly improved thermal stability. The onset of crystallization in the Ti-doped films occurs only at higher temperatures. In particular, the PXRD measurements of the samples annealed at 750 °C and 800 °C show the gradual appearance of diffraction peaks near $2\theta \approx 25\text{-}26°$, which are consistent with the (101) reflection of anatase *a*-TiO_2.

These results demonstrate that *a*-TiO_2 doping significantly enhances the thermal stability of *a*-GeO_2 coatings, while humidity during annealing can alter the hydrogen content of the films.

3.6. Characterization of *a*-SiO_2 Films

In high-reflectivity (HR) multilayer structures, alternating layers of *a*-44%Ti-doped GeO_2 and *a*-SiO_2 are deposited to form a quarter-wave stack designed for 1064 nm. Figure 3.6.1. shows the design of an HR quarter wave stack coating.

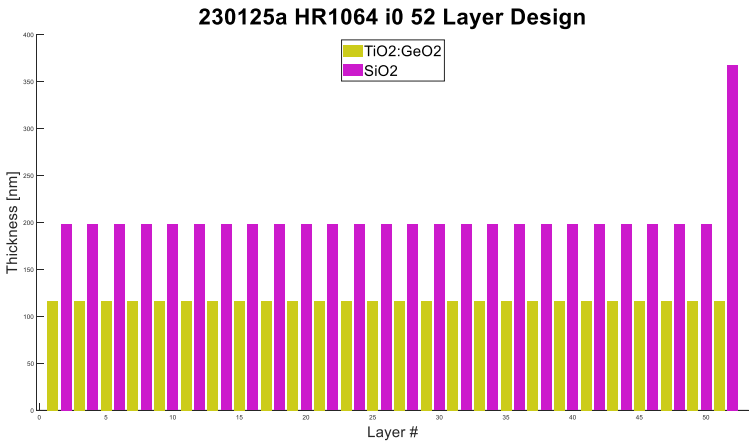

Figure 3.6.1. - Quarter-wave multilayer design of the TiO_2:GeO_2/SiO_2 HR coating deposited at 200 °C. The stack consists of alternating high-index *a*-44%Ti-doped GeO_2 layers and low-index *a*-SiO_2 layers designed for 1064 nm operation [24].

Since water penetration and thermal treatment can affect the stability of multilayer coatings, it is important to understand the structural behavior of the amorphous *a*-SiO_2 layers under the same annealing conditions used for the *a*-44%Ti-doped GeO_2 films.

To investigate this, PXRD and FTIR measurements were performed on *a*-SiO_2 films in the as-deposited, after annealing at 600 °C and after annealing at 600 °C under high humidity conditions (~94 % RH). The PXRD patterns are shown in Figure 3.6.2.

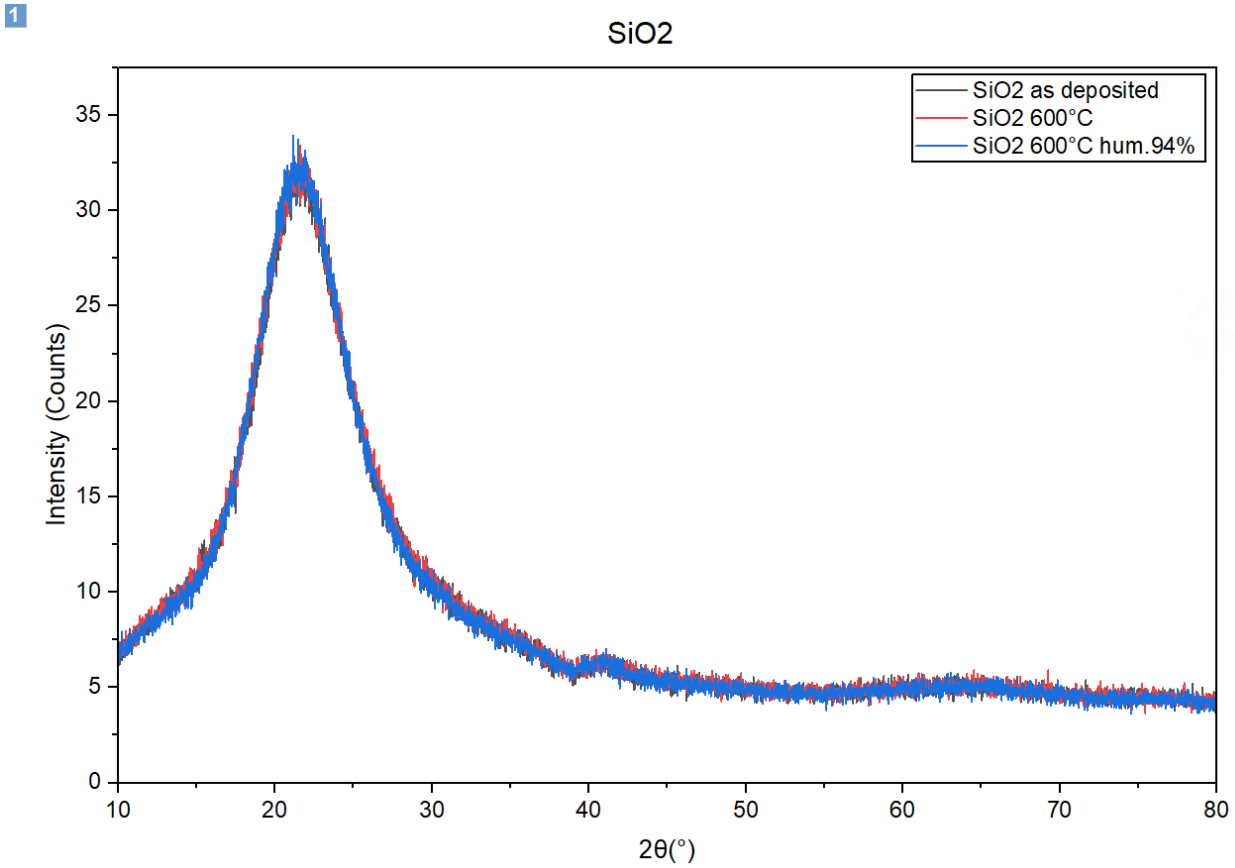

Figure 3.6.2. - XRD patterns of *a*-SiO_2 films in the as-deposited, after annealing at 600 °C and after annealing at 600 °C under high humidity.

The diffraction patterns exhibit a broad diffuse peak centered near 22° (2θ), which is characteristic of amorphous silica. No sharp diffraction peaks corresponding to crystalline silica phases are observed in either sample. The similarity of the three spectra indicates that annealing at 600 °C, even under high humidity conditions, does not induce crystallization in the *a*-SiO_2 films. The films therefore remain structurally amorphous after thermal treatment. This behavior is consistent with the well-known high thermal stability of amorphous *a*-SiO_2, which typically requires significantly higher temperatures to undergo crystallization.

This observation is important for the interpretation of the multilayer coating behavior. Since the *a*-SiO_2 layers do not undergo structural phase transitions under the studied conditions,

any structural changes observed in the multilayer stacks are more likely associated with the *a*-44%Ti-doped GeO_2 layers rather than the silica layers.

The structural stability of the *a*-SiO_2 layers therefore supports their role as thermally stable low-index layers in the *a*-TiO_2:GeO_2/SiO_2 multilayer system.

The optical microscopy image of the *a*-SiO_2 film annealed at 600 °C under high humidity shows a uniform surface. Only a small amount of dark spots are found, which are most likely surface dust particles or minor contamination rather than structural defects.

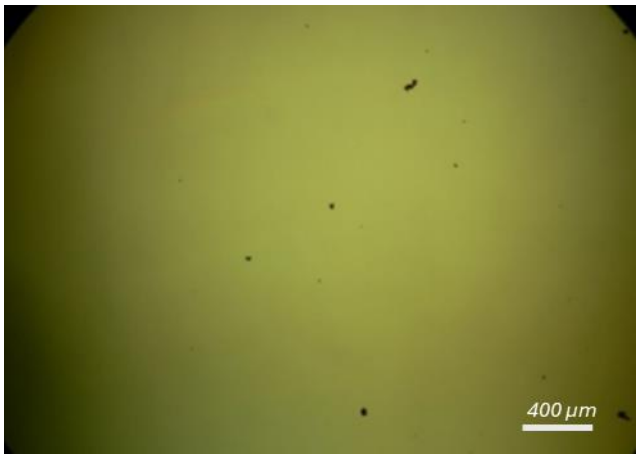

Figure 3.6.3. - Optical microscopy image of the *a*-SiO_2 thin film after annealing at 600 °C under high humidity conditions.

In contrast to the *a*-GeO_2 films, no circular domains or interference patterns are observed. This indicates that humid annealing does not induce significant structural or morphological changes in the *a*-SiO_2 film. The absence of surface modifications is consistent with the PXRD results, which show that the *a*-SiO_2 films remain fully amorphous after annealing.

FTIR spectroscopy was used to evaluate the presence of hydroxyl groups and water-related species in the *a*-SiO_2 films.

The FTIR spectra in the O-H stretching region are shown in Figure 3.6.4.

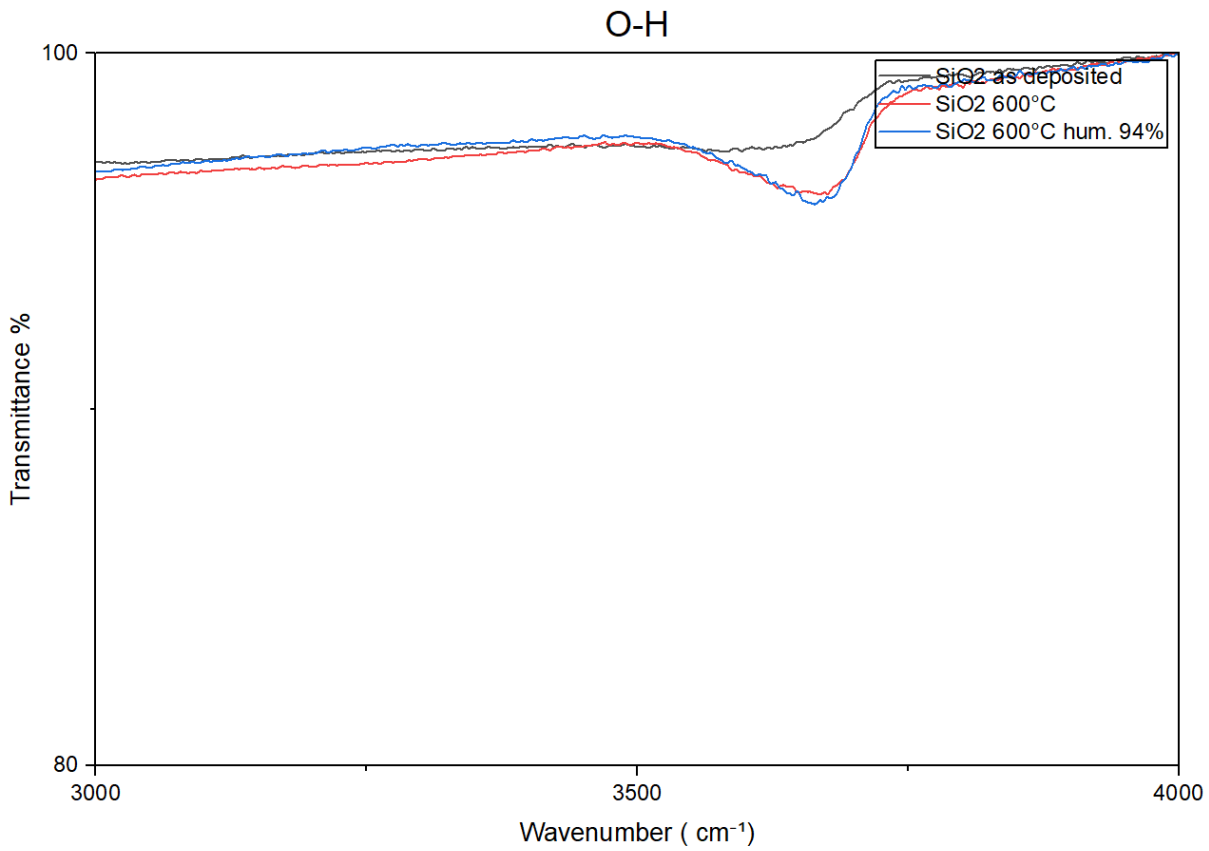

Figure 3.6.4. - FTIR spectra of *a*-SiO_2 films in the O-H stretching region (3000-4000 cm^{-1}) for as-deposited and annealed samples.

A weak and broad absorption band is observed near ~3600–3700 cm^{-1}, which is characteristic of Si-OH stretching vibrations in amorphous silica. The intensity of this feature is very small for all samples, indicating that the *a*-SiO_2 films contain only a low concentration of hydroxyl groups. Comparison of the spectra for the as-deposited, 600 °C annealed, and 600 °C humid-annealed films show only minimal differences. The absence of significant changes in the O-H absorption band suggests that annealing and humidity exposure do not strongly modify the hydroxyl content of the *a*-SiO_2 films.

The FTIR spectra in the 1600-1700 cm^{-1} region, corresponding to the H-O-H bending vibration of molecular water, are shown in Figure 3.6.5.

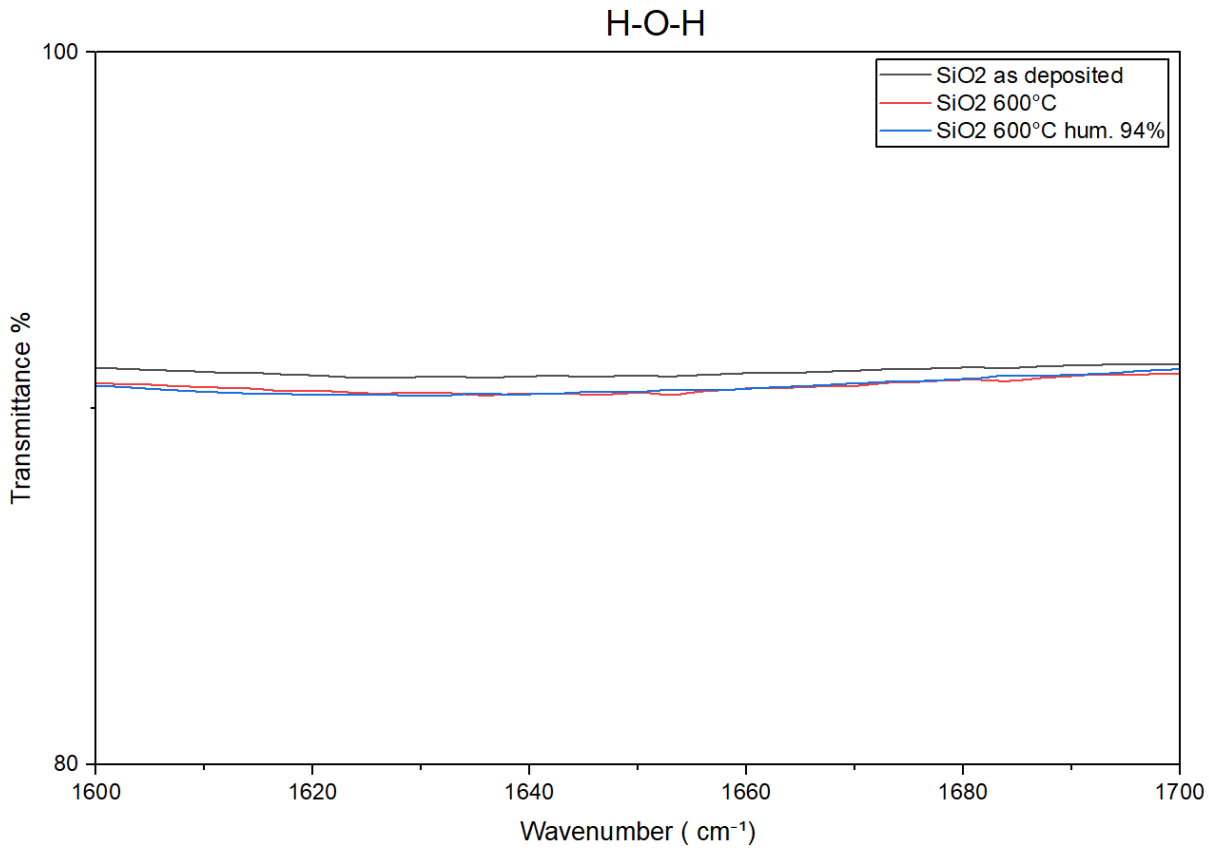

Figure 3.6.5. - FTIR spectra of *a*-SiO_2 films in the H-O-H bending region (~1600-1700 cm^{-1}).

No distinct absorption peak near ~1630 cm^{-1} is observed for any of the samples. This indicates that molecular water is not significantly incorporated into the *a*-SiO_2 films, even after annealing under high humidity conditions.

The FTIR results indicate that the O-H content of the *a*-SiO_2 films remains very low and largely unchanged during annealing, even when the films are exposed to high humidity. This behavior reflects the high structural stability of the amorphous *a*-SiO_2 network, which resists the incorporation of hydroxyl groups and water molecules under the studied annealing conditions.

Combined with the XRD results showing that the films remain amorphous after annealing, these observations confirm that *a*-SiO_2 layers in the multilayer coating remain structurally stable during thermal processing.

3.7. Characterization of multilayer *a*-44%Ti-doped GeO_2 and *a*-SiO_2 coatings

To evaluate the structural stability of the multilayer coatings during thermal processing, two multilayer structures were investigated: a simplified 8-layer stack and a full high-reflectance coating consisting of 60 layers. Both coatings were composed of alternating *a*-44%Ti-doped GeO_2 and *a*-SiO_2 layers deposited by ion beam sputtering and designed as quarter-wave stacks for operation near 1064 nm.

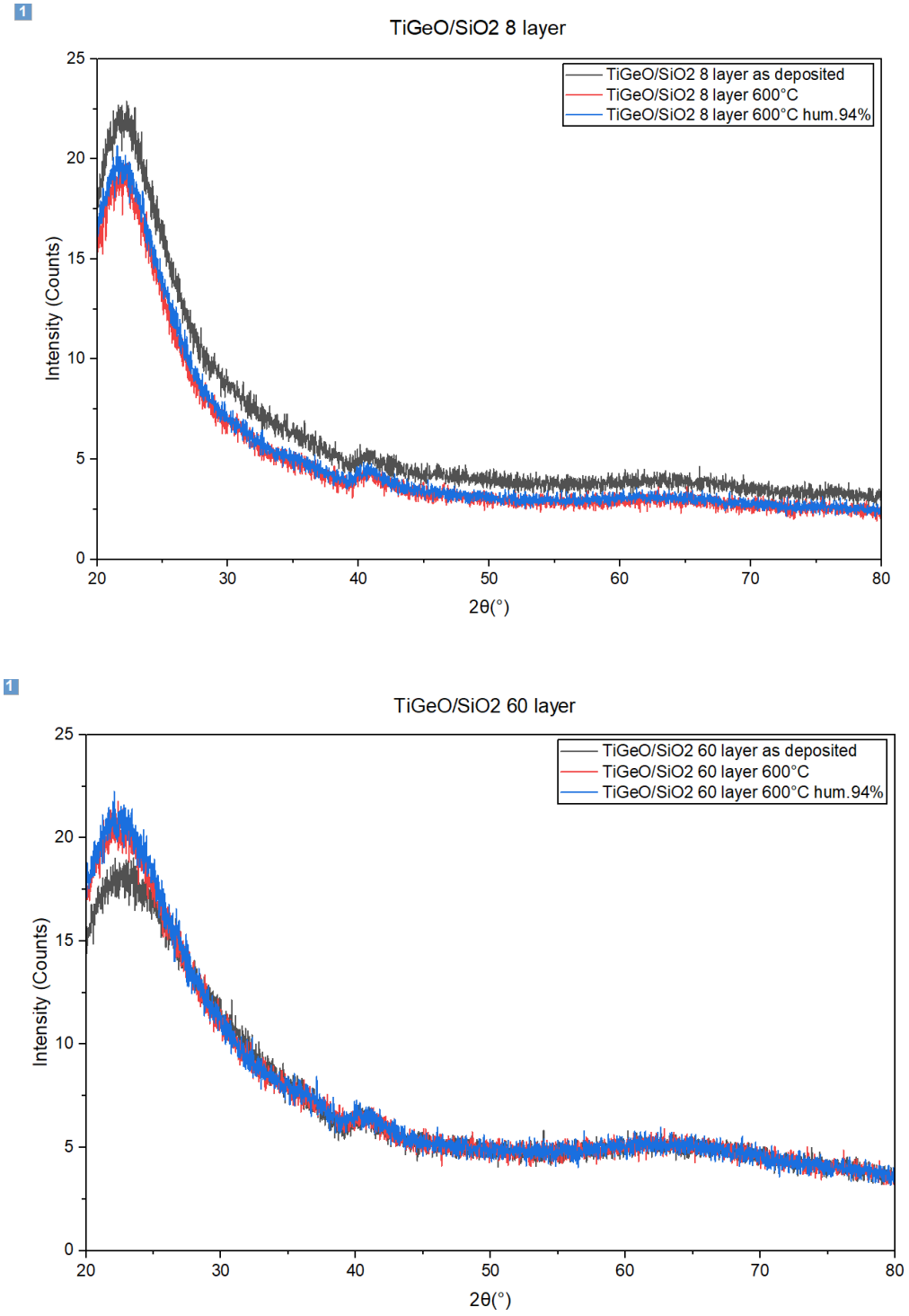

Figure 3.7.1. - PXRD patterns of *a*-44%Ti-doped GeO_2/SiO_2 multilayer stacks.
(a) 8-layer structure and (b) 60-layer high-reflectance coating measured in the as-deposited state and after annealing at 600 °C with and without humidity.

Both multilayer systems exhibit a broad diffuse halo centered near ~22° 2θ, which is characteristic of amorphous silica-based oxide films. No sharp diffraction peaks corresponding to crystalline phases of GeO_2, TiO_2, or SiO_2 are observed in the as deposited samples (Figure 3.7.1.). This indicates that the multilayer stacks deposited by ion beam sputtering form fully amorphous structures. After annealing at 600°C, the diffraction patterns remain amorphous without the appearance of new diffraction peaks. A similar behavior is observed for samples annealed at 600°C under high humidity conditions (~94 % RH). In particular, no diffraction peaks corresponding to crystalline GeO_2 phases (such as the α-quartz-type reflection near ~26° 2θ) are detected in either multilayer structure. This indicates that neither thermal annealing nor humidity exposure induces crystallization within the multilayer coatings.

The absence of crystallization in both the 8-layer test structure and the 60-layer high-reflectance coating suggests that the *a*-44%Ti-doped GeO_2/SiO_2 material system remains structurally stable under the investigated thermal and humidity conditions. The suppression of crystallization is likely related to both the *a*-TiO_2 doping of *a*-GeO_2, which is known to inhibit crystallization.

Maintaining an amorphous structure is desirable for optical coatings, since crystallization can introduce optical scattering, increased absorption, and mechanical stress, potentially degrading coating performance.

Optical microscopy of the *a*-44%Ti-doped GeO_2/SiO_2 multilayer coatings showed significant differences in surface morphology after thermal treatment. The 8-layer stack shows only small blisters in the film located in a certain area; these are the traces of acetone.

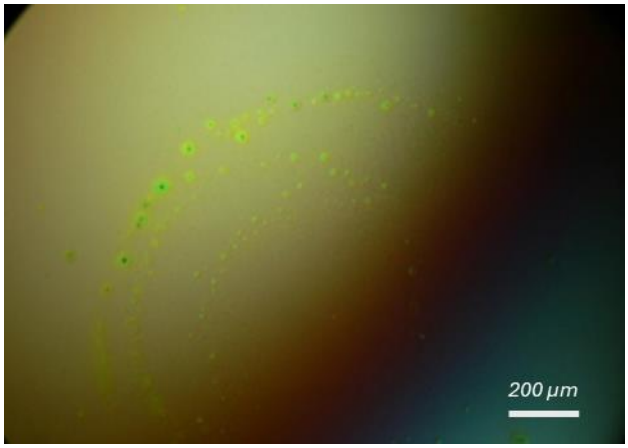

Figure 3.7.2. - Optical microscopy image of the *a*-44%Ti-doped GeO_2/SiO_2 8-layer coating after annealing at 600 °C under high humidity.

The 60-layer stack showed much higher amount of circular bubble structures after annealing, especially under high humidity conditions. Their size and density increased compared to the 8-layer coating. That means that the multilayer structure plays an important role in defect formation.

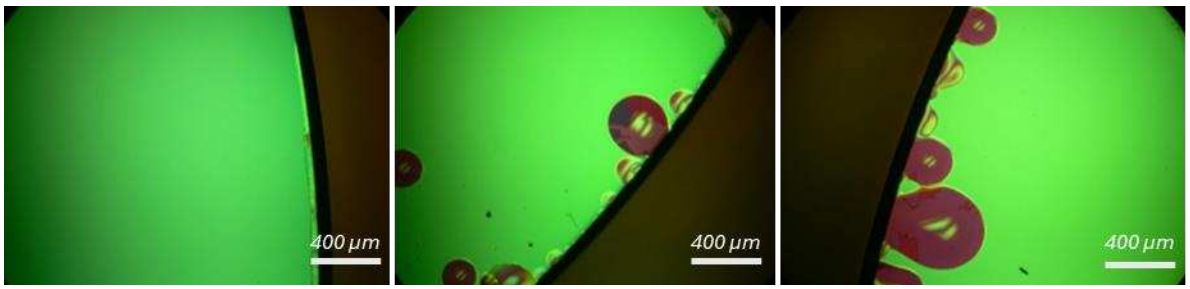

Figure 3.7.3. - Optical microscopy images of the *a*-44%Ti-doped GeO_2/SiO_2 60-layer coating: (a) as-deposited film; (b) after annealing at 600 °C under ambient conditions; (c) after annealing at 600 °C under high humidity (~94 % RH).

FTIR spectroscopy was used to investigate the presence of hydroxyl groups and water-related species in the *a*-44%Ti-doped GeO_2/SiO_2 multilayer coatings. Measurements were performed for both the 8-layer test stack and the 60-layer high-reflectance coating in three

conditions: as deposited, annealed at 600 °C, and annealed at 600 °C under high humidity (~94 % RH).

The spectra were analyzed in two characteristic regions:

- O-H stretching region (3000-4000 cm^{-1})
- H-O-H bending region (1600-1700 cm^{-1})

The corresponding spectra are shown in Figures 3.7.4.-3.7.5.

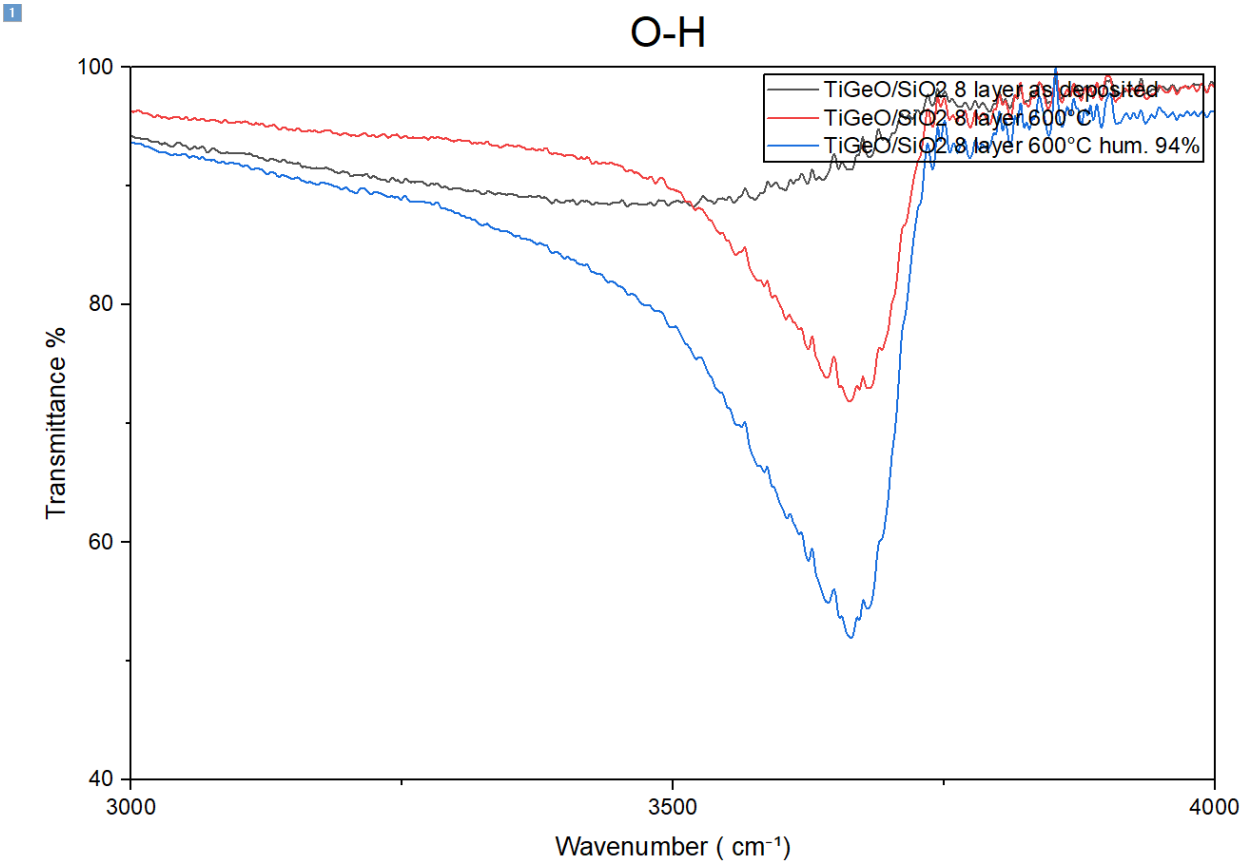
O-H
TiGeO/SiO2 8 layer as deposited
TiGeO/SiO2 8 layer 600°C
TiGeO/SiO2 8 layer 600°C hum. 94%
Transmittance %
100
80
60
40
3000
3500
4000
Wavenumber (cm⁻¹)

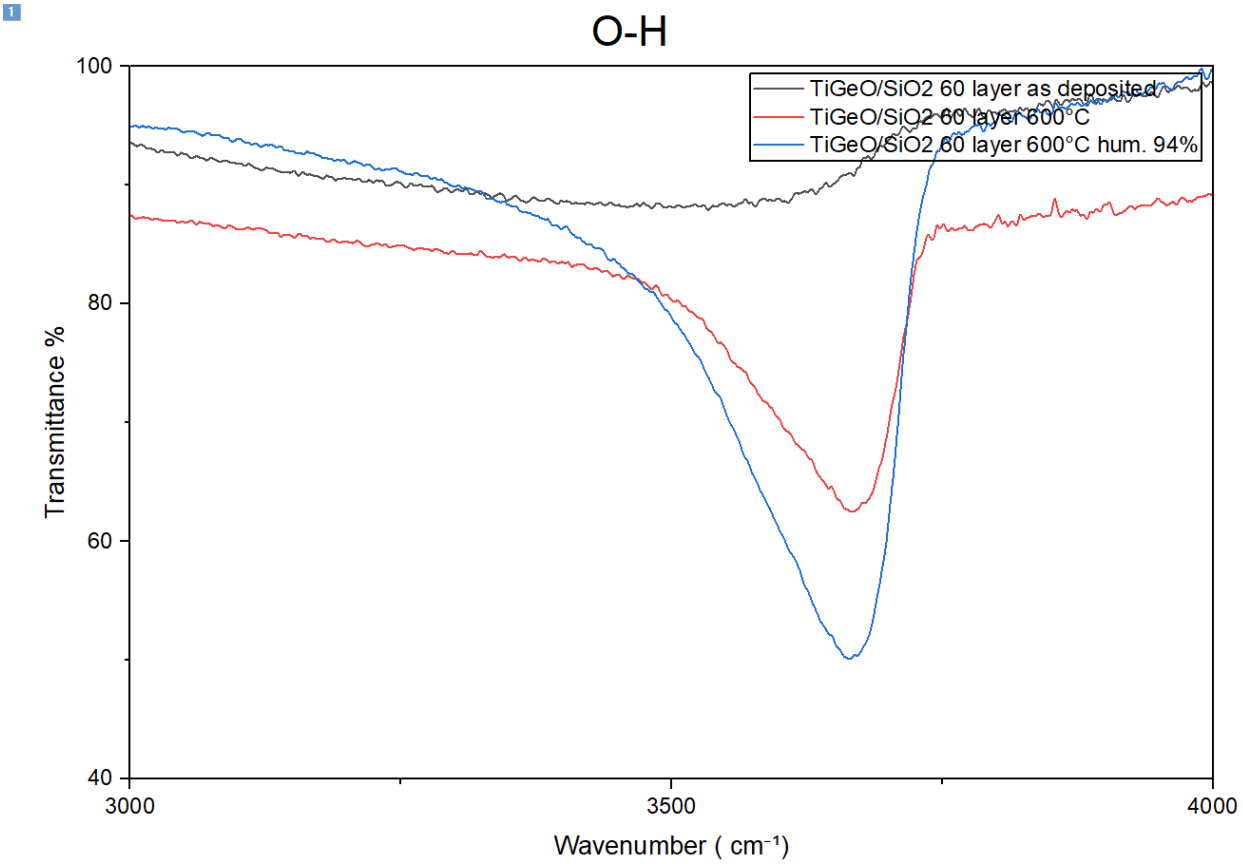

Figure 3.7.4. - FTIR spectra of the *a*-44%Ti-doped GeO_2/SiO_2 films in the O-H bending region (3000-4000 cm^{-1}).

Both multilayer systems exhibit a broad absorption feature near 3600-3700 cm^{-1}, which is characteristic of O-H stretching vibrations associated with hydroxyl groups in oxide films. For both the 8-layer and 60-layer coatings, the as-deposited samples show only a weak O-H absorption feature, indicating a relatively low concentration of hydroxyl groups in the films immediately after deposition.

After annealing at 600 °C, the O-H absorption band slightly decreases in intensity, which suggests partial removal of hydroxyl groups during thermal treatment. This behavior is consistent with dehydroxylation processes commonly observed in oxide thin films during annealing.

However, when annealing is performed under high humidity conditions (~94 % RH), the O-H absorption band becomes significantly stronger for both multilayer stacks.

A similar trend was previously observed for the single-layer *a*-44%Ti-doped GeO_2 films. In both cases, annealing at 600 °C in dry conditions leads to a decrease in the O-H absorption band. When annealing was performed under high humidity conditions, the O-H absorption band increases again, suggesting re-incorporation of hydroxyl species through interaction of water molecules with the oxide network. The multilayer stacks exhibit the same qualitative behavior as the single-layer *a*-44%Ti-doped GeO_2 films. However, the O-H absorption can differ depending on the surrounding layers, since materials such as *a*-SiO_2 or *a*-Al_2O_3 may influence the diffusion of water molecules into the *a*-44%Ti-doped GeO_2 layer.

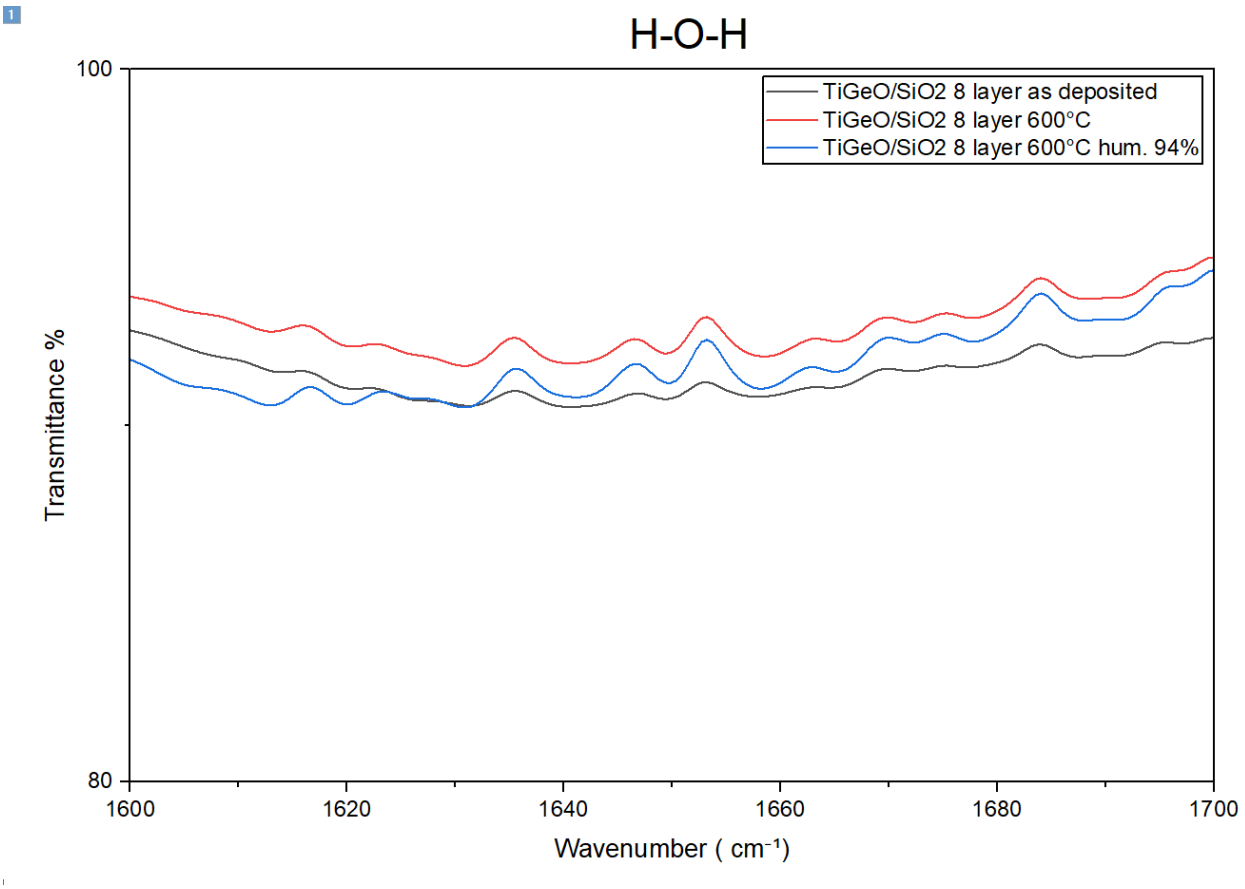

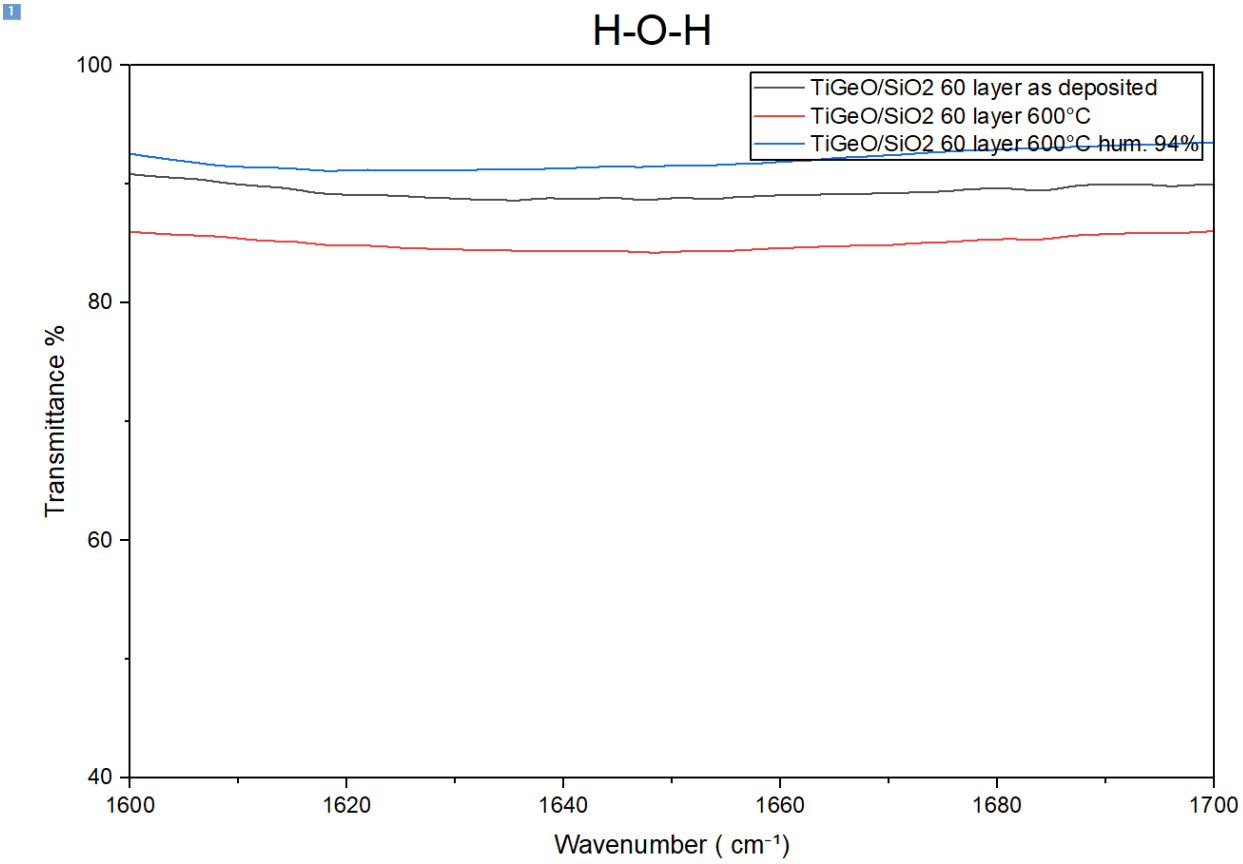

Figure 3.7.5. - FTIR spectra of *a*-44%Ti-doped GeO_2/SiO_2 films in the H-O-H bending region (~1600-1700 cm^{-1}).

The spectra measured in the 1600-1700 cm^{-1} region correspond to the H-O-H bending vibration of molecular water. In contrast to the O-H stretching region, the spectra in this range shows very weak or nearly absent absorption features for all samples. This indicates that molecular water is not significantly trapped within the multilayer coatings, even after annealing in a humid environment.

Instead, the FTIR results suggest that water interaction occurs primarily through hydroxyl bond formation within the oxide network rather than through the presence of free water molecules.

The FTIR results show that both the 8-layer and 60-layer *a*-44%Ti-doped GeO_2/SiO_2 multilayer stacks interact with water during humid annealing, primarily through the formation of hydroxyl groups. While annealing under dry conditions leads to partial removal of hydroxyl groups, annealing under high humidity conditions promotes hydroxyl incorporation into the oxide network.

Despite the increase in hydroxyl content during humid annealing, the PXRD results demonstrate that no crystallization occurs in the multilayer coatings when annealed for 10 hours at 600 C. This indicates that the incorporation of hydroxyl groups does not significantly disrupt the amorphous structure of the multilayer system under the investigated conditions.

In addition to the GeO_2, TiO_2:GeO_2, and SiO_2-based coatings, Al_2O_3 thin films and several three-layer oxide stacks ($SiO_2/GeO_2/SiO_2$, SiO_2/TiGeO/SiO_2, Al_2O_3/TiGeO/Al_2O_3, and $Al_2O_3/GeO_2/Al_2O_3$) were fabricated. Both PXRD and FTIR measurements were performed for the films in the as deposited state, after annealing at 600 °C, and after annealing at 600°C under high humidity conditions (~94 % RH). The results will be present in Appendix A.

3.8 Summary of Results

In this work, the structural stability of *a*-GeO_2, *a*-44%Ti-doped GeO_2 and *a*-SiO_2 thin films deposited by ion-beam sputtering using the bias target deposition system was investigated under different annealing conditions. The films were annealed at 600°C for 10 hours under ambient and high-humidity conditions, and their structural, chemical and surface changes were analyzed using PXRD, FTIR, and optical microscopy.

PXRD measurements showed that *a*-GeO_2 films annealed in high humidity indicate diffraction peak near $2\theta \approx 26.5°$, suggesting the onset of crystallization after the annealing. The

films annealed under ambient conditions remained amorphous, indicating that the presence of water accelerates structural rearrangement and contributes to crystallization of *a*-GeO_2.

FTIR analysis showed the appearance of absorption bands associated with O-H stretching and H-O-H bending modes in humid-annealed samples, confirming that water can be incorporated into the *a*-GeO_2 network during annealing.

For *a*-44%Ti-doped GeO_2 films, the PXRD spectra did not show crystalline peaks after annealing at 600 °C and high humidity, indicating that the addition of Ti stabilizes the amorphous structure and suppresses crystallization under the same conditions as for GeO_2. This suggests that Ti incorporation modifies the network and increases its resistance to humidity.

The *a*-SiO_2 films stayed structurally stable during annealing in both ambient and humid environments. FTIR measurements showed very low O-H absorption and no significant changes after annealing, indicating minimal water incorporation and confirming the high chemical and structural stability of the amorphous *a*-SiO_2 network.

The results demonstrate that the annealing conditions plays an important role in the structural changes of *a*-GeO_2-based coatings. High humidity leads to water incorporation and can accelerate structural changes in *a*-GeO_2 films, while Ti doping improves the stability of the amorphous network. *a*-SiO_2 films show significantly higher resistance to humidity structural changes under the same annealing conditions.

CHAPTER 4 CONCLUSIONS AND FUTURE WORK

4.1 Conclusions

This work investigated the influence of annealing conditions on the structural stability of oxide thin films. Attention was given to the role of the humidity during high-temperature annealing and its effect on *a*-GeO_2, *a*-44%Ti-doped GeO_2, and *a*-SiO_2 thin film coatings.

The experimental results demonstrate that the annealing atmosphere has a significant impact on the structural changes of *a*-GeO_2-based films. PXRD measurements showed that *a*-GeO_2 coatings annealed at 600 °C for 10 hours under high humidity conditions show diffraction peak near $2\theta \approx 26.5°$, suggesting the onset of crystallization after humid annealing, while films annealed in ambient air remain amorphous, which means that the presence of water drives structural rearrangement and reduces the crystallization temperature of *a*-GeO_2 thin films.

FTIR analysis confirms that water incorporates into oxides network during high-humidity annealing. The spectra show increased absorption in the O-H stretching region (~3000-3700 cm^{-1}) and in the H-O-H region (~1630 cm^{-1}). These results suggest that water interacts with the oxide network during annealing, modifying the network structure.

a-44%Ti-doped GeO_2 films remain amorphous after annealing at 600 °C for 10 hours, even under high humidity conditions. PXRD measurements did not show crystalline peaks in these films, indicating that the incorporation of Ti modifies the oxide network and improves the stability of the amorphous structure.

a-SiO_2 films showed the highest structural stability among the investigated films. FTIR measurements showed very weak O-H absorption bands and no significant changes after

annealing under either ambient or humid conditions. This behavior reflects the strong and stable amorphous network structure of *a*-SiO_2, which resists water incorporation and structural rearrangement during annealing.

Optical Nomarski microscopy observations demonstrated surface degradation and severe changes in several samples annealed under high humidity conditions. Bubble formation and partial film delamination were observed in *a*-GeO_2 coatings, whereas *a*-44%Ti-doped GeO_2 and *a*-SiO_2 stayed mostly unchanged, indicating that water incorporation and structural changes may generate internal stresses during thermal treatment.

Overall, the results demonstrate that humidity during annealing plays an important role in the structural changes of *a*-GeO_2-based thin films. Water incorporation can facilitate structural rearrangement and may lead to the onset of crystallization in *a*-GeO_2 coatings, while Ti incorporation improves the stability of the amorphous structure. *a*-SiO_2 films remain mostly stable under the same annealing conditions.

These findings contribute to the understanding of how the humidity effects on structural changes in oxide thin films and provide imagination into the stability of *a*-GeO_2-based coatings under thermal annealing conditions.

4.2 Future Work

Although this work shows the influence of humidity on oxide thin films during annealing, several aspects require further investigation.

First, additional structural characterization can help to clarify the crystallization behavior of *a*-GeO_2 films. High-resolution PXRD measurements and grazing-incidence diffraction scans

could be performed to better separate weak film diffraction signals from strong substrate peaks and to accurately identify the onset of crystallization in the coatings.

Second, ellipsometry measurements should be carried out to find possible changes in film thickness, refractive index, and density after annealing. Variations in optical constants can provide information about structural relaxation, densification, or network expansion associated with water incorporation into the films.

Third, X-ray photoelectron spectroscopy (XPS) measurements can provide important information about the chemical composition and bonding states in the films. XPS analysis can help to identify the possible changes in the chemical environment of Ge, Ti, and O atoms after humid annealing. Such measurements would allow a more direct investigation of water incorporation mechanisms within the oxide network.

Finally, future studies could explore a wider range of annealing temperatures, humidity percentages, and annealing durations. More precise control of humidity and temperature during thermal treatment would help determine the threshold conditions at which water begins to significantly affect to the structural stability of *a*-GeO_2-based coatings.

That would provide a deeper understanding of humidity-induced structural changes in oxide thin films and help improve the stability of optical thin film coatings.

BIBLIOGRAPHY

[1] MacLeod, H. A. Thin-Film Optical Filters, 4th ed. Boca Raton, FL: CRC Press, 2010.

[2] Ristau, D. Laser-Induced Damage in Optical Materials. Boca Raton, FL: CRC Press, 2014.

[3] Wu, J.-Y., Lee, C.-C. "Comparison of silicon oxide films deposited by RF ion beam sputtering and e-beam gun evaporation in visible to UV ranges." Proc. SPIE 5870, 58700G (2005).

[4] Tilsch, M. K., et al. "Effects of thermal annealing on ion-beam-sputtered SiO_2 and TiO_2 optical thin films." Optics & Photonics, 1997.

[5] Ren, W., et al. "Annealing effects on the optical and electrochemical properties of tantalum pentoxide films." Journal of Advanced Ceramics, 2021.

[6] Hsu, C.-H., Geng, X.-P., Wu, W.-Y., Zhao, M.-J., et al. "Air annealing effect on oxygen vacancy defects in Al-doped ZnO films." Molecules 25, 5043 (2020).

[7] Krous, E. M. "Characterization of Scandium Oxide Thin Films for Use in Interference Coatings". M.S. thesis, Colorado State University, 2010.

[8] Gupta, S., et al. "Tuning of optical properties via annealing of $BiFeO_3$ thin films." Open Journal of Applied Sciences 14, 2485–2496 (2024).

[9] Bohď, P., et al. "The optical properties of GeO_2, ZnS and Ge films produced by RF sputtering." Vacuum, 1990.

[10] Fazio, M. A., Vajente, G., Yang, L., Ananyeva, A., et al. "Comprehensive study of amorphous metal oxide coatings." Physical Review D 105, 102008 (2022).

[11] Fazio, M. A., Vajente, G., Sankar, S., Bassiri, R., et al. "Structure and morphology of low mechanical loss TiO_2-doped Ta_2O_5." Optical Materials Express 11, 2120–2132 (2021).

[12] Pérez, I., Sosa, V., Gamboa, F., et al. “Influence of post-deposition annealing on Ta_2O_5 films.” Applied Physics A 124, 792 (2018).

[13] Mori, D., Oka, H., Hosoi, T., Kawai, K., et al. “Comparative study of GeO_2/Ge and SiO_2/Si structures under water adsorption.” Journal of Applied Physics 120, 095306 (2016).

[14] Schmeisser, D., et al. “Surface oxidation states of germanium.” Surface Science, 1986.

[15] Richet, P. “GeO_2 vs SiO_2: Glass transitions and thermodynamic properties.” Physics and Chemistry of Minerals 17, 79–88 (1990).

[16] Hsu, C.-H., et al. “Microstructural and optical properties of GeO_2 thin films.” Crystal Research and Technology, 2011.

[17] Yang, L. A Study of Structural Organizations in Amorphous Oxide Thin Films. Ph.D. dissertation, Colorado State University, 2021.

[18] Yang, L., Vajente, G., Fazio, M., Ananyeva, A., et al. “Enhanced medium-range order in germania glasses.” Science Advances 7 (2021).

[19] Inoue, D., et al. “Structural and optical properties of TiO_2-GeO_2 mixed oxide films.” Journal of Vacuum Science & Technology A 37, 060601 (2019).

[20] Wang, X., Sun, Y., Yu, H., Wang, Y., et al. “Tuning thermal stability of germanium oxide.” Surface and Interface Analysis 50, 1176–1182 (2018).

[21] Stavarache, I., Lepadatu, A.-M., Stoica, T., Ciurea, M. L. “Annealing induced changes in $GeTiO_2$ films.” Applied Surface Science 309, 168–174 (2014).

[22] Hodroj, A., Chaix-Pluchery, O., Audier, M., Gottlieb, U., et al. “Thermal annealing of amorphous Ti-Si-O thin films.” Journal of Materials Research 23, 755 (2008).

[23] Vajente, G., et al. “Low mechanical loss TiO_2:GeO_2 coatings.” Physical Review Letters 127, 071101 (2021).

[24] Davenport, A., Vajente, G., Demos, N., Billingsley, G., et al. “Low thermal noise TiO_2:GeO_2 stacks.” Frontiers in Optics + Laser Science, 2024.

[25] Kaźmierczak-Bałata, A., Bodzenta, J., Szperlich, P., et al. “Impact of annealing in various atmospheres on ITO layers.” Materials 17, 4606 (2024).

[26] Khadri, S. R., Srihari, N. V., Nagaraja, K. K., Murthy, D. H. K. “Annealing atmosphere-dependent defects in $BiFeO_3$.” Materials Advances, 2025.

[27] Pang, X., Gao, K., Luo, F., Yang, H., et al. “Annealing effects on chromium oxide coatings.” Thin Solid Films 516, 4685–4689 (2008).

[28] Woods, K. N., Plassmeyer, G. M., Brizee, E. S., Valley, D. C., et al. “Low-temperature steam annealing of metal oxide thin films.” Chemistry of Materials 29, 8531–8538 (2017).

[29] Uzum, A., Kanda, H., Noguchi, T., Nakazawa, Y., et al. “H_2O/O_2 vapor annealing of alumina thin films.” International Journal of Photoenergy, 2019.

[30] Lee, S. M., Dummer, A., Montcalm, C., Kohli, S. “Annealing effects on optical filters.” Proceedings of SVC, 2002.

[31] Birkholz, M. Thin Film Analysis by X-Ray Scattering. Wiley-VCH, 2006. Chapter 4, pp. 89–120

[32] Wilkins, J. W., et al. “Nomarski microscopy as thickness monitor.” Ultramicroscopy 92, 293–300 (2002).

[33] Mori, D., Oka, H., Hosoi, T., Kawai, K., Morita, M., et al “Comparative study of GeO_2/Ge and SiO_2/Si structures on anomalous charging of oxide films upon water adsorption revealed by ambient-pressure X-ray photoelectron spectroscopy.” Journal of Applied Physics, vol. 120, 095306 (2016).

[34] Castro-Lucas, S. Y., Yang, L., Fazio, M., Markosyan, A., et al. “Structural modifications in oxide nanolaminates.” OIC, 2022.

[35] Ristau, D. “Ion beam sputter coatings for laser technology.” Proc. SPIE, 2005.

[36] Sites, J. R., et al. “Ion beam sputter deposition of optical coatings.” Optical Engineering, 1983.

[37] Zhurin, V. V., et al. “Biased target deposition.” Journal of Vacuum Science & Technology A, 2000.

[38] Ohring, M. Materials Science of Thin Films. Academic Press, 2002.

[39] Mattox, D. M. Handbook of Physical Vapor Deposition Processing, 2nd ed. Elsevier, 2010.

[40] Baldwin, D. A., et al. “Synthesis route to garnet and perovskite thin films.” SVC TechCon, 2009.

[41] Campbell, S. A. Fabrication Engineering at the Micro- and Nanoscale. Oxford University Press, 2008.

[42] Cullity, B. D., Stock, S. R. Elements of X-Ray Diffraction, 3rd ed. Pearson, 2001.

[43] Warren, B. E. X-Ray Diffraction. New York, NY: Dover Publications, Inc., 1990.

[44] Gao, Y., Masuda, Y., Peng, Z., Yonezawa, T., et al. “Room temperature deposition of TiO_2 thin films.” Journal of Materials Chemistry 13, 608–613 (2003).

[45] Griffiths, P. R., de Haseth, J. A. Fourier Transform Infrared Spectrometry, 2nd ed. Wiley, 2007.

[46] Stuart, B. Infrared Spectroscopy: Fundamentals and Applications. Chichester, UK: John Wiley & Sons, 2004.

[47] Moore, C., Perova, T. S., Kennedy, B., et al. “Study of silicon oxides using FTIR and Raman microscopy.” Proc. SPIE, 2002.

[48] Sharma, S., et al. “Growth and etch rate study of low temperature anodic silicon oxide films.”

International Scholarly Research Notices, vol. 2014, Article ID 106029, 2014.

[49] Murphy, D. B., and Davidson, M. W. Fundamentals of Light Microscopy and Electronic Imaging, 2nd ed. Hoboken, NJ: John Wiley & Sons, 2013.

[50] Pluta, M. Advanced Light Microscopy, Vol. 2: Specialized Methods. Amsterdam, Netherlands: Elsevier, (1989).

[51] Schmitt, D.-R. “Characterization of surfaces by Nomarski microscopy.” Precision Engineering 13, 263–269 (1991).

[52] Astuti, B., Tanikawa, M., Abd Rahman, S. F., Yasui, K., et al. “Graphene as buffer layer for SiC structures.” Nanoscale Research Letters, 2012.

[53] West, K. G., Lu, J., Yu, J., Kirkwood, D., et al. “Growth and characterization of vanadium dioxide thin films.” JVST A 26, 133–139 (2008).

[54] Kazmerski, L. L. Polycrystalline and Amorphous Thin Films and Devices. Amsterdam, Netherlands: Elsevier, (2012).

[55] Wang, J., et al. “FTIR study of water thin films on MgO.” Surface Science 487, 261–268 (2001).

[56] Zhang, R., Osovsky, R., Jiang, J., Fry, J. N., et al. “Network structure of TiO_2-doped GeO_2.” Physical Review Materials 10, 013601 (2026).

[57] Stuart, B. H. Infrared Spectroscopy: Fundamentals and Applications. Chichester, UK: John Wiley & Sons, 2004.

[58] Faber, J., Fawcett, T. “The powder diffraction file: present and future.” Acta Crystallographica B 58, 325–332 (2002).

[59] Kamimura, T., Fukumoto, S., Ono, R., Yap, Y. K., et al. "Enhancement of $CsLiB_6O_{10}$ surface-damage resistance by improved crystallinity and ion-beam etching." Optics Letters, vol. 27, no. 8, pp. 616–618 (2002).

[60] Langston, P., Patel, D., Markosyan, A., Krous, E. M., et al. "SiO_2/HfO_2 multilayers: impact of process parameters and stack geometry on the optical and structural properties." In Frontiers in Optics 2008 / Laser Science XXIV / Plasmonics and Metamaterials / Optical Fabrication and Testing. Rochester, NY: Optical Society of America, 2008, paper JSuA27.

APPENDIX A

A.1. Structural and FTIR characterization of Al_2O_3

The PXRD diffraction patterns of the *a*-Al_2O_3 films are presented in Figure A.1.1. The results show that Al_2O_3 remains amorphous under all conditions. No crystalline reflections associated with *a*-Al_2O_3 are observed. These results indicate that annealing at 600 °C for 10 hours, even under high humidity conditions, does not induce crystallization of the *a*-Al_2O_3 films.

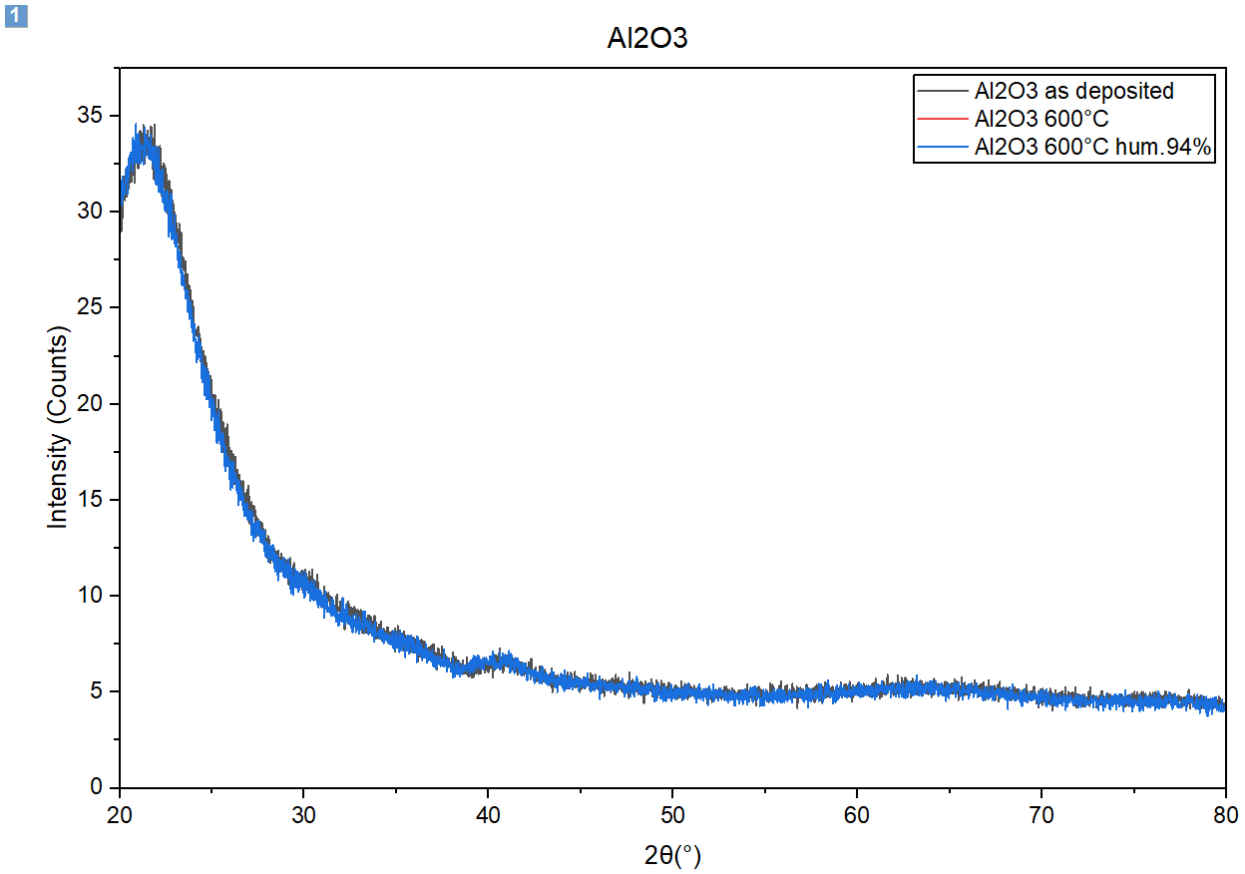

Figure A.1.1. PXRD patterns of *a*-Al_2O_3 films in the as-deposited state, after annealing at 600 °C, and after annealing at 600 °C under high humidity.

The FTIR spectra of the *a*-Al_2O_3 films are shown in Figures A.1.2. and A.1.3.

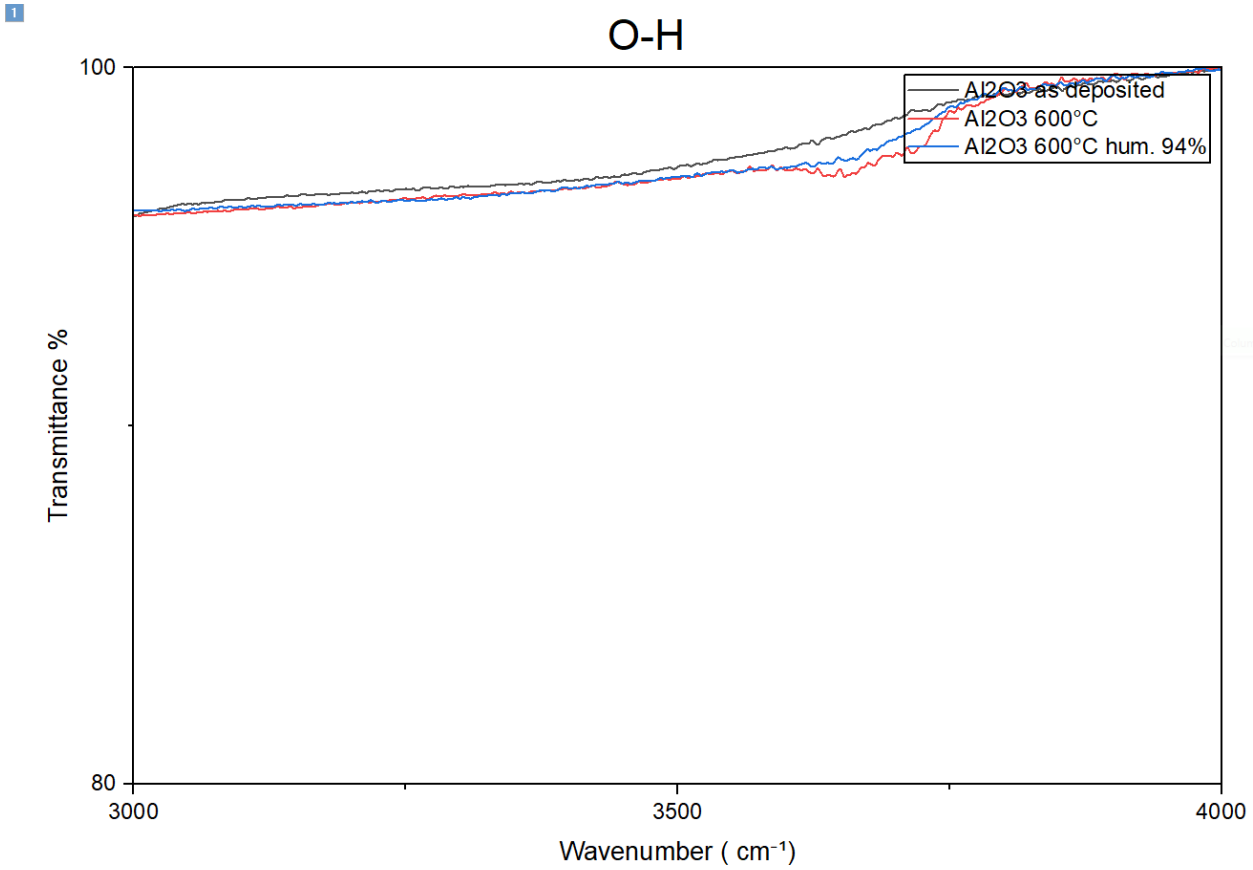

Figure A.1.2. - FTIR spectra of *a*-Al_2O_3 films in the O-H stretching region.

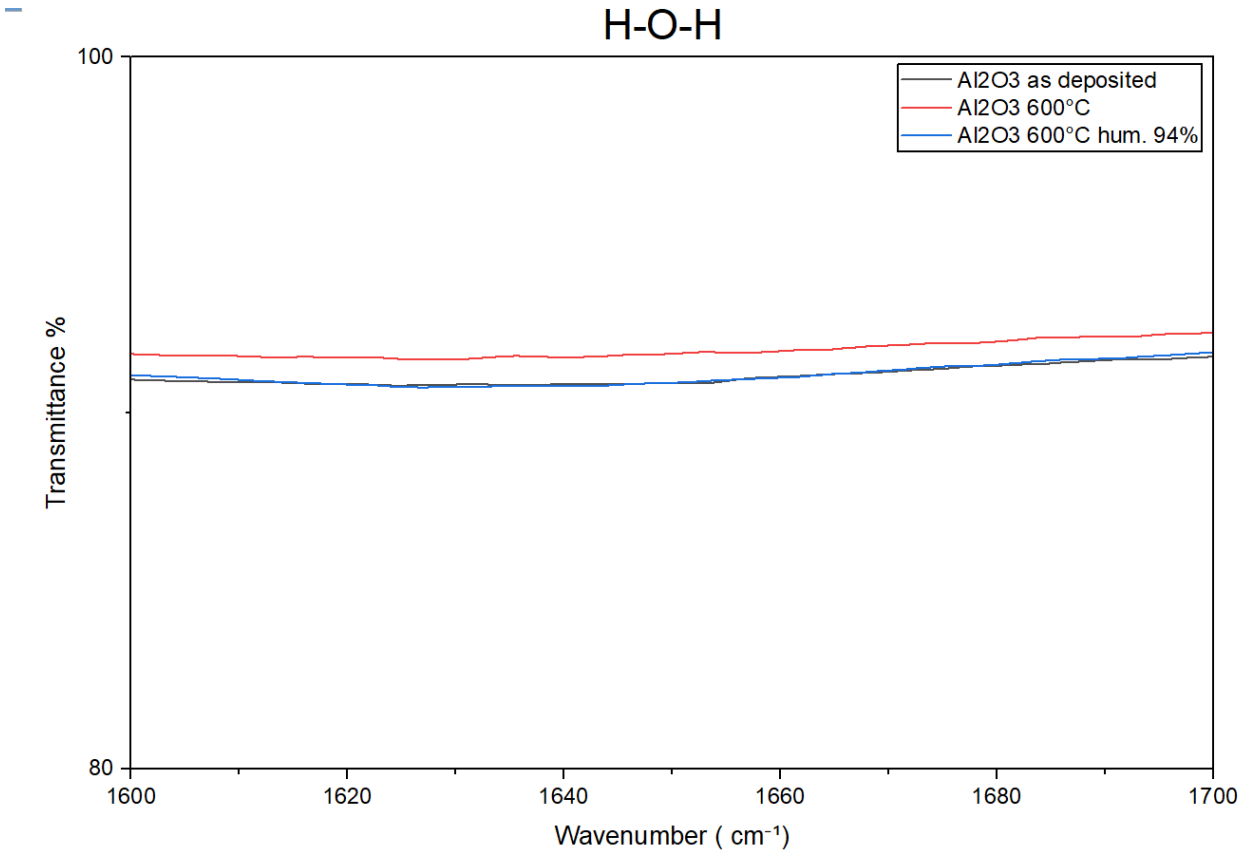

Figure A.1.3. - FTIR spectra of *a*-Al_2O_3 films in the H-O-H bending region.

No absorption band is observed in the 3000-3700 cm^{-1} range, indicating that the concentration of hydroxyl groups in the *a*-Al_2O_3 films is very low. The sample annealed in humidity does not show an increase in absorption, so water incorporation into the *a*-Al_2O_3 is minimal. In the H-O-H region all samples exhibit spectra without a distinct absorption feature. This indicates that molecular H_2O is not incorporated into the *a*-Al_2O_3 films.

The PXRD and FTIR results show that the *a*-Al_2O_3 films remain amorphous and show minimal sensitivity to humidity during annealing.

A.2. Structural and FTIR characterization of three-layer oxide stacks

A.2.1 $SiO_2/GeO_2/SiO_2$ stack

The optical microscopy images show that the $SiO_2/GeO_2/SiO_2$ stack remains smooth after annealing at 600 °C under ambient conditions. The sample annealed at 600 °C under high humidity exhibits circular and textured surface features.

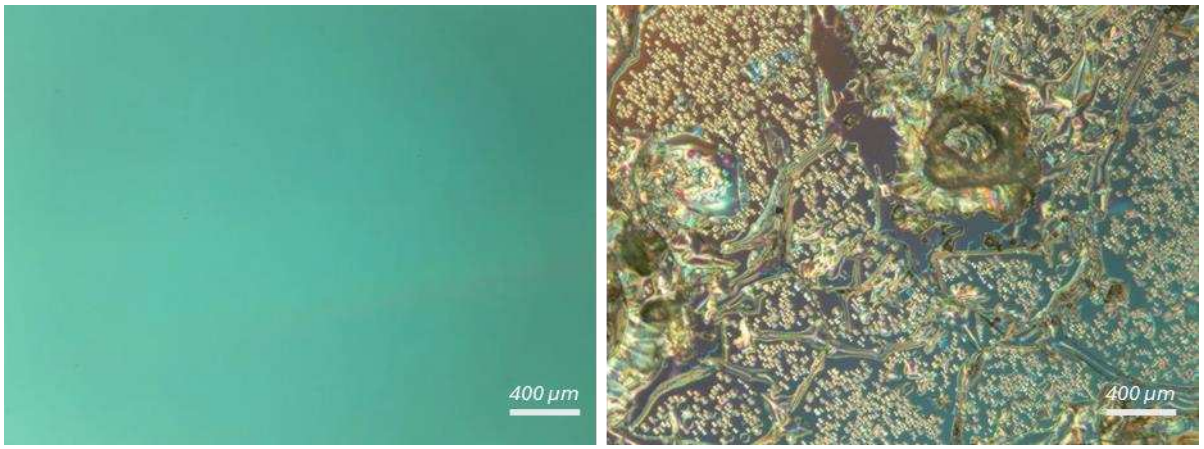

Figure A.2.1.1. - Optical microscopy images of the $SiO_2/GeO_2/SiO_2$ stack: (a) after annealing at 600 °C under ambient conditions; (b) after annealing at 600 °C under high humidity (~94 % RH).

The PXRD results of the $SiO_2/GeO_2/SiO_2$ structure are presented in Figure A.2.1.2. The as deposited and dry-annealed samples remain amorphous oxide films. After annealing at 600 °C under high humidity, the diffraction pattern shows the peaks associated with crystalline *a*-GeO_2. This indicates that humidity leads to crystallization of the *a*-GeO_2 layer within the stack.

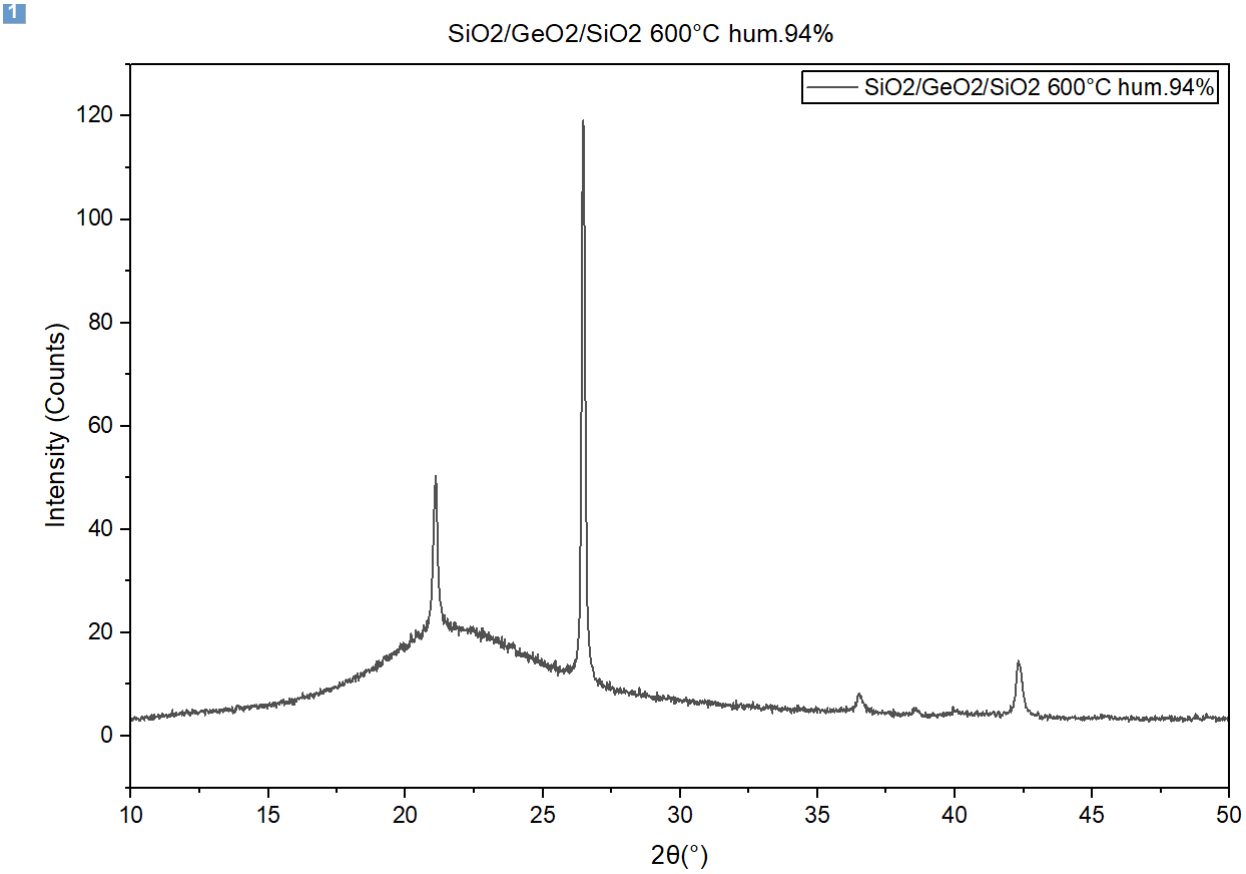

Figure A.2.1.2. - PXRD pattern of $SiO_2/GeO_2/SiO_2$ stacks after annealing at 600°C under high humidity.

The FTIR spectra is shown in Figure A.2.1.3. The humid-annealed sample exhibits a stronger absorption feature in the O-H region compared to the as-deposited and dry-annealed samples, suggesting increased hydroxyl incorporation during humid annealing.

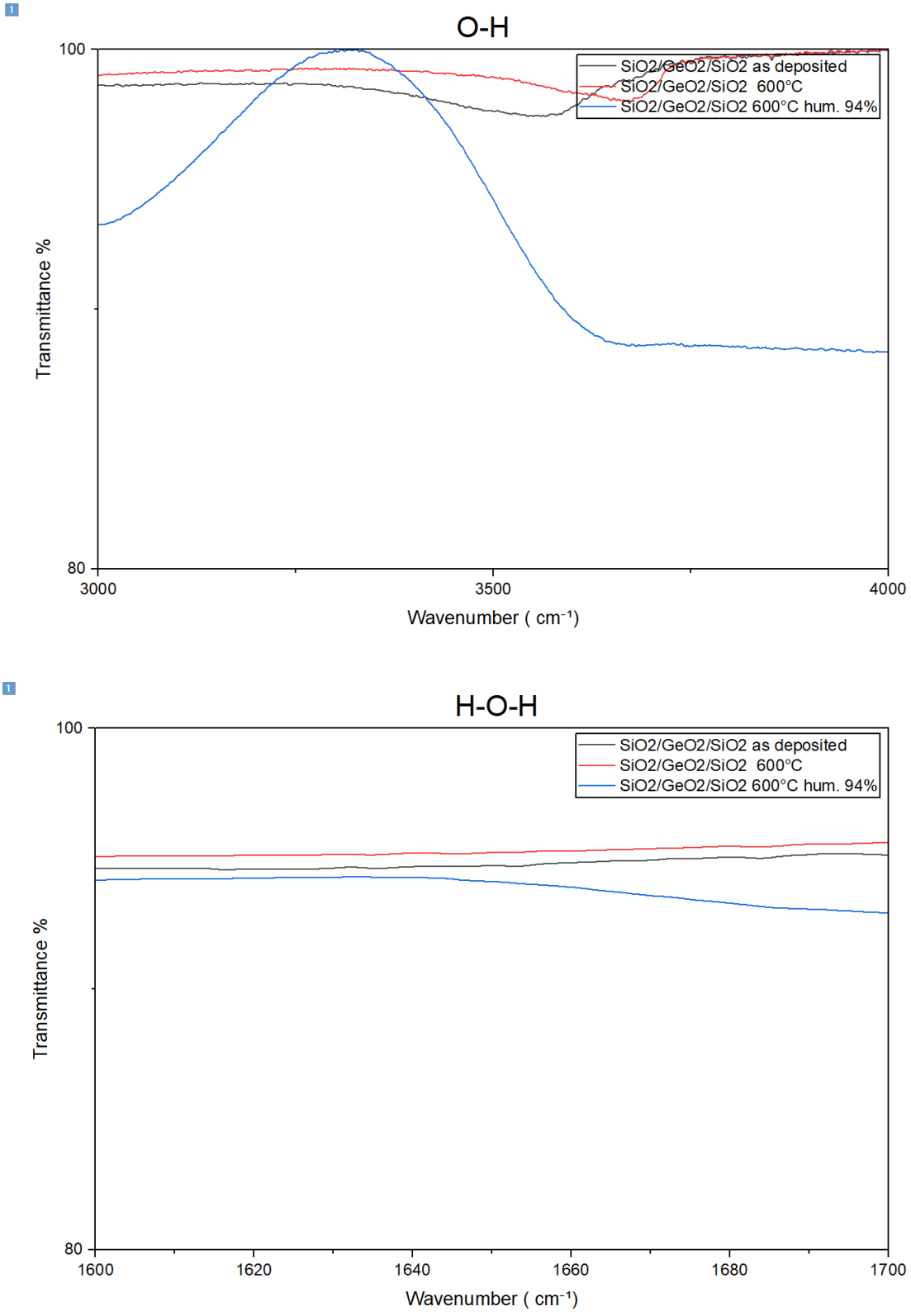

Figure A.2.1.3. - FTIR spectra of $SiO_2/GeO_2/SiO_2$ stacks.

A.2.2. SiO_2/TiGeO/SiO_2 stack

The SiO_2/TiGeO/SiO_2 stack shows a homogeneous surface after a humid annealing condition.

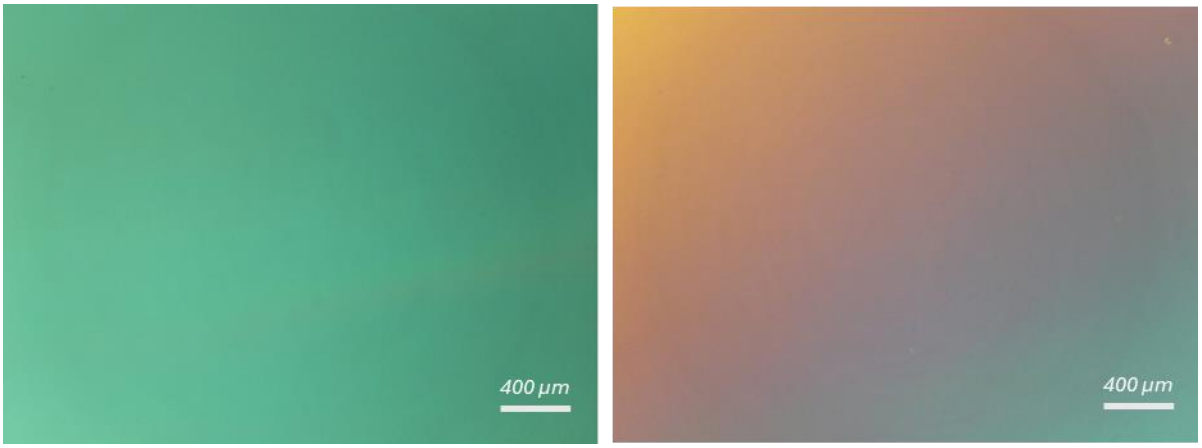

Figure A.2.2.1. - Optical microscopy images of the SiO_2/TiGeO/SiO_2 stack: (a) after annealing at 600 °C under ambient conditions; (b) after annealing at 600 °C under high humidity (~94 % RH).

The PXRD patterns of the SiO_2/TiGeO/SiO_2 annealed at high humidity stack is shown in Figure A.2.2.2. No sharp diffraction peaks observed. This indicates that the *a*-44%Ti-doped GeO_2 layer remains amorphous under humid annealing.

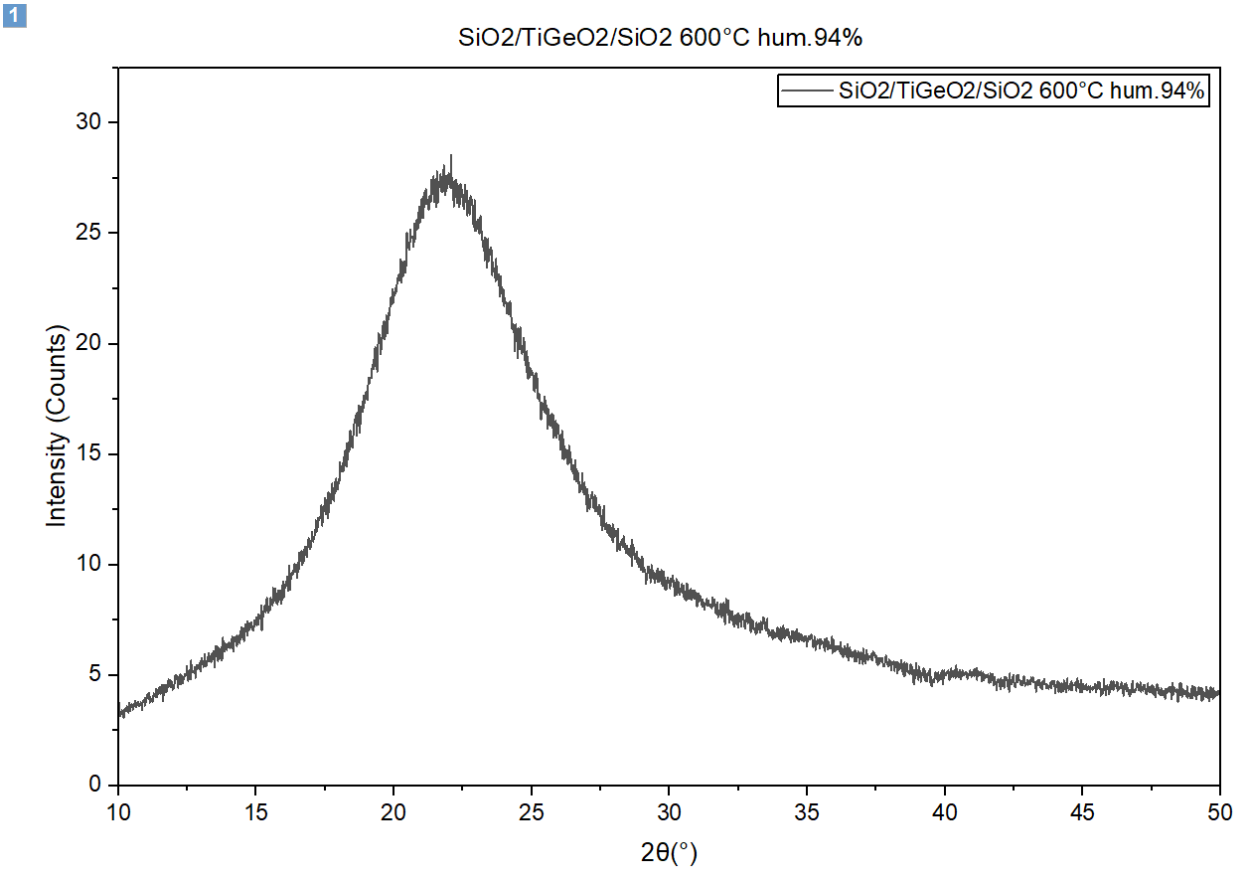

Figure A.2.2.2. - PXRD pattern of $SiO_2/TiGeO/SiO_2$ stacks under high humidity annealing.

The FTIR spectra presented in Figure A.2.2.3. shows the sample annealed at 600 °C under high humidity and a decrease in transmittance in the 3200-3600 cm^{-1} region, corresponding to the O-H stretching vibration.

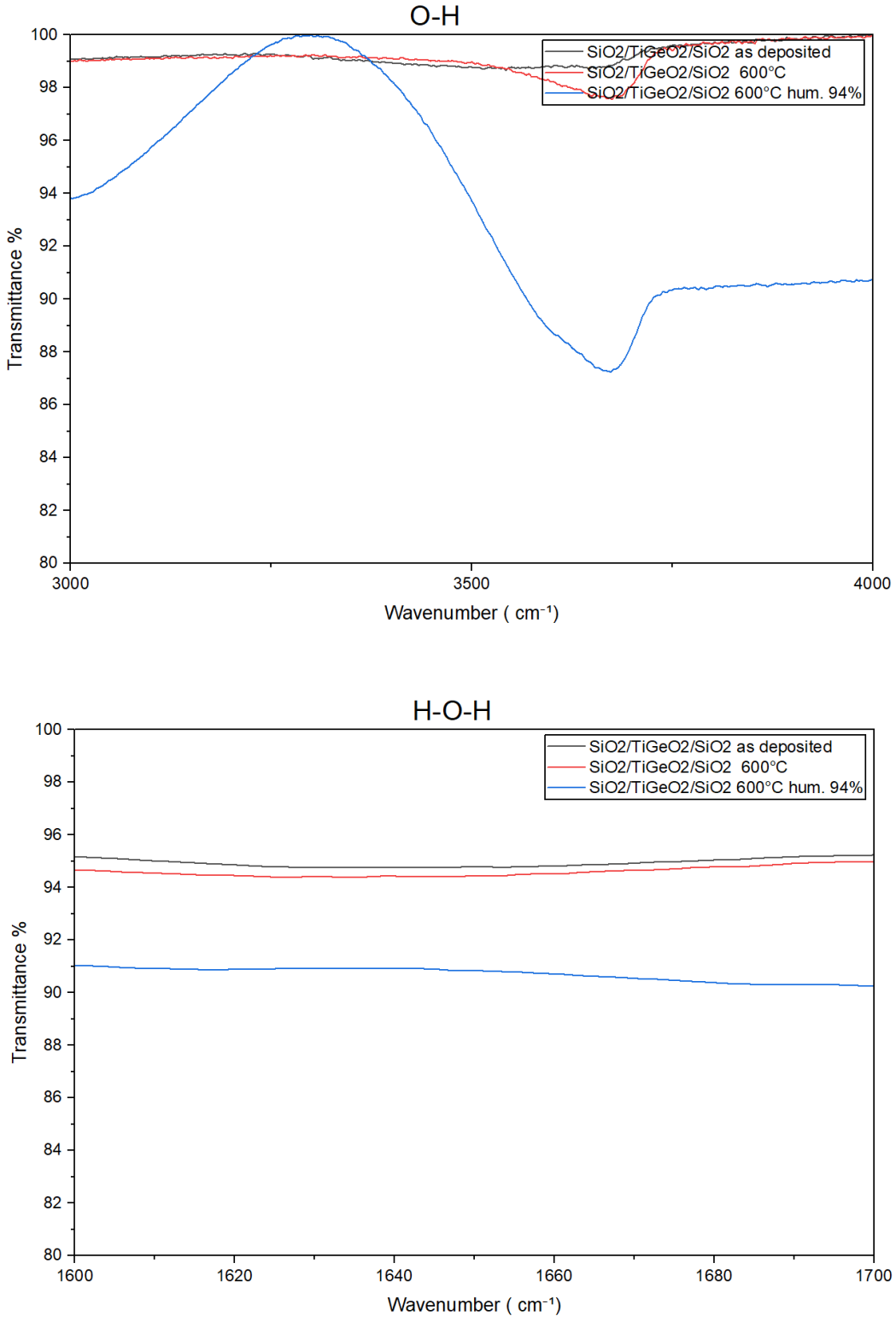

Figure A.2.2.3. - FTIR spectra of SiO_2/TiGeO/SiO_2 stacks.

A.2.3. $Al_2O_3/TiGeO/Al_2O_3$ stack

After annealing at 600 °C, the $Al_2O_3/TiGeO/Al_2O_3$ stack maintains a relatively uniform surface with no major morphological changes. However, the sample annealed at 600 °C under high humidity shows the formation of bubbles features, suggesting defect formation or localized stress relaxation within the multilayer structure.

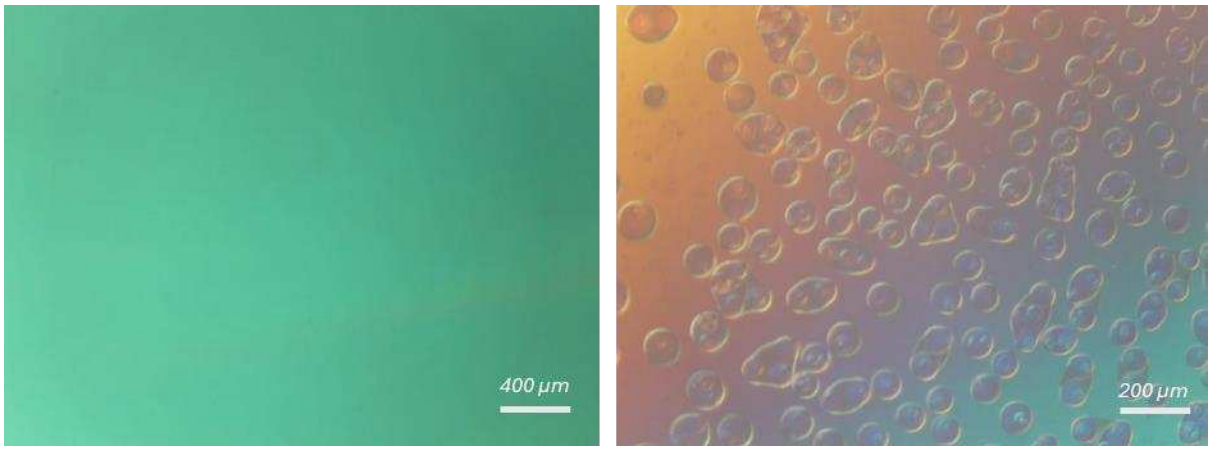

Figure A.2.3.1. Optical microscopy images of the $Al_2O_3/TiGeO/Al_2O_3$ stack:(a) after annealing at 600 °C under ambient conditions; (b) after annealing at 600 °C under high humidity.

The PXRD pattern of the $Al_2O_3/TiGeO/Al_2O_3$ annealed with high humidity conditions are shown in Figure A.2.3.2. Like the *a*-SiO_2-based stack, the diffraction patterns remain amorphous for all annealing conditions.

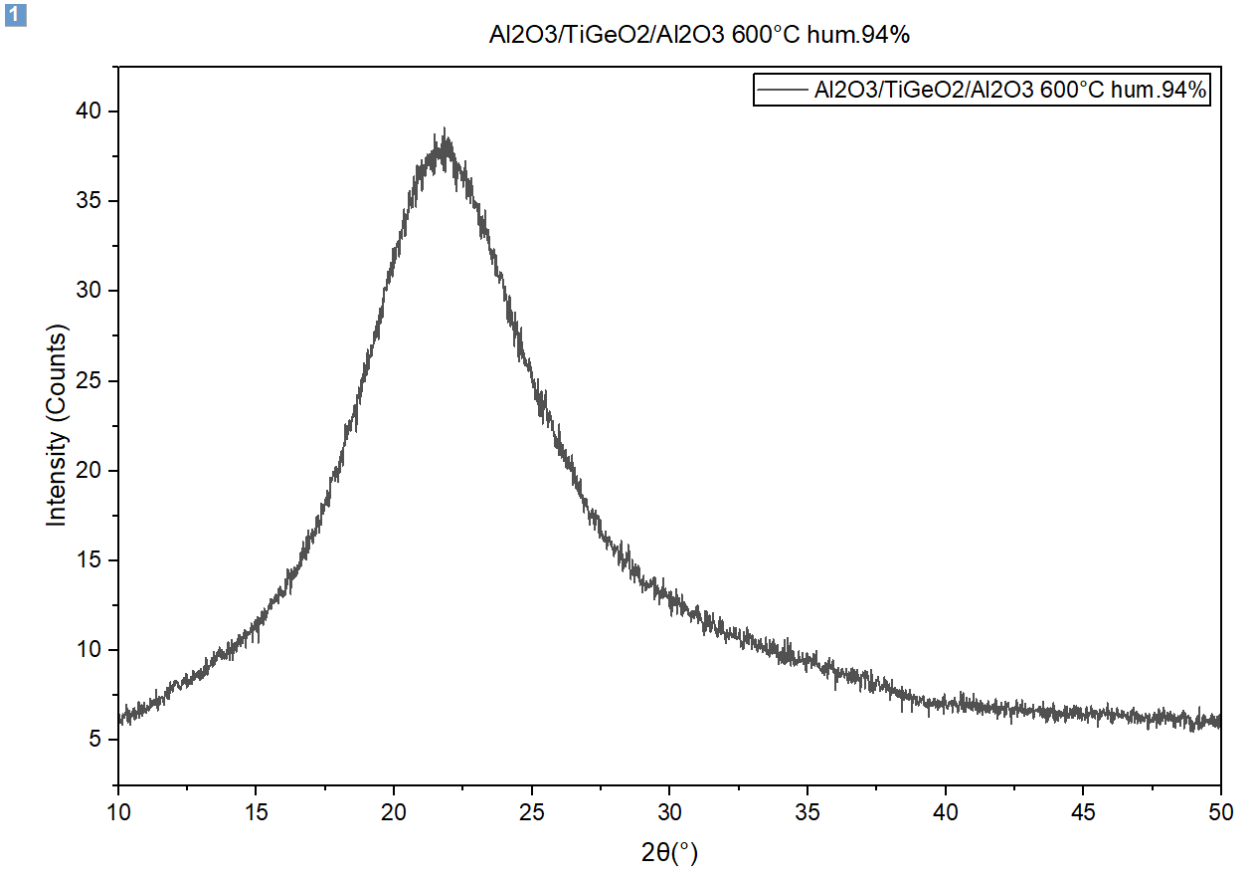

Figure A.2.3.2. - PXRD pattern of Al_2O_3/TiGeO/Al_2O_3 stack.

The FTIR spectra presented in Figure A.2.3.3.

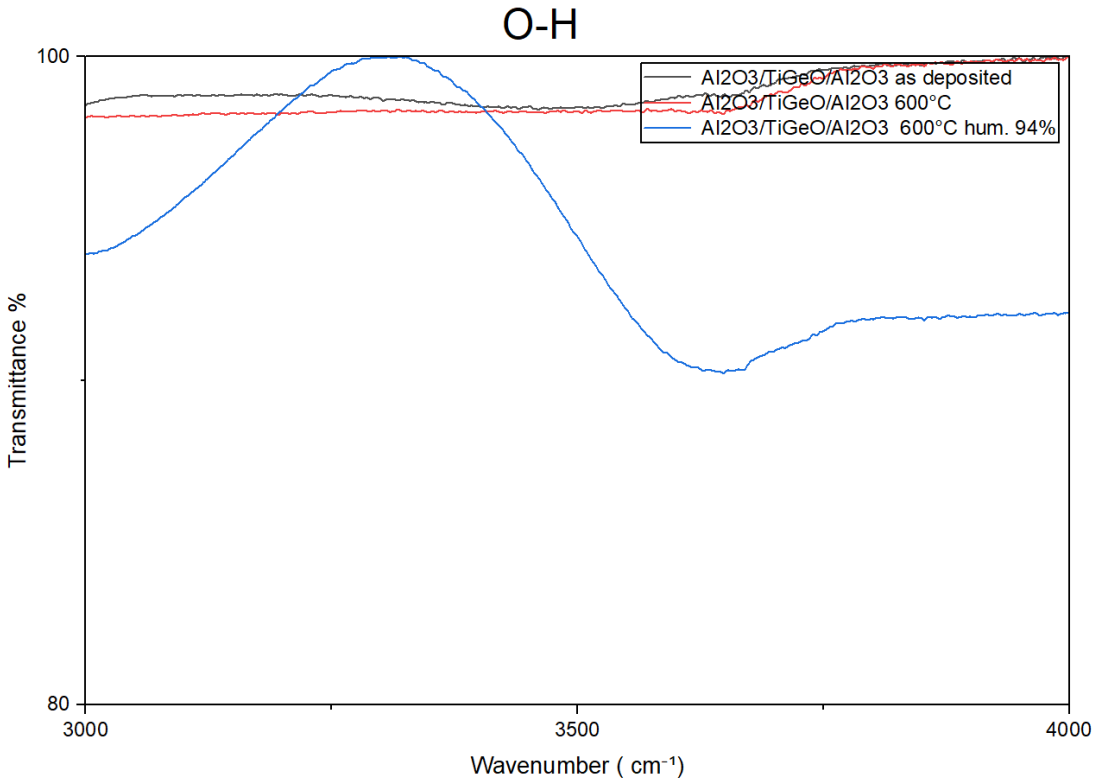

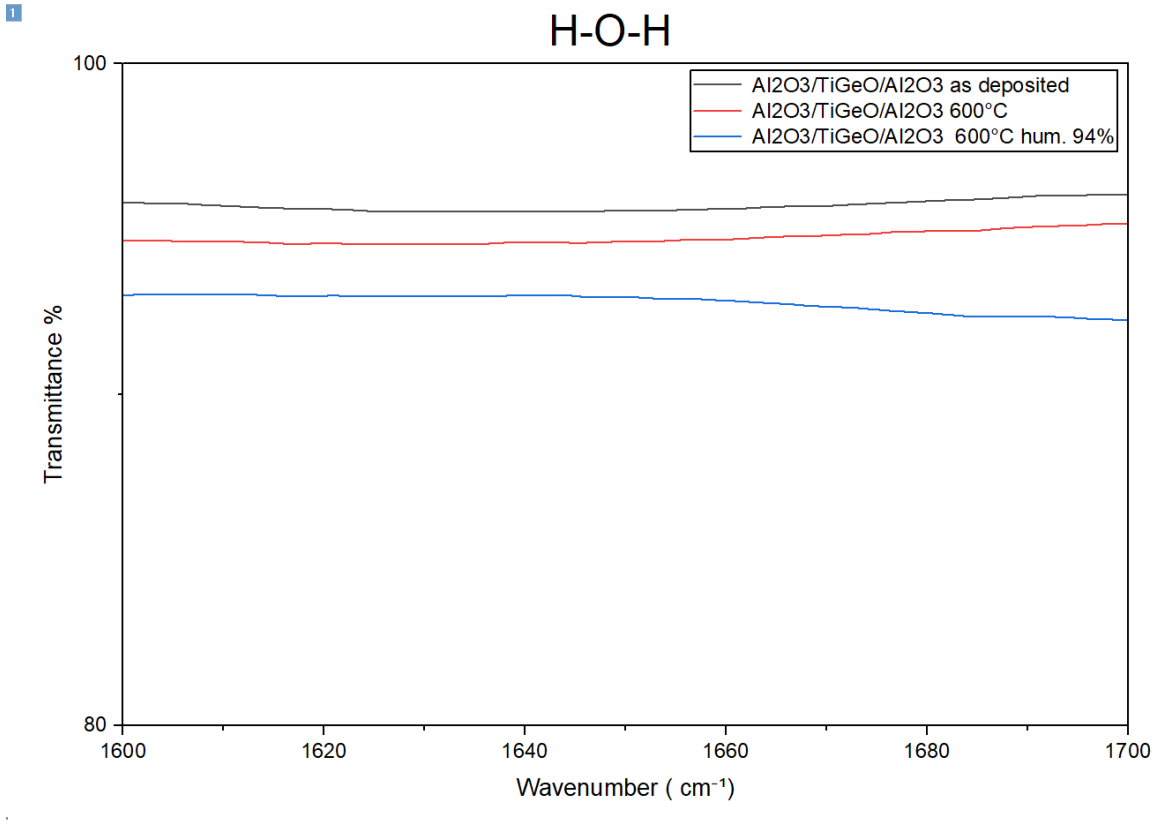

Figure A.2.3.3. - FTIR spectra of Al_2O_3/TiGeO/Al_2O_3 stacks.

A.2.4. Al_2O_3/GeO_2/Al_2O_3 stack

The Al_2O_3/GeO_2/Al_2O_3 stack exhibits noticeable surface changings after annealing at 600°C, suggesting structural changes within the *a*-GeO_2 layer. After annealing at 600°C under high humidity, the surface develops large bubbles patterns, indicating significant crystallization and morphological restructuring of the *a*-GeO_2 layer under humid conditions.

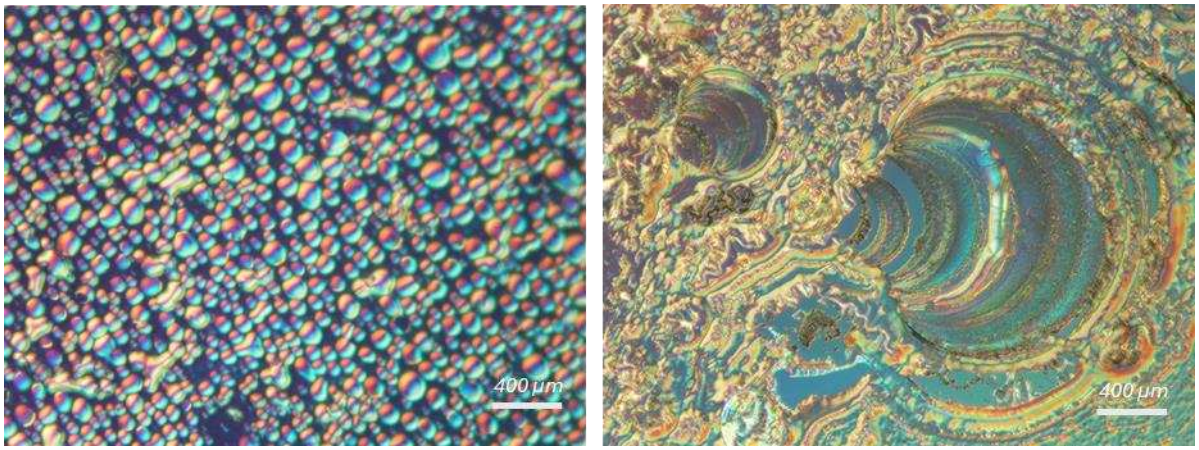

Figure A.2.4.1. - Optical microscopy images of the $Al_2O_3/GeO_2/Al_2O_3$ stack: (a) after annealing at 600 °C under ambient conditions;(b) after annealing at 600 °C under high humidity.

The PXRD pattern of the $Al_2O_3/GeO_2/Al_2O_3$ stack are presented in Figure A.2.4.2. In contrast to the TiGeO-containing stacks, the sample annealed at 600 °C under high humidity has clear diffraction peaks associated with crystalline *a*-GeO_2. This observation indicates that the *a*-GeO_2 layer undergoes crystallization under humid annealing conditions.

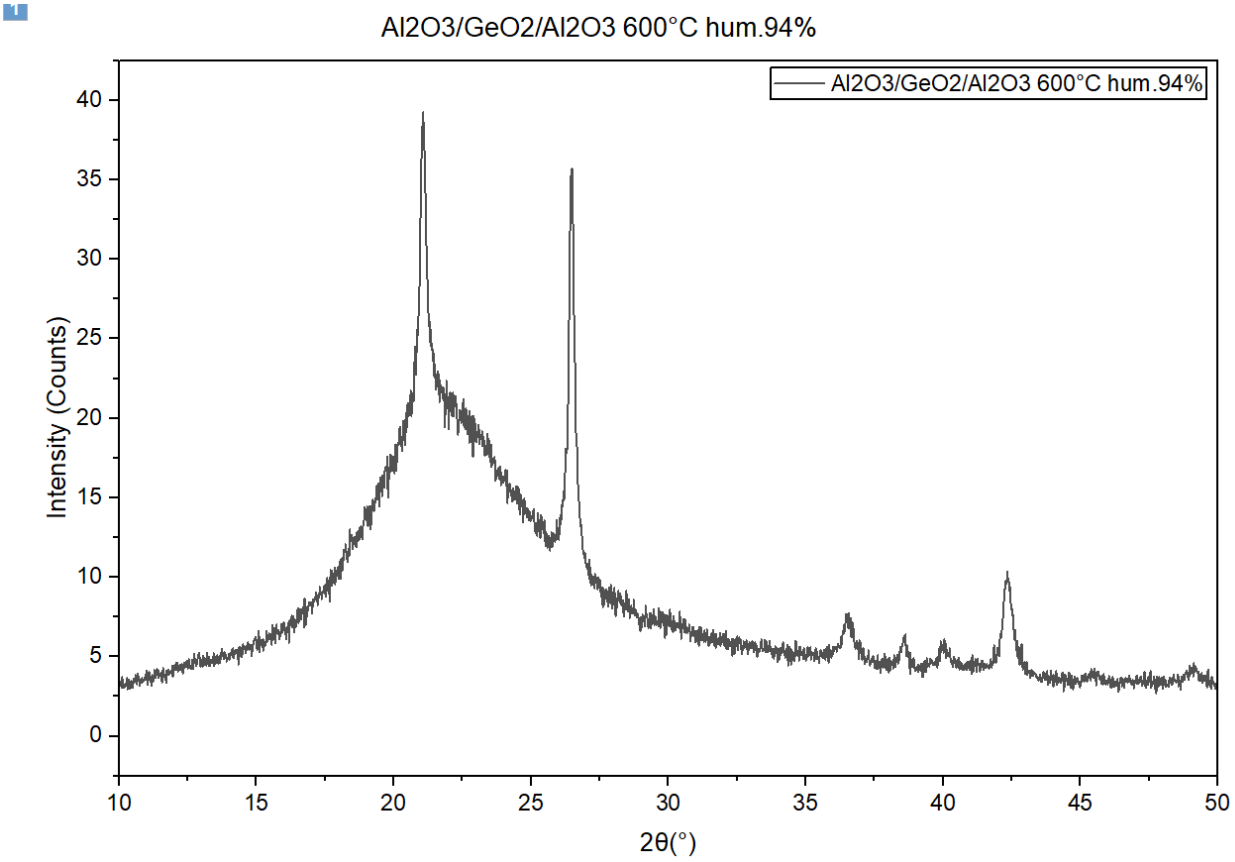

Figure A.2.4.2. - PXRD patterns of $Al_2O_3/GeO_2/Al_2O_3$ stacks.

The FTIR spectra in the Figure A.2.4.3. show increased absorption for the humid-annealed sample compared to the other conditions.

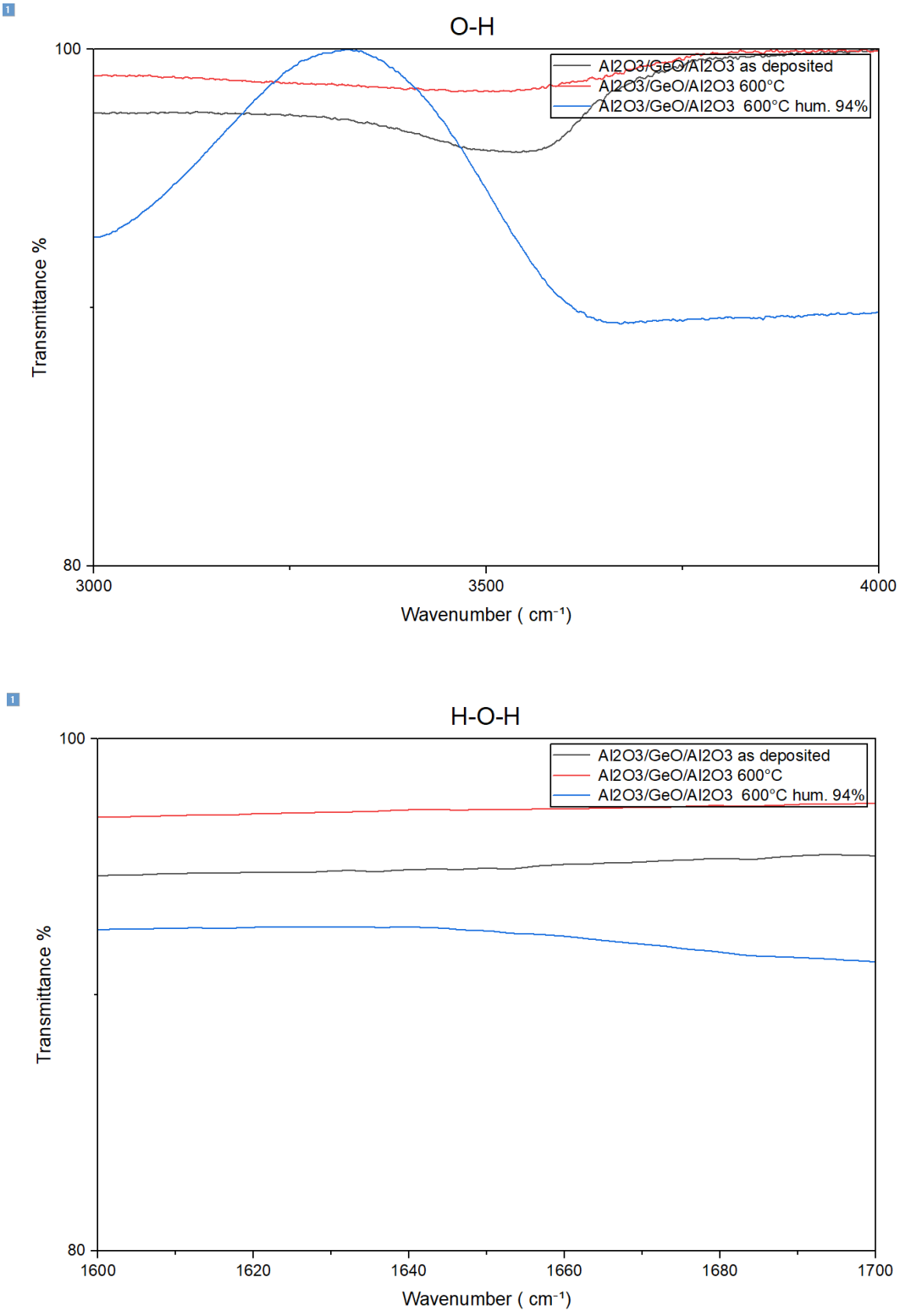

Figure A.2.4.3. - FTIR spectra of $Al_2O_3/GeO_2/Al_2O_3$ stacks in the O-H stretching region.